Deep groundwater characterisation and recharge estimation in the Verlorenvlei catchment

Anya Eilers

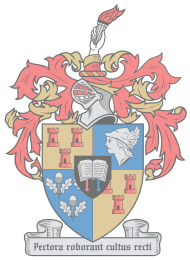

UNIVERSITEIT
iYUNIVESITHI
STELLENBOSCH
UNIVERSITY

Thesis presented in fulfilment of the requirements for the degree Master of Science in Geology/Environmental Geochemistry Stellenbosch University

Supervisor: Dr Jodie Miller

Faculty of Science

Department of Earth Sciences, Stellenbosch University

March 2018

Declaration

I declare that *Deep groundwater characterisation and recharge estimation in the Verlorenvlei catchment* is my own work, that it has not been submitted for any degree or examination in any other university, and that all the sources I have used or quoted have been indicated and acknowledge by complete references.

By submitting this thesis electronically, I declare that the entirety of the work contained therein is my own, original work, that I am the sole author thereof (save to the extent explicitly otherwise stated), that reproduction and publication thereof by Stellenbosch University will not infringe any third party rights and that I have not previously in its entirety or in part submitted it for obtaining any qualification.

Full name: Anya Eilers

Date: December 2017

Dedication

I dedicate this thesis to my beloved parents, Wulf and Inez Eilers, without whom none of this would have been possible. Your emotional, spiritual and financial support throughout the duration of my studies has been a driving force that kept me going, when all I wanted to sometimes do was just give up. Thank you for being my rock and encouraging me every step of the way.

Acknowledgements

I would first like to thank my supervisor Dr Jodie Miller for providing me with the opportunity to complete this study, and guiding me along the way. I would also like to thank Andrew Watson for sharing his knowledge on the study area, reading through drafts, and providing much technical support in the field (particularly for climbing up the Piketberg Mountain to construct the rainfall collector!).

I would like to extend my deepest gratitude to all the farmers who supported this project in terms of groundwater collection. This project would not have been possible without your support. I would particularly like to thank Jacobus Smit, Monique and Danie Vlok, and Jacqui van der Merwe for the long-term rainfall collection, and always being willing to help us in any way needed. Additionally, I would like to thank my fellow students Thendo Sigidi and Jasoyn Samuels for assistance in the field.

The many people who contributed to the data analysis must be thanked, including Mike Butler (iThemba Labs), Riana Rossouw (Department of Earth Sciences, Stellenbosch University) and Lore-Marie Deysel (Institute for Groundwater Studies, University of the Free State). Your contributions made this project possible. I would also like to thank the NRF for personal funding, and the WRC for funding this project.

Finally, I would like to thank all my friends and family for their constant encouragement and support throughout my master's.

Abstract

Secondary aquifers are a primary source of water in many semi-arid regions, and understanding groundwater recharge is necessary for the effective management of this resource. The Chloride Mass Balance (CMB) technique provides low-cost recharge estimates, and has successfully been used in many semi-arid catchments in Southern Africa. It is particularly useful along the west coast of South Africa, where physical data is limited. The west coast hosts the Verlorenvlei catchment and its RAMSAR listed wetland, where it is thought that deep groundwater baseflow sustains the wetland during the dry season. Shallow groundwater salinisation and increasing agricultural activity in the catchment has resulted in more deep groundwater abstraction, threatening the long-term health of the wetland. This study describes how major ion and stable isotope chemistry of ground and rain water can be used to calculate recharge to the secondary aquifer using the CMB technique, and its implications for assessing mechanisms of recharge and salinisation in the catchment. To do this, 102 groundwater samples were collected across the catchment over six sampling seasons. Additionally, 94 rain water samples were collected over the period of eighteen months, with daily rainfall collectors located in the valley, and a cumulative collector erected on the Piketberg mountain range, to assess the contribution of recharge from the Table Mountain Group (TMG) aquifer. CMB recharge estimates in the upper catchment indicate that the TMG aquifer contributes between 40 and 53 mm/a (11.4 – 15.2% MAP) recharge to the secondary aquifer, while direct recharge in the upper valley is between 20 and 27 mm/a (4.2 – 5.6% MAP). These estimates are supported by $\delta^{18}O$ and $\delta^{2}H$ values of rain and groundwater, and correlate well with previous physical methods. $\delta^{18}O$ and $\delta^{2}H$ values also indicate that the upper catchment is likely to be a gaining stream, with deep groundwater contributing to baseflow. The additional input of salts further down the catchment, due to water-rock interaction and the inflow of other deep groundwater, make CMB recharge estimates unreliable in the lower catchment. Furthermore, pumping-induced discharge from the primary to secondary aquifer during the summer months is responsible for a distinct increase in salinity of the secondary aquifer. This is characteristic of a losing stream, with groundwater contributing little to baseflow. Predictions of increasing temperature and decreasing rainfall along the west coast indicate that pumping-induced discharge could become more common in the lower catchment, increasing the threat of secondary aquifer salinisation and a reduction in groundwater baseflow. Overall, the methodology applied in this study can be used for high resolution, at-point CMB estimates in other small catchments, and contribute to long-term groundwater management in semi-arid catchments affected by salinisation.

Keywords: Recharge, Chloride Mass Balance, Verlorenvlei, Deep Groundwater, Semi-arid

Abbreviations and symbols

°C – Degrees Celsius

‰ – Per Mil

$\delta^{18}O$ – Oxygen Isotope value (‰)

$\delta^{2}H$ – Hydrogen Isotope value (‰)

µm – Micrometre

µS/cm – Micro semen per centimetre

AWS – Automatic weather station

CAF – Central Analytical Facility

Cl_p – Chloride in precipitation

Cl_{gw} – Chloride in groundwater

d – Deuterium Excess

EC – Electrical Conductivity

GMWL – Global Meteoric Water Line

HNO_3 – Nitric acid

HRU – Hydraulic Response Unit

IC – Ion Chromatography

ICP-MS – Inductively Coupled Plasma Mass Spectrometry

ICP-OES – Inductively coupled plasma optical emission spectrometer

LMWL – Local Meteoric Water Line

Ma - Million years

MAP – Mean Annual Precipitation

mg/L – Milligrams per litre

ml – Millilitre

mm - Millimetre

mS/m – Millisiemen per metre

PP – Polypropylene

TDS – Total dissolved Solids

TMG – Table Mountain Group

TABLE OF CONTENTS

LIST OF FIGURES

LIST OF TABLES

1. INTRODUCTION

1.1. General Introduction

South Africa is historically a water-stressed country, with rainfall significantly decreasing from east to west (Dennis and Dennis, 2012). Much of the west coast of South Africa receives between 200 and 500 mm rainfall per annum, and is defined as semi-arid (Lloyd, 1986). Low rainfall and the lack of surface water in many parts has resulted in large-scale groundwater abstraction to support agricultural and urban demands. Over-pumping is therefore a cause for concern, and quantifying groundwater recharge is necessary to determine safe aquifer yields, and to assess future groundwater vulnerability (Hugman *et al.*, 2012). Sustainable groundwater management is particularly important along the west coast, where boreholes show less resilience to the effects of climate change in comparison to central South Africa (MacDonald *et al.*, 2011).

Groundwater recharge estimation is particularly important for wetland systems occurring in semi-arid settings, as base-flow derived from groundwater is considered an essential component for sustaining the health of these ecosystems, particularly during low flow periods (Parsons, 2004). In the African context, many wetland systems are threatened by over-exploitation (either at the wetland or upstream) for economic development, as these ecosystems provide a valuable source of both water and nutrients (Schuyt, 2005). Furthermore, high groundwater extraction near streams can result in discharge from the stream to the aquifer, thus reducing baseflow (Chen, 2001). The South African Water Act of 1998 states that groundwater can only be utilised for economic purposes if the annual recharge exceeds the basic environmental and human requirements in both the catchment and downstream. Quantifying groundwater recharge is therefore essential for assessing the contribution of baseflow to wetlands, and the effects of groundwater abstraction on baseflow.

Decades of studies have focused on estimating recharge in semi-arid areas (Fontes and Edmunds, 1989; Gee and Hillel, 1988; Rushton, 1988) and Sub-Saharan Africa (Beekman and Xu, 2003; De Vries *et al.*, 2000; Bredenkamp *et al.*, 1995). These studies indicate that recharge estimation in semi-arid environments is particularly complicated, due to a smaller and more variable recharge flux in comparison to humid areas, and fewer recharge estimation techniques can be successfully used in semi-arid environments (De Vries and Simmers, 2002). No single estimation technique can be used to accurately estimate recharge across a range of environments (Van Tonder and Bean, 2003), but combining physical and natural tracer techniques, as well as numerical modelling, has proven to be a powerful tool for estimating recharge (Scanlon *et al.*, 2002). The Chloride Mass Balance (CMB) technique has

been successfully used to estimate recharge in many semi-arid areas (Lihe *et al.*, 2010; Sami and Hughes, 1996; Bazuhair and Wood, 1996; Wood and Stanford, 1995). Such a method provides cheap estimations that are often easier to obtain than physical methods. It also provides a time-integrated recharge value (Wood and Stanford, 1995) that is particularly useful in semi-arid areas where rainfall varies in both time and space. For the CMB method to effectively work, it must be assumed that all chloride input to the aquifer is derived from rainfall, and that chloride is conservative in the system (Wood, 1999). Groundwater salinisation is common in many semi-arid settings, and as such the CMB method requires the use of additional methods, such as stable isotopes, to effectively constrain flow systems and understand recharge mechanisms (Verhagen, 2003).

The Verlorenvlei is a RAMSAR (#525) listed wetland situated 200 km north of Cape Town in the Sandveld. The intermittent connection between wetland and ocean has created an estuarine environment that supports a high biodiversity of fish and aquatic birds. Agriculture is also an important part of life in the Sandveld, with potato production contributing 15% of the national potato produce and using roughly 20% of the annual recharged groundwater in the Sandveld (Archer et al., 2009). The upper reaches of the Piketberg valley, to the south east of the catchment, also host an increasing number of large-scale commercial farms, particularly producing export quality table grapes. The combination of low rainfall and poor-quality soil results in a large amount of water and fertiliser use, with the introduction of centre-pivot irrigation contributing to both declining groundwater levels, and the salinisation of surface and shallow ground water (Maclear, 1994). The strong interplay between the economic benefit for the agricultural sector, as well as ecosystems that are highly dependent on groundwater, has resulted in a groundwater system that shows significant signs of water stress (Conrad et al., 2004).

There are three aquifers in the Verlorenvlei catchment. A primary, unconfined aquifer is hosted in by quaternary sediments, and is widely used for irrigation in the west of the catchment. It is characterised by high salinity values of up to 1988 mS/m (Sigidi, 2017). The primary aquifer is underlain by a semi-confined secondary aquifer hosted by the Malmesbury Group. It becomes increasingly important towards the east of the catchment, and is characterised by lower salinity values in comparison to the primary aquifer. An additional fractured rock aquifer is hosted the Table Mountain Group (TMG). The primary and secondary aquifers are likely to be in hydraulic connectivity (Conrad *et al.*, 2004), and the effects of over-pumping, in combination with changing climate conditions, could result in regional groundwater depression cones (Yuan *et al.*, 2013), creating a threat of salinisation for both the wetlands and deeper aquifer. The TMG aquifer is also likely to provide the bulk of the recharge to the secondary

aquifer (Watson et al, 2017b; Conrad et al., 2004). The highest recharge to the TMG occurs in the Piketberg mountain range, with groundwater transported primarily through fracture networks down the catchment, due to the high hydraulic gradient (Watson et al., 2017c).Although recharge estimation in semi-arid South Africa has received a lot of attention, limited recharge studies and hydrological data along the west coast makes recharge quantification in this environmentally sensitive area one of the most difficult to characterise. The CMB technique is one of the most common methods used for calculating recharge, but it is difficult to apply in areas of groundwater salinisation, such as along the west coast of South Africa. Furthermore, little research has focussed on the upper reaches of the Piketberg Mountain range, where the bulk of the recharge is suspected to be derived from the TMG aquifer. While some studies have characterised the chemical composition of the secondary aquifer groundwater in the Piketberg valley (GEOSS, 2012; SRK, 2009; GEOSS, 2006), these studies only cover a selected number of boreholes and do not assess long-term seasonal variations.

This study therefore aims to characterise the geochemical and isotopic nature of groundwater from the secondary aquifer in the Verlorenvlei catchment over a period of 18 months. The study is focussed on the Moutonshoek Valley of the Piketberg Mountain range, where there is a high recharge potential and concentrated agricultural activity. Precipitation samples are used in combination with groundwater samples to calculate recharge using the CMB technique, with stable isotopic signatures providing additional insight into recharge processes. This geochemical approach to groundwater characterisation and recharge estimation will provide a good comparison to previous physically-based methods by Watson *et al.* (2017b) and Conrad *et al.* (2004). The methodology used during this study will be used to create a robust filtering technique for ground and rain water collection for CMB estimations in other semi-arid areas where salinisation is a cause for concern. Furthermore, recharge estimates and stable isotope data will be used to establish a conceptual model of recharge mechanisms. This will be used to assess the interaction of the shallow and deeper aquifer, and assess the future health of the groundwater and wetlands based on climate predictions.

1.2. Aims and Objectives

The key aim of this study is to characterise the groundwater originating in the secondary aquifer of the upper Verlorenvlei catchment, and estimate recharge using stable isotopes and the CMB technique. The data will be used to assess the extent of the interaction between the secondary and primary aquifer, the source of salts in the secondary aquifer, and the long-term impacts of climate change and pumping on groundwater quality and quantity. Additionally, the methodology presented for CMB estimation will be evaluated to assess the applicability of

such a method in other semi-arid catchments effected by salinisation, as well as establish a conceptual model of recharge mechanisms.

Key objective one: To characterise deep groundwater and precipitation in the Verlorenvlei catchment.

1. What is the geochemical and isotopic signature of deep groundwater in the Verlorenvlei catchment, and how does this vary spatially and temporally?
2. What is the geochemical and isotopic signature of precipitation in the Verlorenvlei catchment, and how does this vary spatially and temporally?
3. What is the average annual rainfall during this study, and how does it compare to previous years?

Key objective two: To determine the recharge rate to the secondary aquifer of the Verlorenvlei catchment using the chloride mass balance method, and assess the applicability of this method for other semi-arid catchments.

1. What is the recharge rate based on chloride mass balance calculations and stable isotope compositions, and how do these estimates compare to other recharge estimates in the Sandveld?
2. What are the possible recharge mechanisms in the catchment?
3. How can the methodology presented in this study be used for recharge estimation in other semi-arid areas?

Key objective three: To assess the future health of the secondary aquifer and wetlands in the Verlorenvlei catchment.

1. What are the possible sources of salinisation to deep groundwater?
2. What is the extent of the interaction between deep and shallow groundwater, and how could this effect the secondary aquifer?
3. What impacts could regional pumping and climate change have on future groundwater quality and quantity, and how could this impact the wetlands?

2. GROUNDWATER SYSTEMS

2.1. Surface - Groundwater Interaction

The term baseflow refers to the groundwater component of river flow, and groundwater is likely to contribute to surface flow during low rainfall periods. Baseflow may also contribute to wetlands, springs and seepages (Vegter and Pitman, 2003), and provides a minimum estimate of groundwater recharge. Winter *et al.* (1998) divides shallow groundwater and stream interaction into four simplified scenarios: (1) a gaining stream (where the groundwater contributes to stream flow); (2) a losing stream (where stream flow replenishes the groundwater); (3) a disconnected stream (where the stream and groundwater are separated by an unsaturated zone); and (4) bank storage (occurring when stream levels rise higher than the groundwater levels and the stream flow moves into the stream bank) (Figure 1). Connected rivers are common in the lower catchments of humid climates, and often seasonally alternate between losing and gaining streams (Lerner, 2003). Disconnected rivers on the other hand are likely to be smaller streams found in the upper catchments of drier climates, and under these circumstances, it is unlikely that groundwater contributes to stream flow (Lerner, 2003). This surface and sub-surface interaction occurs in the critical zone and is controlled by several factors, including the geological and soil characteristics of the stream beds, seasonal fluctuations, and the position of the water body with respect to groundwater flow paths (Winter, 1999).

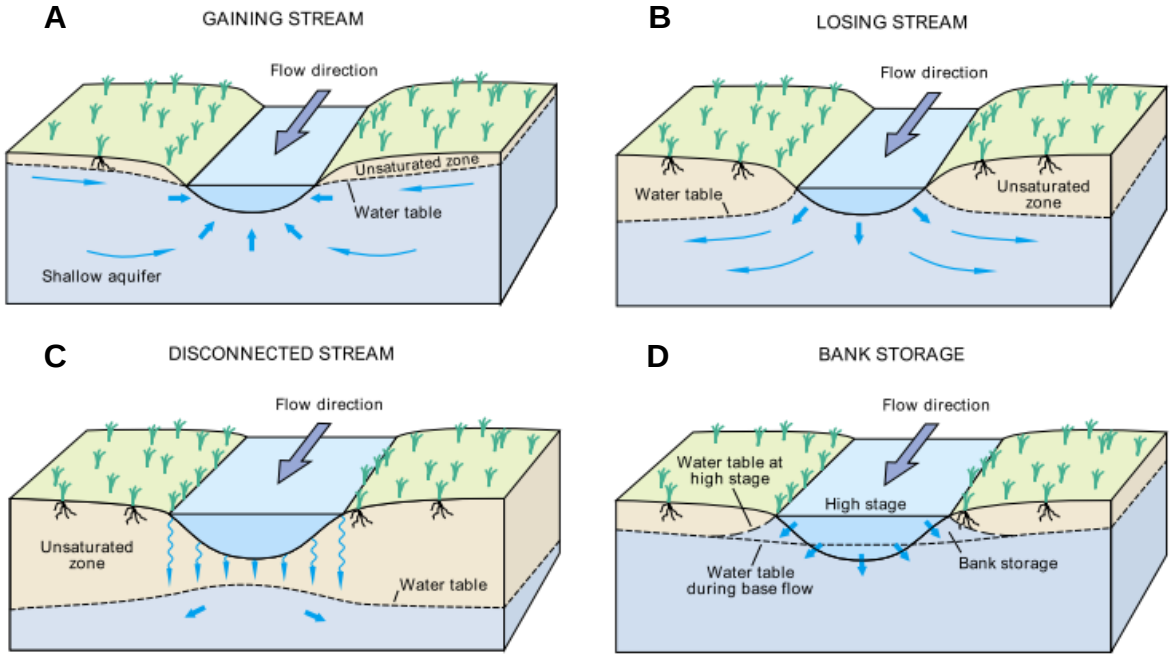

Figure 1: Schematic diagrams of a gaining stream (a), losing stream (b), disconnected stream (c) and bank storage (d) (Winter et al., 1999)

A large portion of the interaction between streams and shallow aquifers is pumping-induced, and large groundwater abstraction could lead to a reverse-hydraulic gradient, where stream water discharges into the aquifer, creating a losing stream (Butler *et al.*, 2001). The induced stream infiltration will result in the reduction of groundwater baseflow and stream flow depletion, and could have serious consequence for the health of wetlands, springs and riparian zones (Hugman *et al.*, 2012). Furthermore, contaminated surface water could result in groundwater contamination (Chen, 2001). Pumping-induced interaction can also occur between a semi-confined and unconfined aquifer that are in hydraulic connectivity. While it is assumed that the hydraulic head in the unpumped aquifer will remain constant, this is not the case for prolonged or heavy pumping (Sayed and Hussainy, 2011). These are known as leaky aquifers, and aquifer drawdown could result in the discharge from one aquifer to the other via the semi-pervious layer.

2.2. Groundwater flow systems

The idea of *groundwater flow systems* was proposed by Toth (1963), who divided groundwater into local, intermediate and regional flow systems. This division supports the complicated nature of groundwater, which is a three dimensional field with components of lateral and vertical flow (Winter *et al.*, 1998). These systems are heavily influenced by topography and follow the undisputed law of the hydrological cycle: topographically high areas are sites for recharge and topographically low areas are sites for discharge (Schwartz and Zhang, 2003). Understanding these flow systems is very useful due to their control on groundwater flux, residence time, depth and chemical properties (Dahl *et al.*, 2007).

Local flow systems are the shallowest and generally smallest, with the greatest variability in their interaction with surface water, as well as larger recharge rates and shorter residence times (Winter *et al.*, 1998). These ‘meteoric waters’ are active participants in the water cycle, and are normally comparatively less saline than their deeper counterparts (Van Weert *et al.*, 2009). In such a local system, the effects of local topographic features, such as depressions, are a key controlling factor. An increase in local slope has the effect of increasing the depth and concentration of these local systems (Dahl *et al.*, 2007). Recharge occurs at a topographic high and discharges to an adjacent lowland. Discharge is seasonal and erratic, and baseflow may not even occur in the dry season. In far-reaching flat areas, no local flow systems may develop, resulting in stratified groundwater (Dahl *et al.*, 2007). Groundwater is generally present in this flow path for less than a year, and surface-groundwater interaction may occur in either direction (Gardner, 1999). Contamination by human activities are most likely to occur in this groundwater system.

Intermediate flow systems occur below local flow systems, but are not as deep as their regional counterpart. The topography and geology within a certain region controls the nature of intermediate flow paths, and they may interact occasionally with surface water. Groundwater residence times may be between 1 and 100 years approximately, and precipitation flowing through the vadose zone may enter the groundwater along this flow path (Gardner, 1999). Groundwater is discharged along a stream or wetland area. Recharge rates are smaller, but discharge into larger streams is continuous and steady throughout the year (Dahl *et al.*, 2007).

Regional flow systems are the deepest, and occur where the regional slope dominates local slope, such as between mountainous and coastal areas. Such systems have the longest flow paths and greatest residence times, as groundwater is primarily traveling through bedrock, and thus they generally contain the most dissolved solids (Winter *et al.*, 1998). Groundwater present in regional flow systems typically has no contact with surface water after recharge, with recharge often occurring at the divide between two catchments (Dahl *et al.*, 2007). This groundwater may have a residence time of thousands of years, and is typically the most resilient to degradation by human intervention (Gardner, 1999).

2.3. Groundwater recharge

The global hydrological cycle is a complex system controlled by the processes of inflow (from precipitation and snow melt), recharge and outflow (from runoff and evapotranspiration), with ground and surface water only forming two components of this system (Freeze and Cherry, 1979). Groundwater is recharged from precipitation, rivers, large water bodies and anthropogenic activities such as irrigation. Recharge is therefore defined as the hydrologic process where the downward flow of water, through infiltration and percolation, contributes to the permanent water table. This recharge value is often represented as the *increase in stored water (ΔS)*, and forms an integral part of the water balance $\Delta S = P - R - E$ where P is precipitation, R runoff, and E actual evaporation (Rushton and Ward, 1979). Understanding groundwater dynamics is particularly important in the modern climate, where rapid urbanisation coupled with expanding industrial and agricultural activities are placing increasing pressure on water requirements. A thorough knowledge of groundwater recharge is therefore necessary to determine the limit for safe groundwater extraction (Hugman *et al.*, 2012), and understand subsurface contamination and ecological impact.

Recharge studies are essential in semi-arid and arid landscapes, where groundwater is the primary water source and prone to depletion (De Vries and Simmers, 2002). Many (semi-)arid areas are facing a water crisis, and this is likely to be exacerbated by population growth and

climate change. The low annual precipitation and high evapotranspiration rates in (semi-)arid environments results in low recharge values that are difficult to determine, and vary considerably in time and space (Scanlon *et al.*, 2002).

2.3.1. Mechanisms of recharge

Lerner et al. (1990) characterised recharge into three principal mechanisms, namely direct/diffuse recharge, indirect recharge, and localised/focused recharge. The first mechanism is the direct diffusion of precipitation, where water percolates vertically through the vadose zone into the groundwater, and will only occur where the additional water is greater than evapotranspiration and the soil-water deficit in the unsaturated zone. Indirect recharge is associated with river beds and defined channels, where water percolation contributes to the recharge of the local water table (Beekman and Xu, 2003). Localised or focussed recharge is a form of indirect recharge, where large water bodies with an absence of channels, such as lakes, act as the hosts for localised recharge, and concentrated infiltration and percolation transfers water through the vadose zone (Robins, 1998).

While such simplified definitions enable us to contextualise recharge processes, they focus on vertical percolation and largely ignore lateral subsurface recharge (Lerner *et al.*, 1990). Sharma and Hughes (1985) showed that even with direct recharge, up to 50% of the recharged water can bypass the soil zone by moving along preferred pathways. Furthermore, in many locations a combination of these mechanisms can occur, in which case the type of percolation can play a significant role. De Vries and Simmers (2002) suggest the primary processes include diffuse percolation (controlled by hydraulic flux in the unsaturated zone and a piston-like flow in the saturated zone), macro-pore flow (along fissures, cracks and root pathways), and preferential flow (caused by different physical characteristics in the soil, such as a sand-clay interface).

2.3.1.1. Humid environments

High water tables are common in humid environments, and the aquifer's ability to store and channel water controls the rate of recharge. Direct infiltration from precipitation is the most common mechanism of recharge, with recharge occurring along topographic highs and discharging at topographic lows, where baseflow and gaining streams are common.

2.3.1.2. Semi-arid and arid environments

The term aridity covers such a large array of studies that it is a somewhat vague concept. However, a few defining characteristics can be used for semi-arid and arid areas: small mean annual precipitation, high daily and seasonal variations in temperature, low humidity in coastal

areas and highly sporadic rainfall over time and area, to name a few (Lerner *et al.*, 1990). Rainfall is therefore a defining characteristic, and the selection criteria is usually dictated by the mean annual precipitation (MAP) in mm. Perhaps the most widely accepted classification was suggested by Lloyd (1986), where hyperarid areas receive 0 - 50 mm, arid 50 - 200 mm, and semi-arid 200 - 500 mm MAP. Allison (1988), on the other hand, defined the MAP of semi-arid environments to be less than 700 mm. For the purpose of this study, the work of Lloyd (1986) will be used to define aridity.

The hydrological processes that control recharge in (semi-)arid areas are identical to those in other climates. However, for increasing aridity, it is important to note that the recharge is likely to be lower and show more temporal and spatial variation (Wood and Stanford, 1995). The pooling of water along topographic depressions and ephemeral streams is characteristic of arid settings, resulting in indirect or localised recharge to unconfined aquifers (Scanlon *et al.*, 2002). Gee and Hillel (1988) identified common flow pathways caused by shrinkage cracks and roots (several centimetres) and topographic or lithologic variations (several metres) as important for localised recharge. A third important flow path, not present in all (semi-)arid settings, is controlled by playa basins and karst sinks, and can be more than several hundred metres in diameter (Gee and Hillel, 1988). Direct recharge can occur, but rapid percolation along preferred pathways is necessary to overcome the effects of evaporation and transpiration. Furthermore, high rainfall events are required for the rewetting of the dry, unsaturated zone, a necessity for effective infiltration and drainage (Van Wyk *et al.*, 2012).

Unconfined aquifers are commonly found in (semi-)arid landscapes and have characteristically deep water tables and losing streams (Scanlon *et al.*, 2002). They are often the most accessible water sources in (semi-)arid regions, making them prone to over-exploitation and contamination (De Vries and Simmers, 2002). The upwards leakage of water from confined aquifers, as well as lateral groundwater movement from areas of higher rainfall, may contribute significant recharge to unconfined aquifers (Fontes and Edmunds, 1989).

Vegetation and soil characteristics also affect the unsaturated zone of shallow, unconfined aquifers. Vegetation has the evolutionary trait of being able to adapt (both in variety and density) to long-term rainfall values, and will extract water depending on the available soil moisture. For this reason, a sparsely vegetated landscape will have a greater recharge per unit rainfall than a denser vegetation, assuming all the other factors are constant (Bredenkamp *et al.*, 1995). However, desert flora have effective transpiration methods, and deep-rooting acacia trees found in the Kalahari may extract water from depths greater than 50 m (De Vries and Simmers, 2002). Where indigenous, shrub-like vegetation has been cleared for shallow-rooted crops and grassland, recharge may increase (Allison, 1988). Soil texture and

permeability are also important parameters for recharge, where coarse-grained soils and sand have higher recharge rates than fine-grained soils and clays (Scanlon *et al.*, 2002). A reduction in the thickness of the soil crust (containing in-washed fine particles) and the unsaturated zone (a host for evapotranspiration processes) will result in an increase in recharge (Balek, 1988).

(Semi-)arid areas occasionally host high-quality groundwater resources, and these are likely to be derived from past climates with higher rainfall and recharge values (Herczeg and Leaney, 2011). They are commonly referred to as *historical groundwaters.* One of the oldest ground waters, with a residence time of 350,000 years, was found in the Great Artesian Basin of Australia (Airey *et al.*, 1979).

2.3.2. Groundwater recharge estimation techniques

A variety of methods are available for estimating the quality and quantity of groundwater recharge and have been outlined by Allison (1988), Beekman and Xu (2003), Bredenkamp et al. (1995), De Vries and Simmers (2002), Gee and Hillel (1988), Lerner et al. (1990) and Scanlon et al. (2002) among others. These techniques are applicable to certain of the three hydraulic zones, namely surface water, the unsaturated zone, and the saturated zone. No single recharge estimation technique can be identified as applicable across a range of groundwater environments, and all the suggested methods give somewhat variable results (Simmers, 1988). The technique must be selected based on the temporal and spatial scales of the study, as well as the recharge flux and estimated groundwater age (Beekman and Xu, 2003). (Semi-)arid environments present a particularly complicated setting for recharge estimations, with the recharge flux becoming smaller and more variable with increasing aridity. Fewer estimation methods can therefore be successfully used in (semi-)arid settings, and the effects of urbanisation and changing land practices on recharge are not always fully understood (De Vries and Simmers, 2002).

Although indirect recharge mechanisms are important in (semi-)arid settings (Scanlon *et al.*, 2002), the methods for estimating direct recharge mechanisms are more reliable and still form the basis of many techniques (Lerner *et al.*, 1990). Methods for estimating indirect recharge commonly make use of ‘at-point’ hydraulic properties from isotope and chemical tracers in the unsaturated zone, or water balance approaches (where the surface runoff is an important component) (De Vries and Simmers, 2002). These methods therefore estimate the potential recharge or drainage (Scanlon *et al.*, 2002). The term ‘potential recharge’ was first proposed by Rushton (1988) to distinguish between the actual recharge, which reaches the water table, and the potential recharge, estimated from surface water and unsaturated zones and may not actually reach the water table. Evaporation and transpiration, as well as the inconsistent

spread of soil and vegetation type, can affect the recharge in these localised, near-surface environments (Koeniger *et al.*, 2016). The application of these 'at-point' assessments may prove troublesome on a regional scale, where small spatial variability is negligent, but do provide invaluable information about local water quality and waste-disposal sites (De Vries and Simmers, 2002).

Recharge techniques addressing the saturated zone are more applicable for assessing direct recharge mechanisms over larger areas, and they represent the actual recharge that contributes to the groundwater. However, a time delay exists between when the meteoric water enters the saturated zone, and when this water becomes available as a consumable groundwater resource (Balek, 1988). This could result in further chemical and isotopic alteration, and uncertainties regarding the origin of the recharge.

Common recharge estimations are differentiated between physical techniques, tracer techniques and groundwater modelling. Multiple recharge estimation techniques should be used to reduce the uncertainties of each approach.

2.3.2.1. Physical techniques

Physical methods rely on direct measurements and produce quantitative results. In (semi-)arid environments, low hydrological fluxes may result in minor changes in hydrological parameters, which may prove difficult to detect (Allison, 1988). Due to the high variability of (semi-)arid rainfall, the measurements should be captured over multiple years to establish mean values.

(a) Water Table Fluctuation (WTF)

The water-table fluctuation (WTF) method is based on a simple concept; a rise in the water table during the rainy season is a direct result of recharged water reaching the unconfined aquifer. The recharge is calculated as (Scanlon *et al.*, 2002):

$$R = S_y \frac{\Delta h}{\Delta t}$$

Where S_y is the specific yield of the aquifer, h is the height of the water table, and t is time. This method is ideally suited for short time periods and unconfined aquifers, where shallow water tables display sharply increasing and decreasing water levels (Scanlon *et al.*, 2002). Difficulties arise in determining the specific yield and the effects of pumping and atmospheric pressure on water level responses, and it is often used in combination with other estimation techniques (Lerner *et al.*, 1990).

(b) Lysimeter

Lysimeters are physical measuring devices that measure evapotranspiration. They are used for recharge estimations in the unsaturated zone and provide point measurements. They are the most direct form of recharge estimation, and have been used extensively to monitor the evapotranspiration and hydrochemistry of agricultural soils (Bredenkamp *et al.*, 1995). However, only a few studies have yielded successful recharge estimations. The rate of water drainage out the bottom of the lysimeter is measured, and is assumed to be proportional to the recharge or moisture flux (Beekman and Xu, 2003). Lysimeters are typically up to 10 metres in all three dimensions to minimise the effects of local soil, vegetation and climate differences (Lerner *et al.*, 1990). They are expensive to construct and maintain, and experiments are often abandoned before a wide range of data can be collected.

2.3.2.2. Natural tracer techniques

Multiple review papers focus specifically on the use of chemical and isotopic tracer techniques for assessing groundwater recharge (Fontes and Edmunds, 1989; Geyh, 2001; Herczeg and Leaney, 2011; Koeniger *et al.*, 2016). Natural tracer techniques have an added advantage over physical techniques in semi-arid environments as the accuracy of recharge estimates do not decrease with increasing aridity and decreasing moisture flux to groundwater (De Vries and Simmers, 2002). They provide long term estimates, but little detailed information on a short time scale (Scanlon *et al.*, 2002).

(a) Chloride Mass Balance

The use of the chloride ion as a tracer was first applied in the saturated zone by Eriksson and Khunakasem (1969) to estimate recharge rates to a coastal plain aquifer in Israel. This method assumes that chloride is conservative, and therefore the input of atmospheric chloride is equivalent to chloride flux in the subsurface. Since 1969, the use of chloride tracers in the saturated zone are now universally referred to as the *Chloride Mass Balance* technique and has been used in numerous recharge studies. Allison and Hughes (1978) have also successfully showed the use of chloride in the unsaturated zone as a technique for estimating recharge.

Wood and Stanford (1995) assessed the validity of the study of Eriksson and Khunakasem (1969). They argued that the CMB results lacked validation from physical methods, but demonstrated that under certain conditions and assumptions, this method can be used in (semi-)arid areas to calculate regional recharge rates comparable to physical methods. Wood (1999) suggests that the following four statements must hold true for the CMB technique to be

successfully used: (1) all chloride in the groundwater must originate from precipitation directly infiltrating the aquifer; (2) chloride in the aquifer is conservative; (3) the chloride-mass flux has been consistent over time; (4) chloride is not recycled or concentrated in the aquifer. In the case of recharge estimations by Eriksson and Khunakasem (1969), it is now known that sea-water intrusion effected the validity of these results.

A limiting factor in some areas of South Africa is the absence of long term rainfall values. However, Sami and Hughes (1996) successfully used the technique to calculate recharge in a Karoo aquifer, with results comparable to physical techniques. For CMB, the general equation used is:

$$\boldsymbol{R = \frac{P \times Cl_p}{Cl_{gw}}}$$

Where R is recharge (mm/a), P is annual precipitation (mm), Cl_p is chloride concentration in rainwater, and Cl_{gw} is chloride concentration in groundwater.

Care must be taken when applying this technique as it is not suitable for higher recharge rates, and many discrepancies are caused by preferential flow (Wood, 1999). Pollution during rainfall collection and sampling is an area of concern, as well as the effects of dry aerosol deposition, particularly in coastal areas and during the dry seasons when vegetation cover is limited (Van Tonder and Bean, 2003). Although not as accurate as other methods, differences in recharge estimation are within a factor of five, and the relative simplicity and cost-effectiveness of this method make it highly recommended (Beekman and Xu, 2003). The CMB technique provides point estimates for spatial scales that range from ~200 m to several kilometres, and time scales of decades to thousands of years (Scanlon *et al.*, 2002). It is mainly used for recharge on a local-scale recharge, and seldom applied to regional-scale recharge (Wood, 1999).

(b) Stable O and H isotopes

Verhagen (2003) eloquently describes the use of stable isotope data in the saturated zone as a "snapshot" of recharge studies, as it provides a broad visual understanding of the hydrological cycle, and can form a helpful contribution to other estimation techniques. While stable isotopes can help delineate the water's origin and evaporative history, they cannot be used to quantitatively estimate recharge (Bredenkamp *et al.*, 1995). The natural process of fractionation between heavier and lighter isotopes supports their applicability to identify groundwater infiltrating at high altitude regions or during a colder climate, as well as water where evaporation has occurred after recharge (Bredenkamp *et al.*, 1995). The large

fluctuations in δ-values of precipitation are largely homogenised by the time this rainfall reaches the water table (Allison *et al.*, 1983), and isotopic ratios remain conservative at ambient temperatures (Gat, 1996). (Semi-)arid areas typically have groundwater with a more negative stable isotopic ratio in comparison to surface water, supporting recharge that is derived from prolonged, intense rainfall events or during a previous climatic period (Bredenkamp *et al.*, 1995). In both humid and semi-arid environments, precipitation and groundwater both obey the LMWL (Dansgaard, 1964).

Stable isotopes have also been used in the unsaturated zone. Allison et al. (1983) suggested that a relationship existed between the deuterium deficit of the soil moisture (in comparison to the LMWL), and the recharge in the unsaturated zone:

$$Deuterium\ deficit \propto \frac{1}{\sqrt{Recharge}}$$

While Allison et al. (1983) could validate this relationship in a wide variety of climatic regimes, with moisture fluxes less than 10 mm/year, this relationship did not prove applicable in other studies. This could be due to variations in vegetation and seasonal changes in the stable isotope composition of rainfall (Herczeg and Leaney, 2011).

(c) Event markers

Nuclear weapon testing during the late 1950s and early 1960s released large amounts of ^{36}Cl and ^{3}H into the atmosphere, which are now referred to as historical tracers or event markers. These isotopes can be used as tracers of soil water movement, and can be used to calculate recharge or water flux in the unsaturated zone. Where Δz is the depth of the ^{36}Cl or ^{3}H peak in the soil, θ is the average water content above the peak of the tracer, and Δt is the time between the tracer fallout and sampling, recharge rates can be calculated as (Scanlon *et al.*, 2002):

$$R = \frac{\Delta z}{\Delta t}\,\theta$$

This calculation is applicable for recharge rates between 10 and 50 mm/a (Scanlon *et al.*, 2002). Tritium and chlorine-36 also prove useful for outlining preferential flow paths in the unsaturated zone. This is noticeable where soil profiles show deeper tritium concentrations in comparison to chlorine-36, as tritium has a greater affinity for the liquid phase (Scanlon *et al.*, 2006).

Applied in the saturated zone, ^{3}H is only able to differentiate between recharge that occurred during the peak of bomb fallout, and that which occurred before or after (Cook and Solomon, 1997). It is therefore a suitable tracer for shallow groundwater that has recharged in the past 50 years. However, with a short half-life of 12.28 years, tritium concentrations have drastically reduced due to radioactive decay. This is further exacerbated in the southern hemisphere, where tritium concentrations increased by one order magnitude between 1963 and 1965, comparatively less than an increase of three orders of magnitude in the northern hemisphere (Allison and Hughes, 1977). As it becomes increasingly difficult to differentiate between natural and bomb-pulse tritium in precipitation, other methods have become necessary to determine groundwater ages

(d) Groundwater age dating

Tracers such as CFCs, ^{3}H/^{3}He, ^{14}C and ^{16}Cl can be used to calculate groundwater age. Using the specific radioactive decay of isotopes, groundwater age can be inferred from the time between when the isotope was isolated from the atmosphere (recharge) and when sampling occurred (Bredenkamp *et al.*, 1995). CFCs and ^{3}H/^{3}He are used to estimate recharge rates in shallow, unconfined aquifers, where groundwater flow is predominantly vertical. Scanlon *et al.* (2002) suggested that these isotopes may only prove useful where water tables are less than 10 m deep. The noble gas helium-3 is the daughter product of tritium, and will increase in comparison to tritium as the groundwater age increases. The groundwater age can be calculated using ^{3}H and tritiogenic ^{3}He, where $t_{1/2}$ is the half-life of tritium (Scanlon *et al.*, 2002):

$$t = -\frac{1}{\lambda}\ln\left(1 + \frac{^{3}He}{^{3}H}\right) \qquad \lambda = \frac{ln2}{t_{1/2}}$$

Due to the diffusive properties of tritium in the unsaturated zone, the ^{3}H/^{3}He technique cannot produce reliable recharge rates where this value is less than 30 mm/a (Cook and Solomon, 1997). CFCs have lower diffusion coefficients and may prove more effective at lower recharge rates. Additional helium-4 may also enter the groundwater from the aquifer material or an inflow from the mantle (De Vries and Simmers, 2002).

Confined, deeper aquifers have horizontal flow velocities, and these can be estimated using radioactive decay of ^{14}C and ^{36}Cl, making them particularly useful in (semi-)arid areas where groundwater typically has longer residence times. Carbon-14 and Chlorine-36 have a half-life of 5 730 years and 300 000 years respectively, and chlorine-36 is used to date groundwater with ages in excess of 50 000 years (Mook, 2001).

2.3.2.3. Numerical modelling

Recharge and hydraulic conductivity often exhibit good correlations, and numerical models make use of available hydraulic information to simulate recharge estimations (Scanlon *et al.*, 2002). These simulated predictions are a useful tool in collaboration with tracer and physical techniques. The water budget method, founded on the water balance, forms the basis of this method. The accuracy is therefore largely dependent on the quantity of data, as well as the quality of the spread of boreholes, frequency of captured data and correct predictions of aquifer boundary conditions (Van Tonder and Bean, 2003). Numerical models have the added benefit of not only predicting the rate of recharge, but also the distribution of the recharge, assuming that the parameters for the model are well established (Sanford, 2002). In most hydraulic settings, where groundwater flows paths are controlled by the climate, land-surface features and geological units (Winter, 2001), models typically use a framework that incorporates all three parameters. Although a powerful tool, their use is cautioned in (semi-)arid settings where hydraulic-conductivity data is limited, and low recharge results in limited groundwater fluctuations.

(a) Cumulative Rainfall Departure (CRD)

The CRD is based on the principle that over time, an aquifer will reach equilibrium. At such a state, the loss of groundwater will be equal to recharge. Thus, any groundwater fluctuation must be a result of rainfall departing from the mean annual precipitation, where a groundwater rise will result in a positive CRD value and vice versa (Xu and Van Tonder, 2001). Bredenkamp *et al.* (1995) showed the success of this method in South Africa. Based on the water balance equation, a simple equation shows the calculation or recharge (Xu and Van Tonder, 2001):

$$R_t = rCRD_i = S_y \left[\Delta h_i + \frac{Q_{pi} + Q_{outi}}{AS_y}\right]$$

Where r is the fraction of a CRD during month i that contributes to recharge, S_y is the specific yield of the aquifer, Δh_i is the water level change during the month (L), Q_p is the groundwater abstraction (L^3/T), Q_{out} is natural outflow, A is the recharge area (L^2), and P_i is rainfall (L/T). An optimisation process during simulation can estimate r/S_y which will minimise the differences between actual and calculated fluctuations over time (Beekman and Xu, 2003). The added benefits of such an equation is the incorporation of the effects of outflow and pumping, which the Water Table Fluctuation method cannot accomodate. This method is particularly useful for fractured, unconfined aquifers with a small storativity, as the effects of rainfall recharge on water tables are more pronounced (Beekman and Xu, 2003).

3. ENVIRONMENTAL SETTING

The Verlorenvlei is a RAMSAR listed wetland, situated 200 km north of Cape Town, in the Sandveld region along the west coast of South Africa. The vlei extends between the villages of Elands Bay and Redelinghuys, making it one of South Africa's largest estuarine lakes. The lake is an important feeding ground for a variety of endangered bird species and has a high biodiversity profile due to the interaction between the fresh and marine water systems. The lake itself is relatively shallow but extends over a significant area (15 by 1.5 km) and as a result, evaporative losses from the lake are significant. However, the vlei has to date never run dry (although lake water levels are variable), and this is because the lake is fed by both surface water and groundwater from the Verlorenvlei catchment (Conrad *et al.*, 1999). The Verlorenvlei catchment covers an area approximately 1890 km^2, and is bounded by the Swartberg and Olifantsrivier mountains in the east and north-east, and the Piketberg Mountain range in the west and south-west (Noble and Hemens, 1978). Climate change coupled with a large amount of agriculture has had an impact on the quantity and quality of water in the major rivers that feed the lake.

3.1. Geology

The Malmesbury Group (~750 Ma) is the host of the oldest rocks found in the area, and forms the Precambrian (Neoproterozoic) basement upon which all younger geological deposition occurred. Hartnady *et al.* (1974) divided this group into three 'terranes', namely the northeastern Boland, central Swartland and southwestern Tygerberg terranes, suggesting that tectonic processes have controlled the formation of the three terranes. The existence of these terranes has however been questioned by Kisters *et al.* (2002). These tectonic processes form part of the Pan-African Orogeny (~600 Ma), where the Malmesbury Group forms part of the low-grade Saldania belt, and northwesterly striking faults zones divide the group into the terranes, all of which display a NW-SE trending structural grain (~600 Ma) (Gresse *et al.*, 2006). The northeastern Boland and central Swartland terranes are separated by the Piketberg-Wellington fault, which lies just to the south-east of the catchment boundary (Figure 2). It is believed to be tectonically linked to the Krom Antonies lineament, which represents a zone of crustal weakness in the Malmesbury Group (Rozendaal *et al.*, 1994). The Krom Antonies lineament marks the western boundary of the Riviera pluton, with a possible downthrow of ~450 m (Rozendaal *et al.*, 1994). The Redelinghuys fault, running through the centre of the catchment, is associated with the Piketberg-Wellington fault and a product of Pan-African tectonics (De Beer, 2003) (Figure 2). The Swartland Terrane is in turn separated from the southwestern Tygerberg Terrane by the Colenso (Piketberg-Wellington) fault.

While the Verlorenvlei catchment lies in the Boland Terrane, a small portion of the Moorreesburg Formation of the Swartland Terrane outcrops on the eastern edge of the catchment, and consists predominantly of greywacke and phyllite (Gresse *et al.*, 2006) (Figure 2). The sediments of the Malmesbury Group are likely to have been deposited on a passive continental margin; including ocean basin (turbidite sequences of the Tygerberg Terrane), ocean shelf (Swartland Terrane), and near-shore environments (Boland Terrane) (Rozendaal and Scheepers, 1995), although the Boland terrane may be the only one that is autochtonous in nature (Kisters *et al.*, 2015). The lowermost Piketberg Formation of the Boland Terrane is exposed between the towns of Piketberg and Redelinghuys, although outcrops are only poorly seen against hill slopes and along road cuts. It is a highly foliated and lineated argillaceous rock comprised of greywacke, sericitic schist, feldspathic limestone, conglomerate and quartzite (Rozendaal *et al.*, 1994). The Porterville Formation (Boland Terrane) covers a large area in the eastern catchment and consists mainly of greywacke, phyllite and shale (Gresse *et al.*, 2006).

The Tygerberg and Swartland Terranes in particular are host to a large number of granite intrusions of the Cape Suite (Rozendaal *et al.*, 1994). The Cape Granite Suite intruded the meta-volcano-sedimentary rocks of the Malmesbury Group syn- and post- tectonic (~510 Ma), with the northwest trending Colenso and Wellington faults controlling the spatial distributions of these S- and I- type granites (Kisters *et al.*, 2015). The Boland Terrane has only two exposed plutons, 150 km southeast of Piketberg, but drilling has revealed the presence of other plutons at depth. Of significance is the Riviera granite pluton in the Moutonshoek valley, that intruded a NW-trending fold structure in the Malmebsury group. Tungsten and molybdenite mineralisation are associated with the deposit, but no mining has occurred yet (GEOSS, 2012). Elevation of the pluton, followed by erosion and recent sedimentary deposition, has placed the pluton in a near-surface environment (Rozendaal *et al.*, 1994). The pluton is terminated on the western, eastern and northern boundaries by fault systems.

The Malmesbury Group and Cape Granite Suite are unconformably overlain by the Cambrian Klipheuwel Group and its Populiersbos Formation, which outcrops in the Redelinghuys area. It is characterised by red to purple shale, conglomerate and arkose (De Beer, 2003).

Quartzose sandstones of the Table Mountain Group (TMG) form the Piketberg and Cederberg mountain ranges that flank the eastern ridge of the Sandveld. These sedimentary rocks form part of the Cape Supergroup that was deposited in a passive margin basin following the end of the Pan-African Orogeny (~500 Ma), and shows a sedimentary succession that includes sandstone, shale and small amounts of conglomerate (Tankard *et al.*, 2009). The TMG forms the lower most unit of the Cape Supergroup (~450 Ma), and unconformably overlies the

Malmesbury basement rocks (Thamm and Johnson, 2006). The depositional environment of the TMG ranges from shallow marine to fluvial, with glacial deposits. The TMG is hard and resilient in nature, forming a stark contrast against the easily weathered rocks of the surrounding Malmesbury Group. The Sandveld region is dominated by the Pikenierskloof, Graafwater, Peninsula and Cedarberg Formations of the TMG. The oldest Piekenierskloof Formation consists of course-grained sandstone, conglomerate and minor amounts of shale. It has a thickness of 390m west of Eendekuil (Figure 2), comparative to a maximum thickness of 900 metres to the northwest of Citrusdal (Rust, 1967). This is overlain by the quartzose sandstone, shales, siltstones and occasionally conglomerates of the Graafwater Formation (Thamm and Johnson, 2006). The sandstone component varies between 50 and 100% of the total formation (De Beer, 2003). The Peninsula Formation is the main unit of the Cape Supergroup, with a maximum thickness of up to 2000 metres around Citrusdal (Thamm and Johnson, 2006). It consists mainly of quartz arenite, and contains small amounts of conglomerate and shale, and is characterised by bedding planes of one and four metres in thickness (De Beer, 2003). It caps the Piketberg Mountain range, and covers an extensive area in the north of the catchment, with an average thickness of 900 m at Piketberg (Rust, 1967). The glacially deposited Pakhuis formation is not present in the catchment, and uppermost Cedarberg Formation only thinly outcrops across the catchment, and is characterised by shale and siltstone that is typical of an offshore shelf. The uppermost unit of the Table Mountain Group, the Nardouw subgroup, only crops out in a small area in the central catchment. It is comprised of a thick layers of quartzose sandstone (Thamm and Johnson, 2006). Deformation and low-grade metamorphism caused by tectonism during the Cape Fold Belt event (~250 Ma) has caused an overprint that hinders the identification of original Malmesbury lithostratigraphy (Rozendaal and Scheepers, 1995).

The Sandveld Group of Cenozoic deposits is the youngest geological unit that covers the southwestern coast from False Bay to Elands Bay. A range of depositional environments (including shallow marine, Aeolian, estuarine and fluvial) have contributed to this rather thin deposit (Roberts *et al.*, 2006).

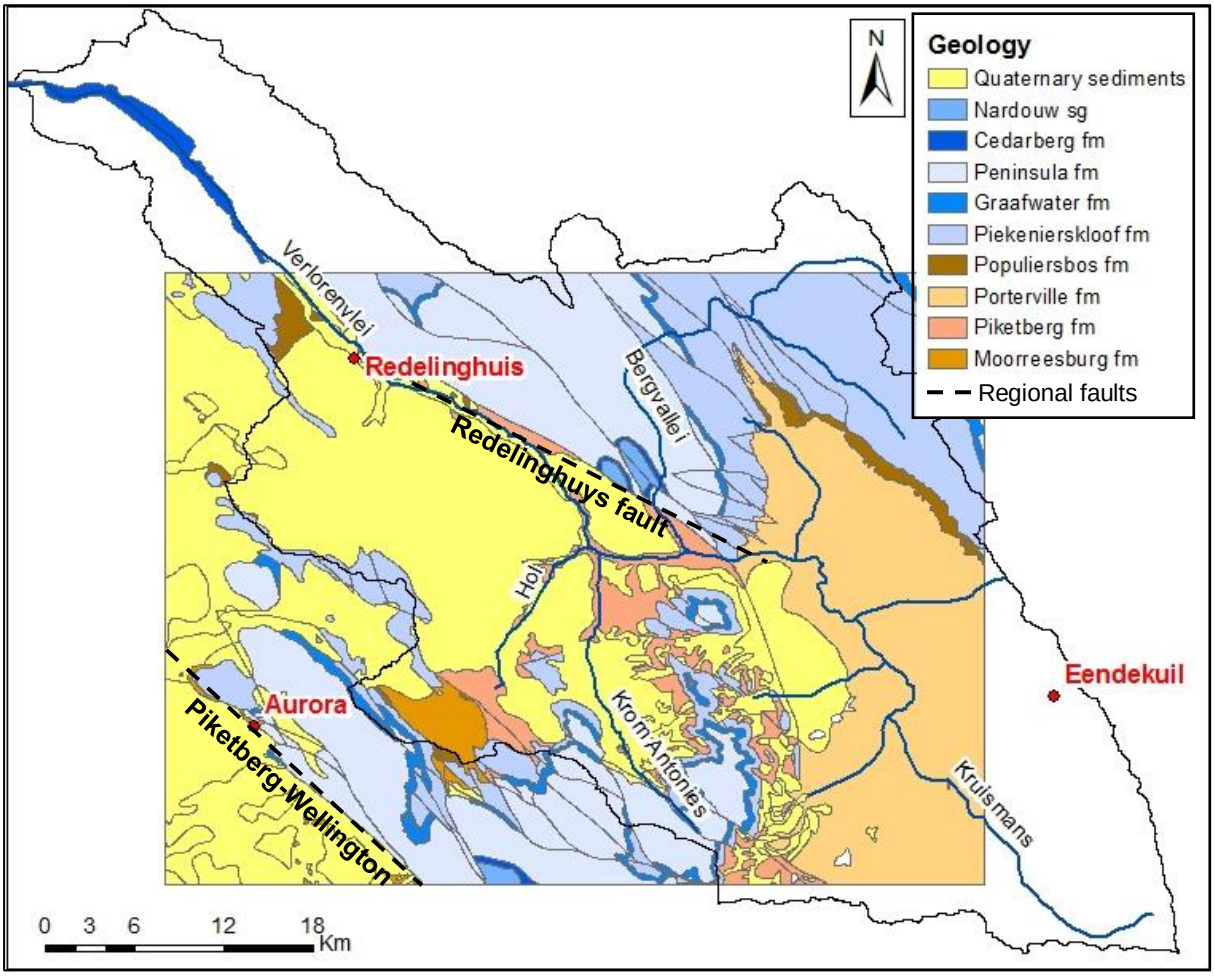

Figure 2: Geology of the Verlorenvlei catchment (courtesy of the Council for Geoscience), including the distribution of regional faults

3.2. Geomorphology

The low-lying areas to the west of the catchment are covered by littoral sands, likely to be of aeolian origin, providing relatively infertile soils with low water retaining capacity (Maclear, 1994). They have a low amount of weatherable minerals, as well as little clay or silt. The soil tends to be acidic, but becomes more alkali towards the coast due to the accumulation of lime (CSIR, 2009). The banks of the Verloren River and tributaries are areas of highly fertile soil where plant material has accumulated. The comparatively fertile Krom Antonies river valley has an upper alluvial sandy soil layer ~3-12m thick, and an underlying clay layer ~3-25m thick (SRK, 2009). The Piketberg Mountain range enclosing the Krom Antonies River in the east has the highest topographic elevation (1446m), and thus mark the eastern boundary for the catchment, which extends towards Elandsbaai.

3.3. Hydrology and Hydrogeology

The Verloren River contributes the bulk fresh water input to the Verlorenvlei estuarine system. It flows mainly during winter and early summer, with its flow being reduced to a trickle in the dry summer months (Sinclair *et al.*, 1984). It has four main tributaries which drain three of the four quaternary catchments (G30B, G30C and G30D) (Figure 3). At a length of 50 km, the Kruismans River is the longest tributary and drains the extensive, low-lying Kruismans basin between the Olifantsrivier Mountains and the Piketberg Mountain range. The Bergvallei River drains the Swartberge and flows into the Kruismans River. It is mostly dry, and the lack of surface water flow has resulted in parts of the river beds being ploughed for agriculture (CSIR, 2009). The Hol and Krom Antonies rivers drain the same quaternary catchment, with the Hol River only flowing sporadically after very good rains. The Krom Antonies River is the shortest tributary of the Verlorenvlei, but arguably the most significant in terms of freshwater input, as it drains the Mountonshoek Valley of the Piketberg Mountain range. The point where the Krom Antonies joins the Hol River has been termed the confluence.

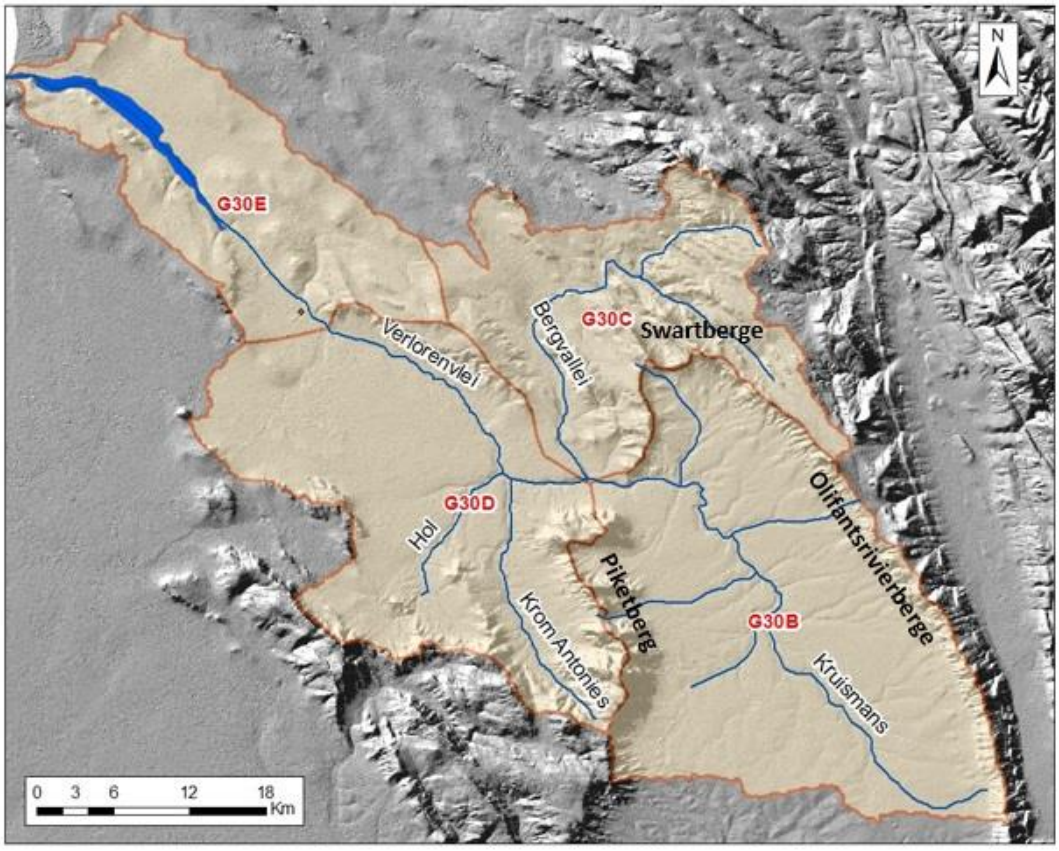

Figure 3: Quaternary catchment of the Verlorenvlei

The Verlorenvlei catchment has both unconsolidated primary and fractured-rock secondary aquifers. The unconfined primary aquifer is hosted by coarse grained, unconsolidated sands, with a flow direction that follows the topography and tributaries (GEOSS, 2006; Watson *et al*.,

2017a). It produces high yielding boreholes, and dominates the west of the Verlorenvlei catchment. Due to its shallow, unconfined nature, it is prone to contamination from anthropogenic activities, with salinity increasing towards the coast (Conrad *et al.*, 2004). The primary coastal aquifers may have also experienced marine transgression in the past (DWAF, 2004). An unconfined, primary aquifer is present in the Moutonshoek Valley of the Piketberg Mountain range, but decreases in thickness as the sediments in the valley give way to the sandstone formations of the Table Mountain Group.

The primary aquifer is underlain by a semi-confined to confined secondary aquifer hosted by the Malmesbury Group, with a partial clay aquitard (Conrad *et al.*, 2004). Faults, weathering zones and bedding planes are the primary features that control groundwater flow (Conrad *et al.*, 2004). The secondary aquifer is associated with high yielding artesian boreholes and good quality groundwater (particularly along the Krom Antonies River). The primary and secondary aquifer are likely to be hydraulically connected, and as the piezometric head is generally higher than the water table, Conrad *et al.* (2004) suggests that the secondary aquifer discharges into the primary aquifer. The primary aquifers to the west of the catchment are characterised by low recharge, due to low rainfall and thick sands (DWAF, 2004).

The TMG rocks of the Piketberg Mountains host an additional fractured rock aquifer system. While the primary aquifer is recharged directly from rainfall, the secondary aquifer does not show any response to rainfall (Watson *et al*., 2017b). It is therefore likely that the secondary aquifer is recharged directly by the TMG aquifer at the top of the Moutonshoek catchment as a result of a high hydraulic gradient, and groundwater flow following a SE-NW direction, primarily controlled by faults (Watson *et al.,* 2017b; Munch *et al*., 2013; GEOSS, 2006; Conrad *et al.,* 2004; Timmerman, 1986). This is supported by the high potential evaporation in the valley, ~1600 mm/a (Watson *et al*., 2017b), which limits vertical recharge from rainfall. The majority of the TMG groundwater occurs in the Peninsula Formation of the Piketberg Mountain range, and shows a dip of 13 degrees (Watson *et al.*, 2017c).

Stratigraphy					Hydrostratigraphy	
Age range (Ma)	**Supergroup**	**Group**	**Formation**	**Description**	**Unit**	**Terminology used in this thesis**
2 - 0		Sandveld	(Various)	Alluvium	Quaternary Aquifer	Primary Aquifer
~~Major unconformity~~~~						
417 - 443	Cape	Table Mountain	Cedarberg	Shale; siltstone	Table Mountain Group Aquifer	TMG Aquifer
			Peninsula	Quartz arenite		
			Graafwater	Sandstone; shale; siltstone		
			Piekenierskloof	Course-grained sandstone; conglomerate		
~~Major unconformity~~~~						
545 - 750		Malmesbury	Porterville	Greywacke; phyllite; shale	Malmesbury Group Aquifer	Secondary Aquifer
			Piketberg	Greywacke; schist; limestone; conglomerate; quartzite		
			Moorreesburg	Greywacke; phyllite		

Table 1: Stratigraphy and hydrostratigraphy of the Verlorenvlei catchment

While the Krom Antonies, Hol and Verloren Rivers drain a single Groundwater Resource Unit (GRU), as defined by GEOSS (2006), the Kruismans River drains the quaternary catchment G30B with a GRU that is fundamentally different. Unlike the mountainous area of Moutonshoek, the Kruismans River drains the flat lying plains of the Malmesbury Group, which is low yielding and results in limited groundwater abstraction (GEOSS, 2006). The Bergvallei River similarly crosses three GRUs (GEOSS, 2006). The most lower reaches of the Bergvallei River (in close proximity to its confluence with the Kruismans River) occur in the same groundwater setting as the Krom Antonies, Hol and Verloren Rivers. An increase in elevation along the Bergvallei marks the change to a new GRU, which is characterised by high-yielding primary aquifers and groundwater flow directions directed towards the coast (GEOSS, 2012), suggesting that this groundwater contributes little to the Verlorenvlei system.

3.4. Climate and vegetation

The Verlorenvlei is described as a Mediterranean climate, with 80% of the rainfall occurring in the winter months between April and September (CSIR, 2009). The highest rainfall occurs in the Piketberg mountains to the southeast of the catchment, which is the origin of the Krom Antonies River. An average annual precipitation of around 550 mm/year is recorded on the Piketberg mountain range (Lynch, 2004). Towards the east of the catchment this value decreases drastically, with Elands Bay (the mouth of the Verlorenvlei) receiving around 210 mm/year. These rainfall patterns are extremely variable, and a single, rare heavy shower can contribute up to one year worth of precipitation (CSIR, 2009). The winter rainfall period corresponds to lower average temperatures between 8 and 13 °C, with average summer temperatures of 17 to 23 °C (Schulze *et al.*, 2008). Evaporation increases towards the coast, with the upper reaches of the Mountonshoek valley experiencing a potential evaporation rate

of 950 mmm/year (Watson *et al.*, 2017b). At the confluence of the major tributaries, the mean annual precipitation is greatly exceeded by a potential evaporation rate of 1460 mm/year (Watson *et al.*, 2017b).

Most of the indigenous vegetation in the catchment is Strandveld Fynbos; a semi-succulent vegetation that is described as a transition between Coastal Fynbos and Succulent Karoo vegetation (CSIR, 2009). These both ecologically important biomes, and have been identified by the government of South Africa as being a top conservation site (Archer *et al.*, 2009).

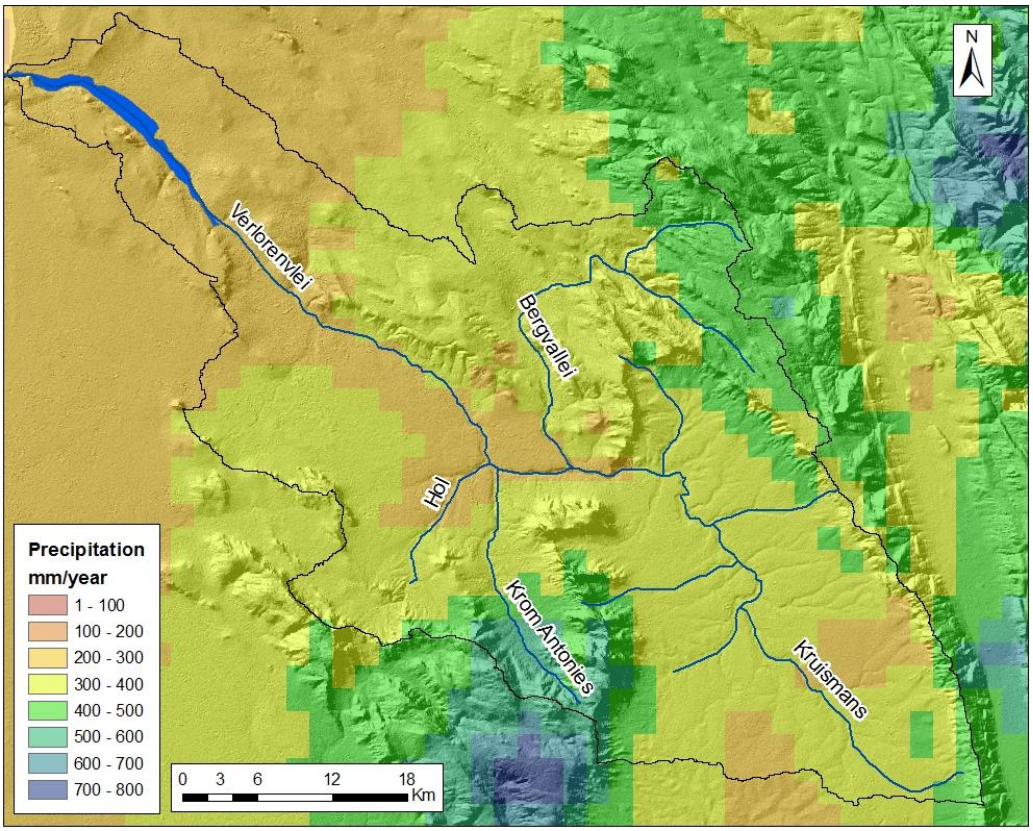

Figure 4: Mean annual precipitation in the Verlorenvlei (Lynch, 2004)

3.5. Land use and cover

Agriculture is the predominant water user in the catchment, and accounts for more than 90% of the total water demand (Archer *et al.*, 2009). Seed and table potatoes are the primary food crop grown, and potato crop circles, using centre pivot irrigation, are visible from high elevations (Figure 5). In 2002, 7500 hectares of land was cultivated for potato production (DWAF, 2003) and used roughly 20% of the annual recharged groundwater (Archer *et al.*, 2009). Sandveld potatoes are grown in the sandy soils typically found in the lower parts of the catchment. While such a setting results in high yields, the use of extensive fertiliser and water is required. Some fields are also left to stand bare between crop rotation (as groundcover plants may host potato pests), which results in soil erosion (CSIR, 2009). Rooibos tea

production covers a significant area of the land. This arid crop relies predominantly on rainfall and therefore contributes little to the water demands. Likewise, natural vegetation provides grazing lands for livestock. Citrus and viticulture production also occur, particularly in the upper reaches of the Moutonshoek (where high rainfall and good quality groundwater are prevalent), as well as in the Kruismans basin. These crops require a large amount of water.

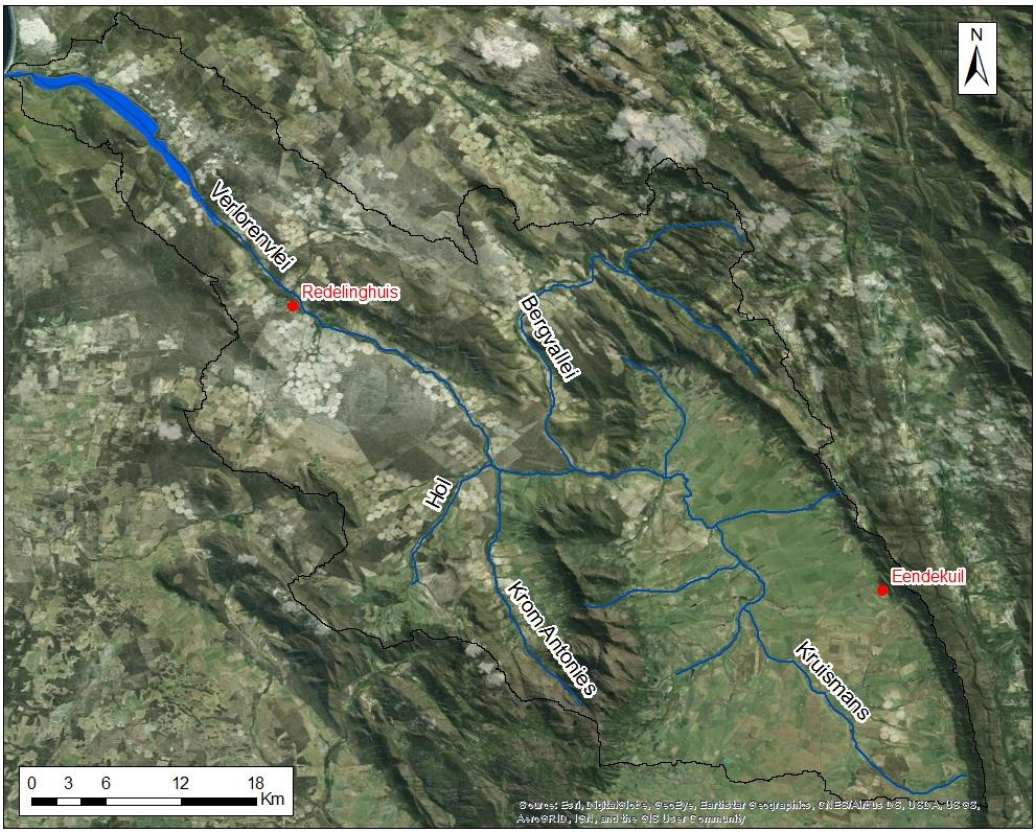

Figure 5: Satellite image of the Verlorenvlei catchment

3.6. Previous recharge estimates

Using the chloride mass balance technique, Weaver *et al.* (1999) calculated a recharge of 5 - 16% to the TMG aquifer in the area of Struisbaai, and Miller *et al.* (2017) a maximum recharge of 27% to the TMG aquifer in Paarl. Parsons (2002) estimated a recharge of 5% in areas of lower rainfall, and >20% in areas receiving rainfall of more than 600 m/a. Hay and Hartnady (2002) support this with recharge estimations between 7 and 44% in the Citrusdal area, and with a spatial average of ~23%. Weaver *et al.* (1999) furthermore shows that a recharge as high as 50% is likely to occur in the TMG mountains surrounding the Agter-Witzenberg valley near Ceres.

The west coast has significantly fewer recharge studies, and CMB results show that very little rain water recharges the primary aquifers of quaternary catchment G30E (DWAF, 2004). This is likely due to the fact that no recharge occurs in alluvial aquifers that receive rainfall of less

than 375mm/a, which is applicable to the lower areas of the catchment where rainfall is less than 300mm/a (DWAF, 2004). This is supported by Conrad *et al.* (2004) who estimates a recharge of ~2.8% in the valley of the Krom Antonies river and further along the Verloren River, and 13 – 20% in the Piketberg Mountains of Moutonshoek.

4. METHODOLOGY

4.1. Study area

Groundwater occurring along the Krom Antonies, Hol, Kruismans and upper reaches of the Verloren Rivers were selected for a detailed study, as these are the main tributaries contributing to the Verlorenvlei wetland. The Krom Antonies River forms the central component of this study area as it is likely to be the main contributor of fresh groundwater to the Verlorenvlei, with high recharge derived from the TMG aquifer of the Piketberg Mountain range. Additionally, there are many boreholes tapping into the secondary aquifer, as this area supports the highest agricultural activity in the catchment.

Natural tracer techniques have been selected for recharge estimation in the Verlorenvlei catchment, largely due to their cost effectiveness, accuracy in semi-arid environments and ability to provide long term estimates. The chloride mass balance (CMB) technique is used as the primary method for calculating recharge in this study. This method was selected based on the availability of anion analytical facilities in South Africa, the size of the study, and the semi-arid nature of much of the catchment (< 500 mm/a). Furthermore, the collection of rainfall samples will provide a platform for a citizen science component where local residents will contribute to the project. These chemical-based recharge estimates will offer an independent comparison to the recharge estimates obtained by the physical and modelling techniques of Watson *et al.* (2017) and Conrad *et al.* (2004). Stable isotopes of ^{18}O and ^{2}H were utilised as a supplementary method to the CMB technique. Although stable isotopes cannot produce direct recharge estimates, a comparison between stable isotope compositions of rain and ground water proved useful in delineating the water's origin and evaporative history, as well as identifying spatial and temporal aspects of recharge and possible recharge mechanisms.

4.2. Field sampling

In June 2015, a reconnaissance site visit was undertaken to locate deep boreholes tapping into the secondary aquifer, as well as to identify local residents who would assist with the collection of rain water. From this visit, eight daily rainfall collection points were identified (Figure 6). These were selected in such a way as to cover a large area of the catchment. In addition to the eight daily rainfall collection points, a cumulative rainfall collector (M-R) was erected on the Piketberg mountain range. The cumulative collector M-R was erected in March 2016, and the sample collected in September 2016.

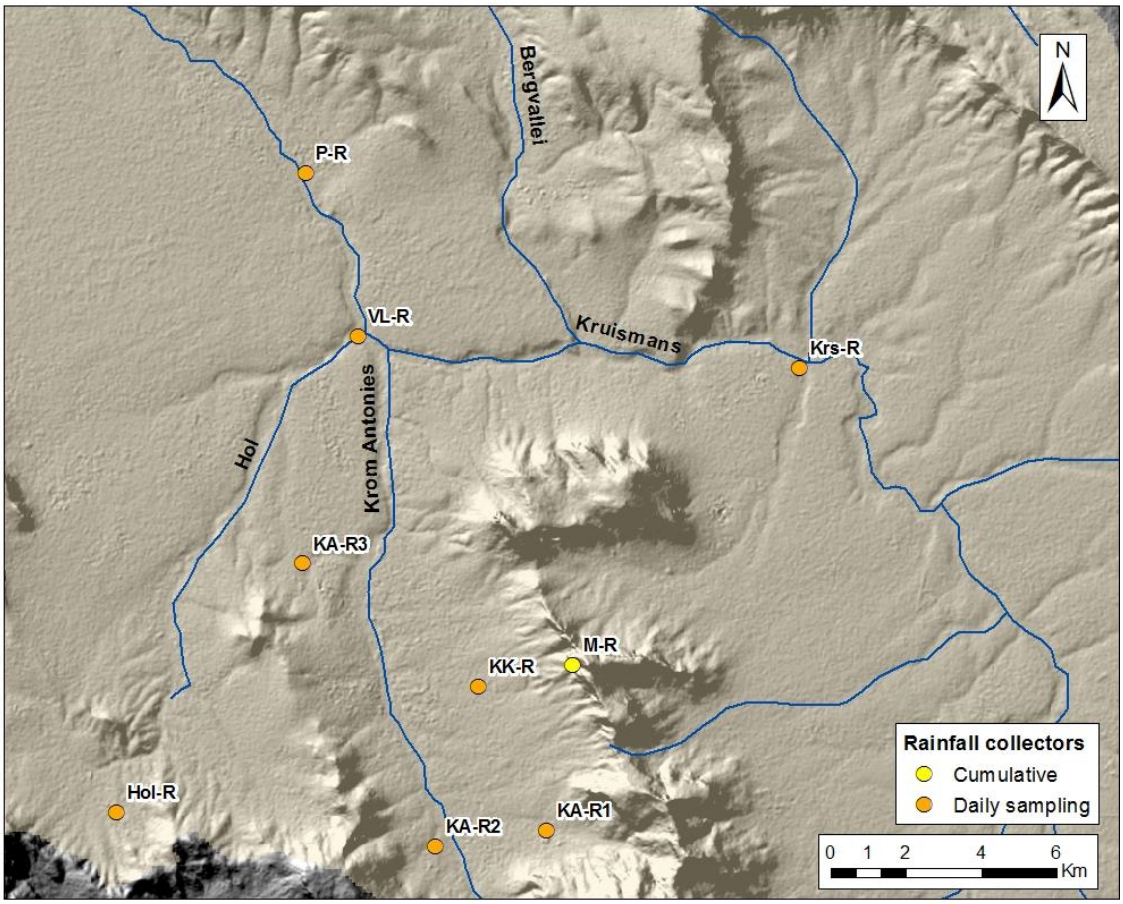

Figure 6: Eight daily rainfall collection points (orange) and one cumulative rainfall collector (yellow) in the Verlorenvlei catchment

Deep boreholes were selected for sampling during subsequent field trips, based on their proximity to the rainfall collectors, distribution across the catchment, and willingness of the farmers to assist with regular sampling. Due to time limitations and unforeseeable events, such as broken pumps, not all boreholes were able to be sampled during every field trip. In total, 41 boreholes were sampled across the catchment during the six sampling trips (Figure 7).

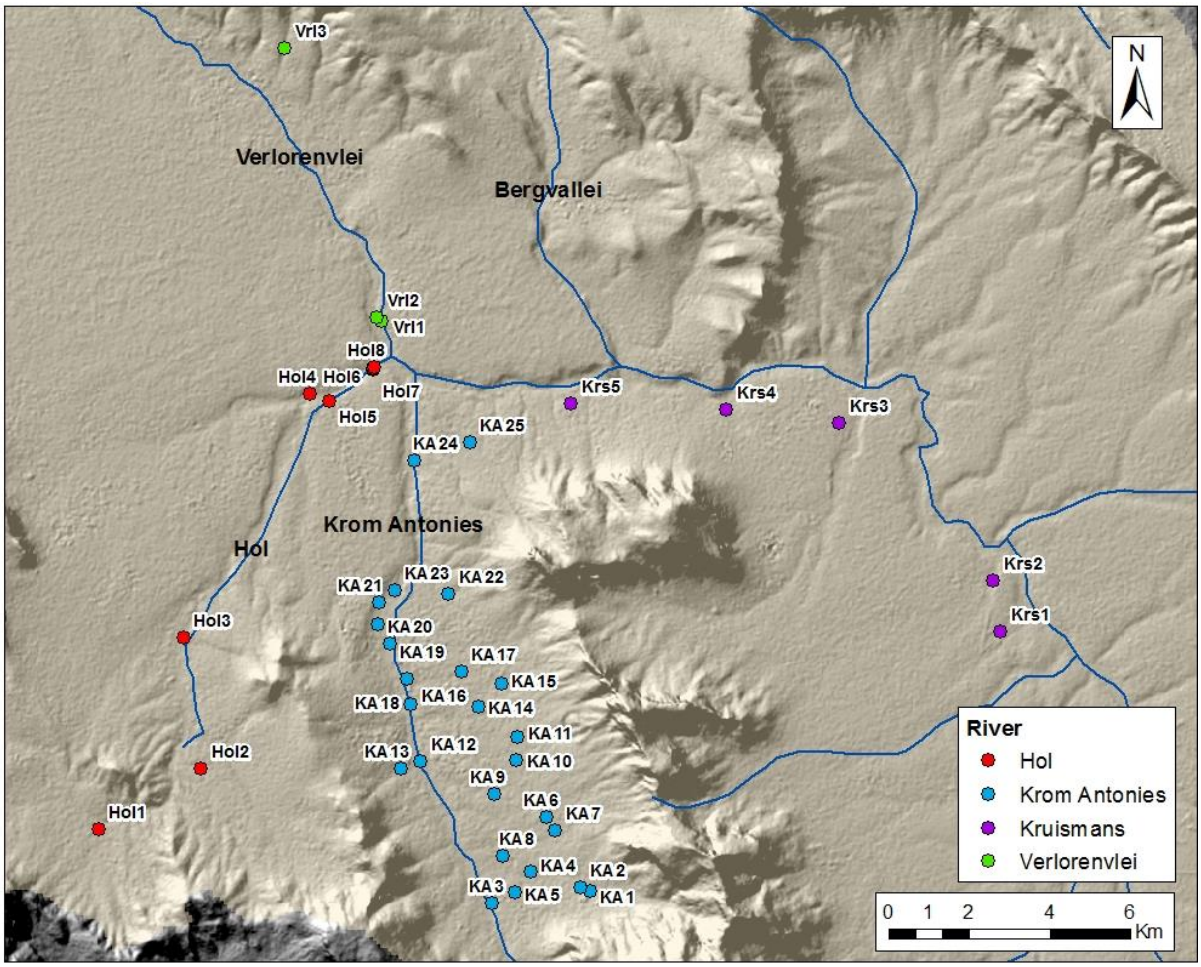

Figure 7: 41 boreholes sampled across the Verlorenvlei catchment

4.2.1. Groundwater collection

Six groundwater sampling trips took place during 2015 (June, September, November) and 2016 (March, June, November), with 102 samples collected from 41 boreholes across the catchment (Table 2). Groundwater was only sampled from deep boreholes tapping into the secondary aquifer, with 64 samples collected in 2015, and 38 in 2016. An electric pump was fitted to 38 of the boreholes, allowing them to be purged before sampling (Figure 8b). Artesian aquifers KA12, KA17 and KA19 flow throughout the year and were sampled directly (Figure 8b). The borehole and sampling locations were situated at a maximum distance of 300 metres from one another, and flowed through steel or PVC piping. Where possible, a sample was taken directly from the source. The sampling points for a single borehole occasionally differed between sampling seasons as the groundwater had been redirected for irrigation purposes.

The boreholes were purged until the electrical conductivity (EC) had stabilised, indicating a homogenous, “fresh” groundwater source. EC, pH and water temperature were measured with portable EXTECH EC500 pH/conductivity probes. All probes were calibrated in the morning and afternoon, to accommodate for temperature fluctuations. They were calibrated against pH

standards of 4, 7 and 10, and EC standards of 1413 µS/cm and 12200 µS/cm. Upon return from a sampling trip, EC was also measured in the laboratory of the department of Soil Science (Stellenbosch University) using a Eutech con700 EC meter, to validate the values obtained by field probes. Major cations, anions and selected trace elements were collected in clean 50 ml Polypropylene (PP) tubes. The cation samples were acidified with nitric acid to prevent the precipitation of metals. Stable isotopes of oxygen and hydrogen were collected in a clean 15 ml PP tube. All samples were filtered through a 0.45 µm cellulose acetate filter, and the tubes were thoroughly rinsed with filtered water. Samples were double bagged and placed in a cooler box with ice during the day, and moved to a refrigerator every evening. Upon return from the field, these samples were stored in laboratory fridges.

Table 2: Deep groundwater sampling points in the catchment; 41 boreholes and 102 samples in total.

River	Borehole	Jun '15	Sep '15	Nov '15	Mar '16	Jun '16	Nov '16
Krom Antonies	KA1	x		x	x	x	
	KA2	x	x	x	x	x	
	KA3	x	x		x	x	
	KA4	x					
	KA5	x					
	KA6				x	x	x
	KA7				x	x	
	KA8				x	x	
	KA9	x	x	x	x	x	x
	KA10	x					
	KA11	x	x	x	x	x	x
	KA12	x					
	KA13	x		x			
	KA14	x					
	KA15	x		x			
	KA16	x					
	KA17	x					
	KA18	x					
	KA19	x					
	KA20					x	
	KA21	x	x	x	x		
	KA22	x					
	KA23	x		x			
	KA24	x		x			x
	KA25	x		x			
Kruismans	Krs1	x					
	Krs2	x					
	Krs3	x	x	x	x	x	
	Krs4	x			x		x
	Krs5	x					
Hol	Hol1	x		x			
	Hol2	x	x	x	x	x	x
	Hol3	x		x			
	Hol4	x		x			x
	Hol5	x		x			
	Hol6	x	x	x	x	x	x
	Hol7	x			x	x	
	Hol8	x					
Verloren	Vrl1	x	x	x	x	x	x
	Vrl2	x					
	Vrl3	x					

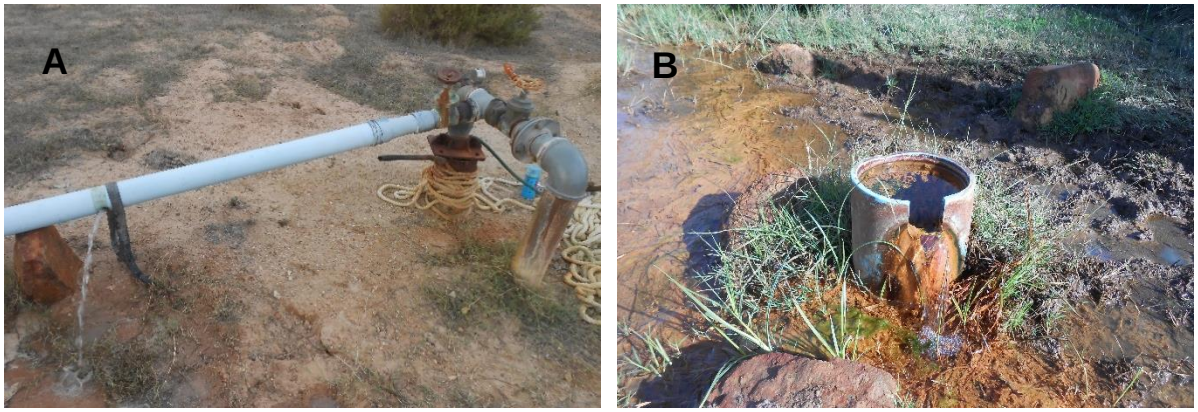

Figure 8: Sampling of an electrical pump operated borehole KA11 (A) and an artesian borehole KA17 (B) along the Krom Antonies River

4.2.2. Rain water collection

As part of the WRC's citizen science initiative, local residents were encouraged to become actively involved in the sampling of daily rainfall events. The eight residents who agreed to contribute to the project were instructed in the correct protocol for rainfall sampling. It was firstly ensured that all rainfall gauges were located at least five metres from any tree or construction, and were not near any large dirt roads, to minimise dust pollution. The residents were instructed to collect a rainfall sample at 8am after every rainfall event, to minimise the effects of evaporation. The collection procedure involved transferring the rain water from the gauge to a clean 50 ml PP tube, labelling the tube with the date, time and amount of rainfall (which is read off the gauge before decanting it), and then refrigerated until collection during the following field trip. Upon return to Stellenbosch, the samples were filtered into two clean 15 ml PP tubes using a 0.45µm cellulose acetate filter, and sent off for chloride and stable isotope analysis. One day of rainfall therefore translates to a single rain water sample.

Of the eight daily collection points, three collectors (KA-R1, Hol-R and P-R) did not accurately record rainfall, and could therefore not be used for recharge estimates. This could be due to confusion regarding the sampling protocol, as well as a change in management (as was the case for KA-R1). The remaining five collection points were assessed by calculating the percentage of total rainfall days that were sampled, and the percentage of the total rainfall (in mm) that was sampled. The accuracy of samples for KA-R2, KK-R, VL- R and Krs-R were validated against the farmers' rainfall records (Table 3). KA-R3 is validated against a Davis Automatic Weather Station (AWS) that is located 100 metres from the rainfall gauge (Table 3). Sampling at KK-R, VL- R and KA-R3 commenced in June 2015, and KA-R2 and Krs-R in July 2015. KK-R, KA-R3 and Krs-R collected samples for one year until June 2016. KA-R2 and VL-R continued collecting samples until October and September 2016 respectively.

Table 3: Inclusivity of rain water collection, in comparison to farmer's records (KA-R2, KK-R, VL-R and Krs-R) and the records of an AWS (KA-R3)

Rainfall records	**2015**													
	Jan	**Feb**	**Mar**	**Apr**	**May**	**Jun**	**Jul**	**Aug**	**Sep**	**Oct**	**Nov**	**Dec**		
KA-R2 (Farmer's rainfall records)														
Total rainfall (mm)	21	6	11	2	21	102	126	31	10	12	13	2	**356**	**28%**
Rainfall sampled (mm)							55	25	8	0	10	0	**98**	
No. rainfall days	3	3	3	1	5	9	7	6	5	4	3	1	**50**	**22%**
No. samples							2	4	3	0	2	0	**11**	
KK-R (Farmer's rainfall records)														
Total rainfall (mm)	10	8	10	1.5	26	97	103	34	10	12	12	3	**327**	**50%**
Rainfall sampled (mm)						39	98	21	6	0	0	0	**164**	
No. rainfall days	1	3	3	1	5	8	9	6	4	3	3	2	**48**	**27%**
No. samples						4	6	2	1	0	0	0	**13**	
VL-R (Farmer's rainfall records)														
Total rainfall (mm)	7	0	6	1	15	55	56	10	4	11	4	0	**169**	**49%**
Rainfall sampled (mm)						19	53	8	3	0	0	0	**83**	
No. rainfall days	2	0	2	1	5	5	5	3	2	1	1	0	**27**	**37%**
No. samples						3	4	2	1	0	0	0	**10**	
Krs-R (Farmer's rainfall records)														
Total rainfall (mm)	0	4	7	0	3	59	36	19	9	0	10	0	**147**	**26%**
Rainfall sampled (mm)							20	18	0	0	0	0	**38**	
No. rainfall days	0	2	3	0	1	3	5	2	2	0	1	0	**19**	**16%**
No. samples							2	1	0	0	0	0	**3**	
KA-R3 (AWS rainfall records)														
Total rainfall (mm)	12	2	14	2	13	38	57	19	7	5	11	1	**182**	**43%**
Rainfall sampled (mm)						19	47	7	5	0	0	0	**78**	
No. rainfall days	4	3	4	2	8	9	11	10	7	3	3	1	**65**	**14%**
No. samples						2	5	1	1	0	0	0	**9**	

Rainfall records	**2016**													
	Jan	**Feb**	**Mar**	**Apr**	**May**	**Jun**	**Jul**	**Aug**	**Sep**	**Oct**	**Nov**	**Dec**		
KA-R2 (Farmer's rainfall records)														
Total rainfall (mm)	9	1	23	45	11	158	101	43	71	10	2	5	**477**	**87%**
Rainfall sampled (mm)	0	0	22	33	9	130	99	43	70	9			**415**	
No. rainfall days	3	1	4	7	3	7	8	4	10	3	1	2	**53**	**62%**
No. samples	0	0	2	4	2	5	7	3	9	1			**33**	
KK-R (Farmer's rainfall records)														
Total rainfall (mm)	8	0	24	31	14	161	99	15	66	7	0	1	**426**	**32%**
Rainfall sampled (mm)	0	0	17	18	8	94							**137**	
No. rainfall days	2	0	4	5	3	8	10	3	10	1	0	1	**47**	**15%**
No. samples	0	0	1	2	1	3							**7**	
VL-R (Farmer's rainfall records)														
Total rainfall (mm)	0	0	16	18	3	106	55	18	37	4	0	2	**259**	**76%**
Rainfall sampled (mm)	0	0	4	17	2	104	55	10	4				**196**	
No. rainfall days	0	0	4	5	3	6	6	3	5	1	0	1	**34**	**56%**
No. samples	0	0	1	4	1	5	6	1	1				**19**	
Krs-R (Farmer's rainfall records)														
Total rainfall (mm)	5	0	13	19	11	78	26	18	13	2			**185**	**27%**
Rainfall sampled (mm)	0	0	0	0	0	50							**50**	
No. rainfall days	1	0	1	2	3	3	2	3	2	1			**18**	**6%**
No. samples	0	0	0	0	0	1							**1**	
KA-R3 (AWS rainfall records)														
Total rainfall (mm)	4	0	8	30	7	73	54	28	25				**229**	**22%**
Rainfall sampled (mm)	0	0	0	0	0	51							**51**	
No. rainfall days	2	0	7	8	7	14	12	13	15				**78**	**5%**
No. samples	0	0	0	0	0	4							**4**	

Limited rain water samples were collected at Krs-R (four samples for both 2015 and 2016), making it an unreliable source for rain water characterisation and recharge estimates. Furthermore, only nine rain water samples were collected at KA-R3 in 2015, and four in 2016. This corresponds to 43% of the total rainfall in 2015 and 27% of the total rainfall in 2016, and is thus an unreliable source for rain water characterisation. The results obtained from Krs-R and KA-R3 were therefore not used for this project.

KA-R2 (Figure 9a), KK-R (Figure 9b) and VL-R (Figure 9c) collected a minimum of 20 samples each over the minimum period of one year and one month (from 1 June 2015 to 30 June 2016). These correspond to a minimum of 28% of the rainfall days being sampled, and a minimum of 59% of the total rainfall being sampled. KA-R2 collected the largest percentage of total rainfall (28% for 2015 and 87% for 2016), with KK-R collecting the smallest percentage of total rainfall (50% for 2015 and 32% for 2016). The cumulative rainfall collector M-R (Figure 9d) was erected on the Piketberg mountain range in March 2016, and sampled in September 2016. The collector was equipped with a measuring gauge to assess the total rainfall, as well as a mesh covering and bird spikes to prevent any solid deposition from contaminating the sample. In total, 34 rain water samples were collected and analysed in 2015, and 60 in 2016.

Figure 9: Daily rainfall collectors KA-R2 (a), KK-R (b), VL-R (c) and cumulative rainfall collector M-R (d)

The weighted mean values of chloride in rain water were calculated by multiplying the daily precipitation amount (mm) with the chloride concentration in the rainwater (mg/L) for the sample taken that day. These were calculated using the equation:

$$Weighted\ average\ Cl_p = \sum P * Cl_p$$

Where P is the daily recorded precipitation amount (in mm) and Cl_p the chloride concentration of the rainwater sample corresponding to that day of rainfall (in mg/L). Weighted average compositions for $\delta^{18}O$ and $\delta^{2}H$ are calculated in the same manner.

4.3. Analytical techniques

4.3.1. Major cations and anions

Major cations (Na^+, Mg^{2+}, Ca^{2+}, K^+) and anions (Cl, SO_4^{2-}, HCO_3^-, CO_3^{2-}) in groundwater were analysed after each of the six field trips. Alkalinity was measured within one day of sampling at the Department of Soil Science, Stellenbosch University, using a Metrohm 702 SM Tritrino Autotitrator. Volumes obtained for EP1 (CO_3^{2-}) and EP2 (HCO_3^-) were converted to mg/L. For all samples, total alkalinity was equal to the bicarbonate alkalinity (mg/L HCO_3^-). Cation (Na^+, Mg^{2+}, Ca^{2+}, K^+) and anion (Cl^-, SO_4^{2-}) analyses were completed at respective laboratories in the University of Stellenbosch and the University of the Free State (Table 4), due to laboratory problems at the University of Stellenbosch. The TDS (total dissolved ions) is defined as the total sum of major anions and cations for each sample, and is presented as mg/L.

Table 4: Number of groundwater samples analysed for cations (Na^+, Mg^{2+}, Ca^{2+}, K^+) and anions (Cl, SO_4^{2-}) at the University of the Free State and Stellenbosch University

	Facility	University	2015			2016		
			Jun	Sep	Nov	Mar	Jun	Nov
cation	CAF (Department of Soil Sciences)	Stellenbosch University	37					
	CAF (Department of Earth Sciences)	Stellenbosch University		9	18	15	14	9
anion	CAF (Department of Microbiology)	Stellenbosch University	37					
	Institute for groundwater studies	University of the Free State		9	18	15	14	9

A total of 94 rain water samples were analysed for chloride. Chloride analysis on rain water was completed at the CAF laboratories of the Department of Soil Science (Stellenbosch University) and the Institute for Groundwater studies (University of the Free State). From this total, 27 samples (collected in 2015) were analysed at the Department of Soil Sciences only, and 60 samples (collected in 2016) were analysed at the Institute for Groundwater Studies only. A random selection of 7 samples (collected in 2015) were analysed at both the

Department of Soil and Sciences and the Institute for Groundwater Studies, for comparative purposes.

Major cation analysis was performed on field acidified samples at the Central Analytical Facilities (CAF) of Stellenbosch University at the department of Earth Sciences and Soil Sciences, using an Argillent 7700 ICP-AES and a thermo iCAP inductively coupled plasma optical emission spectrometer (ICP-OES) respectively. The instruments are calibrated daily, using the standards framework set out by the National Institute of Standards and Technology (NIST). Anion analysis was completed at the CAF laboratories of the Department of Soil Sciences and Microbiology at Stellenbosch University, and the Institute for Groundwater Studies at the University of the Free State. An Ion Chromatography (IC) on a Waters 432 Conductivity detector, connected to a Waters 717 plus Auto sampler and an Agilent 1100 series binary pump, was used in the Department of Microbiology. A DionexDX-120 IC and DionexDX-129 IC were used at the Institute for Groundwater Studies and the Department of Soil Sciences respectively. The instruments are calibrated daily against six prepared standards of NaCl and Na_2SO4, where the relative standard deviation is less than 2%. The anions have minimum and maximum detection limits which can be detected by the IC, and high concentrations are diluted based on the corresponding EC values.

An average charge balance of 7.0% was obtained for the 102 groundwater samples. The 37 samples collected in June 2015 showed an average charge balance of 10.1%. The remaining 65 samples, analysed at Earth Sciences (Stellenbosch University) and the Institute for Groundwater Studies (University of the Free State), show an average charge balance of 5.1%. For piper diagrams and bulk ion chemistry, only samples with a charge balance of less than 10% will be considered. However, since poor charge balance is most likely to do with HCO_3^-, all chloride data was used in the CMB calculations.

The 7 rain water samples analysed for chloride at both the IGS (University of the Free State) and the Department of Soil Sciences (Stellenbosch University) show a good correlation, aside from a single outlier (Figure 10). This outlier shows a concentration of 0 mg/L, as measured by the Department of Soil Sciences, which is unlikely. Furthermore, charge balances from groundwater results support the accuracy of the anion data from the IGS. Where possible, chloride in rain water data obtained from the IGS will be used, implying that samples collected in 2016 will have priority over those collected in 2015.

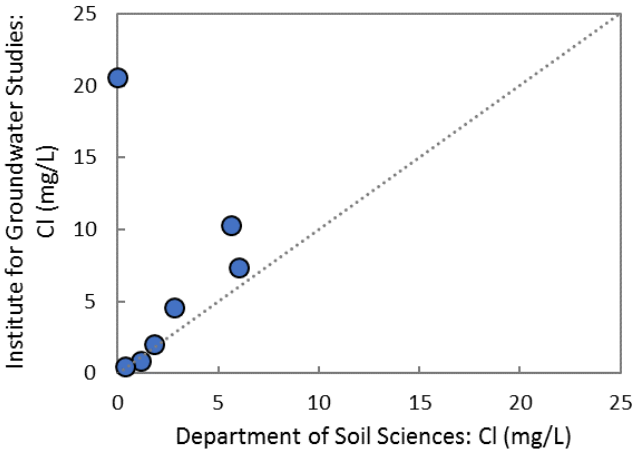

Figure 10: Comparison of analytical results for chloride concentrations in rain water from the Institute for Groundwater Studies (University of the Free State) and the Department of Soil Sciences (Stellenbosch University)

4.3.2. Stable isotopes

Oxygen and hydrogen isotope analysis was completed on 102 groundwater samples and 94 rain water samples. For stable isotope analysis, $\delta^{18}O$ and $\delta^{2}H$ isotope values were analysed relative to Standard Mean Ocean Water (SMOW). The results are presented in the common δ-notation, which shows a deviation (in parts per thousand) from SMOW:

$$\delta^{18}\mathrm{O}\ (‰) = \left[\frac{(^{18}O/^{16}O)sample}{(^{18}O/^{16}O)standard} - 1\right] \times 1000$$

$$\delta\ ^{2}H\ (‰) = \left[\frac{(\ ^{2}H/\ ^{1}H)sample}{(\ ^{2}H/\ ^{1}H)standard} - 1\right] \times 1000$$

Stable isotopes in rain water and ground water were analysed by the Environmental Isotope Group (EIG) at iThemba Laboratories in Gauteng. A PDZ Europa GEO 20-20 gas mass–spectrometer was used for analysis, and has been connected to a peripheral sample preparation device. The analysis technique uses a PDZ water equilibration system (WES), where a dual inlet mode is used for isotopic analysis of oxygen and hydrogen in water. Laboratory standards are analysed with each sample batch. The results are all within the expected error limits, and the analytical precision is estimated to be 0.1‰ for oxygen and 0.5‰ for hydrogen.

Deuterium excess (d) was calculated according to: $\mathrm{d} = \delta^{2}\mathrm{H} - 8\ \delta^{18}\mathrm{O}$

5. RESULTS

5.1. Physical rainfall

5.1.1. Rainfall amounts

Monthly precipitation values from 2015 and 2016 are presented for collector KA-R2 (
Figure 11a), and collectors KK-R (
Figure 11b) and VL-R (
Figure 11c) (Watson et al.*, 2017b). The total precipitation that was collected and analysed is presented as a percentage of the annual precipitation for each collector for 2015 and 2016 (*
Figure 11). which is located at an elevation of 620m (comparative to 53m, 145m and 111m at VL-R, KK-R and KA-R2 respectively).

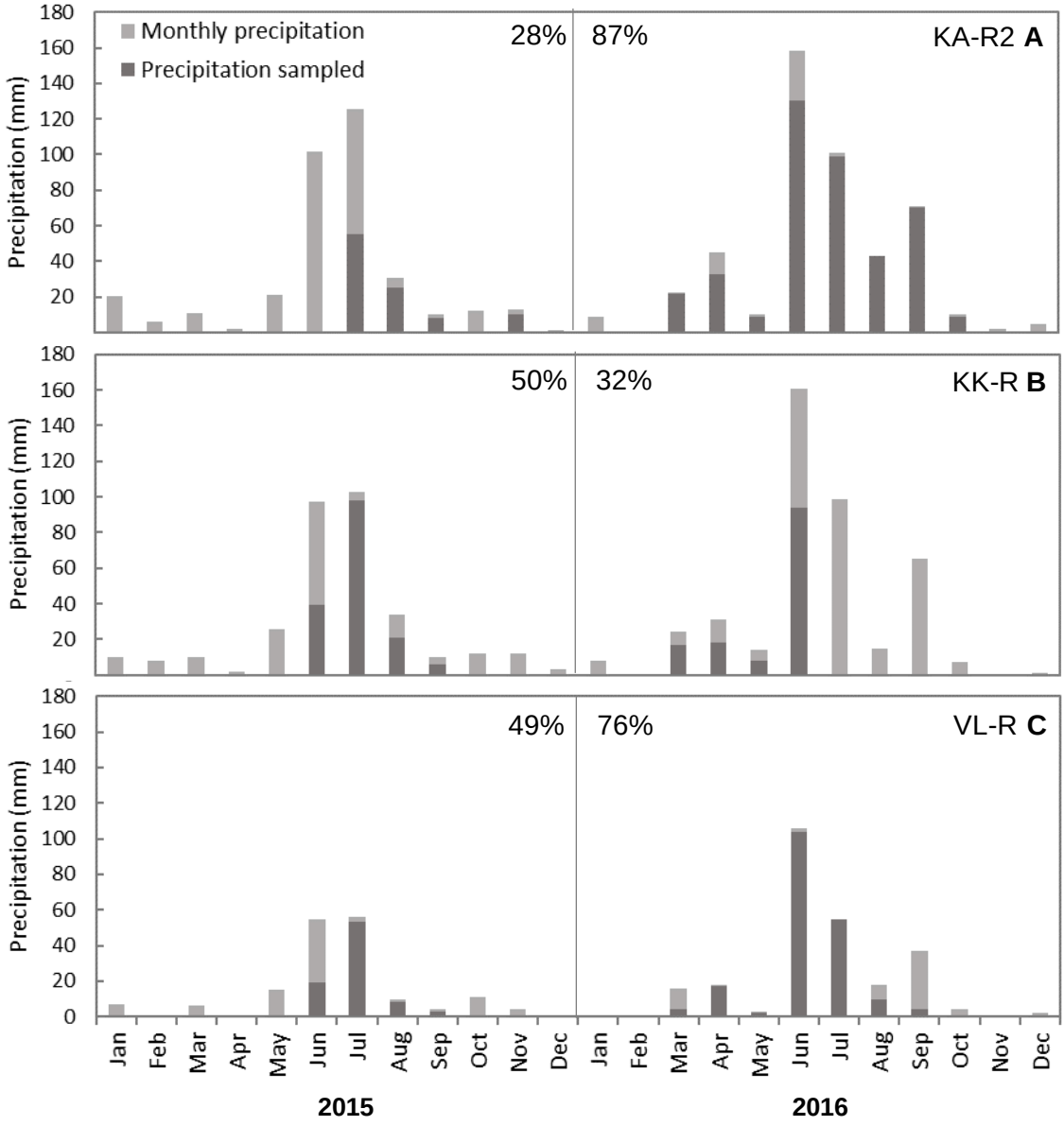

Figure 11: Monthly precipitation values at KA-R2 (a), KK-R (b) and VL-R (c)

KA-R2 received the most rainfall in the catchment (356 mm for 2015 and 477 mm for 2016), followed by KK-R (327 mm for 2015 and 426 mm for 2016), with the least rain measured at VL-R (169 mm for 2015 and 259 mm for 2016). This represents a decrease in rainfall from the top of the catchment towards the confluence. All collection points received on average 28% less rainfall in 2015 when compared to 2016. While the farmers did not collect rainfall for a full calendar year, they did sample for a minimum of one year, from the month of July 2015 to June 2016. During this time frame, VL-R collected the most rainfall (84%), KA-R2 the second most (67%) and KK-R the least (64%). An automatic weather station (C-AWS) is located 400 metres from VL-R, and agrees with the rainfall measurements within approximately 8mm (Watson *et al.*, 2017b). A second automatic weather station (M-AWS) was constructed in March 2016 (Watson *et al.*, 2017b), and is located 3km east of KA-R2. For the ten months between March and December 2016, KA-R2 and M-AWS agree within 15mm, which represents a difference of only 3% of the total rainfall that fell during that time frame.

Cumulative rainfall collector M-R is located at an elevation of 620m (comparative to 53m, 145m and 111m at VL-R, KK-R and KA-R2 respectively). It was constructed in early March 2016, and sampled late September 2016, collecting a total of 330 mm for these seven months. During the same time, 94% (451 mm) of the annual rainfall for 2016 was recorded at KA-R2, 96% (410 mm) at KK-R, and 98% (253 mm) at VL-R.

5.1.2. Rainfall events

A single rainfall event has been described as the total rain that fell over a 24-hour period, from 8 am to 8 am the following day. The total number of rainfall events recorded and sampled at the daily rainfall collectors are presented in Figure 12. The nature of the rainfall event is characterised by the amount of precipitation recorded, where <5mm has been allocated as the smallest rainfall event, and >20mm the largest rainfall event.

The heaviest showers were recorded at KA-R2 for 2016, where six rainfall events >20mm occurred in 2016. The lightest showers were recorded at VL-R, with no showers >20mm occurring in 2015, and only three recorded in 2016. KA-R2 and VL-R show the best distribution of rainfall events collection, particularly for 2016. KK-R on the other hand shows the least representative collection of rainfall events, where no events of <5mm were collected.

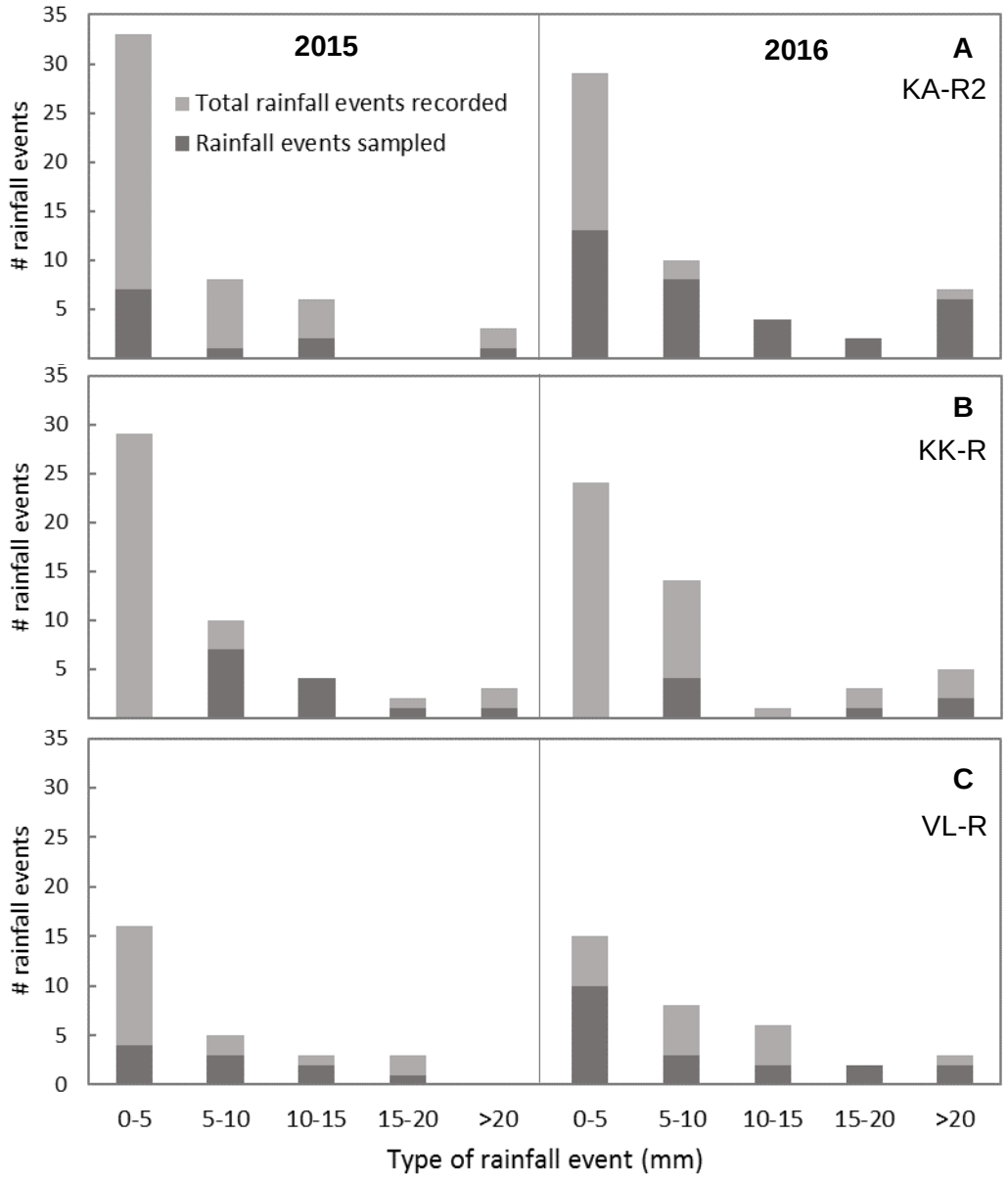

Figure 12: Total number of rainfall events recorded and sampled at daily rainfall collectors KA-R2 (a), KK-R (b) and VL-R (c) for 2015 and 2016

5.2. Compositional rain water

A single rain water sample was collected at cumulative collector M-R on the Moutonshoek mountain range in September 2016, with the results presented in Table 5. Daily rainfall samples were collected at four stations across the field area, with results presented for KK-R (Table 6), VL-R (Table 7) and KA-R2 (Table 8). Weighted averages were calculated from the entire sampling season.

Table 5: Stable isotope and chloride concentration at cumulative rainfall collector (1 sample)

M-R

Latitude: -32.67638 Longitude: 18.74424

Year	Month	Day	Cl_p	δ^2H	$\delta^{18}O$	d-excess	Precipitation
			mg/L	*‰*	*‰*	*‰*	*mm*
2016	September	20	7.10	-15.9	-4.27	18.26	330

Table 6: Stable isotope and chloride concentrations at daily collector KK-R (20 samples)

KK-R

Latitude: -32.68107 Longitude: 18.71758

Year	Month	Day	Cl_p	δ^2H	$\delta^{18}O$	d-excess	Precipitation
			mg/L	*‰*	*‰*	*‰*	*mm*
2015	June	11	1.71	-9.0	-1.39	2.2	8
2015	June	16	2.33	6.4	-0.91	13.7	9
2015	June	17	20.59	-21.8	-3.87	9.1	7
2015	June	24	3.37	-4.6	-2.57	16.0	15
2015	July	12	3.82	-6.5	-2.19	11.0	12
2015	July	17	4.15	-0.8	-3.11	24.1	7
2015	July	18	0.90	-10.4	-3.44	17.1	36
2015	July	24	1.72	-20.5	-4.88	18.5	10
2015	July	30	3.58	3.5	-2.31	22.0	18
2015	July	31	2.08	-14.4	-3.65	14.8	15
2015	August	4	4.60	5.5	-0.81	12.0	7
2015	August	14	3.41	-0.3	-0.88	6.8	14
2015	September	8	10.33	5.8	-0.27	7.9	6
2016	March	27	7.16	-2.1	-3.22	23.7	17
2016	April	23	2.74	-13.2	-2.96	10.5	8
2016	April	29	1.67	-4.6	-1.90	10.6	10
2016	May	24	3.33	6.0	-1.55	18.4	8
2016	June	10	1.22	1.1	-2.08	17.7	22
2016	June	14	0.53	-3.8	-1.91	11.5	9
2016	June	15	0.27	-14.8	-3.51	13.2	63
	MAXIMUM		*20.59*	*6.4*	*-0.27*	*2.2*	
	MINIMUM		*0.27*	*-21.8*	*-4.88*	*24.1*	
	WEIGHTED AVERAGE		*2.73*	*-6.9*	*-2.71*	*14.8*	

Table 7: Stable isotope and chloride concentrations at daily collector VL-R (29 samples)

VL-R

Latitude: -32.59653 Longitude: 18.68548

Year	Month	Day	Cl_p	δ^2H	$\delta^{18}O$	d-excess	Precipitation
			mg/L	*‰*	*‰*	*‰*	*mm*
2015	June	10	4.41	-3.9	-0.61	1.1	5
2015	June	16	9.77	1.5	-0.80	7.9	7
2015	June	24	7.37	-8.1	-2.62	12.9	7
2015	July	11	2.35	-12.1	-3.51	16.0	11
2015	July	18	0.49	-13.4	-3.07	11.2	13
2015	July	23	1.02	-20.4	-5.31	22.1	9
2015	July	30	3.21	-10.2	-2.94	13.3	20
2015	August	4	11.05	1.2	-0.76	7.3	3
2015	August	31	4.11	12.1	1.03	3.9	5
2015	September	7	2.39	2.6	-0.12	3.5	3
2016	March	30	13.07	8.1	-1.00	16.0	4
2016	April	20	14.90	9.9	0.35	7.1	3
2016	April	21	19.55	-8.0	-3.33	18.6	5
2016	April	22	2.29	-12.4	-3.51	15.7	5
2016	April	29	5.14	2.3	-0.60	7.0	4
2016	May	13	2.31	13.3	-0.22	15.1	2
2016	June	10	1.68	0.9	-1.66	14.2	15
2016	June	14	0.46	-9.4	-2.88	13.6	40
2016	June	15	0.45	-16.1	-3.18	9.4	20
2016	June	19	0.83	-21.6	-3.90	9.6	20
2016	June	27	5.34	1.0	-0.68	6.4	9
2016	July	1	6.93	1.5	-1.59	14.2	5
2016	July	6	12.54	1.3	-1.92	16.7	6
2016	July	15	14.21	4.9	-0.41	8.2	2
2016	July	21	1.98	-1.1	-1.06	7.4	26
2016	July	22	12.35	0.1	-2.66	21.4	4
2016	July	29	6.12	-25.3	-4.38	9.7	12
2016	August	3	8.66	-42.5	-6.50	9.5	10
2016	September	1	13.18	9.2	0.02	9.0	4
	MAXIMUM		*19.55*	*13.3*	*1.03*	*1.1*	
	MINIMUM		*0.45*	*-42.5*	*-6.50*	*22.1*	
	WEIGHTED AVERAGE		*3.98*	*-8.9*	*-2.56*	*11.5*	

Table 8: Stable isotope and chloride concentrations at daily collector KA-R2 (44 samples)

KA-R2

Latitude: -32.71908 Longitude: 18.70420

Year	Month	Day	Cl_p	δ^2H	$\delta^{18}O$	d-excess	Precipitation
			mg/L	*‰*	*‰*	*‰*	*mm*
2015	July	30	1.85	1.8	-3.10	26.5	40
2015	July	31	1.68	-15.0	-3.57	13.5	15
2015	August	4	5.4	4.8	-1.20	14.4	5
2015	August	14	2.01	-2.8	-1.26	7.3	13
2015	August	25	2.49	5.5	-0.36	8.4	4
2015	August	31	1.5	16.9	2.13	-0.1	3
2015	September	7	5.38	3.5	-0.02	3.7	4
2015	September	9	2.4	0.5	-0.23	2.3	3
2015	September	15	9.02	7.1	0.78	0.8	1
2015	November	20	12.06	13.5	0.46	9.9	6
2015	November	21	4.55	-13.7	-3.97	18.1	5
2016	March	25	9.44	-2.4	-2.64	18.7	18
2016	March	30	7.18	8.2	-1.34	18.9	4
2016	April	21	2.31	4.1	-0.81	10.6	4
2016	April	22	1.55	-5.5	-2.78	16.7	10
2016	April	23	2.35	-17.0	-3.54	11.4	8
2016	April	28	1.10	-1.9	-1.44	9.6	11
2016	May	18	2.60	10.7	-0.54	15.1	3
2016	May	24	2.41	7.3	-1.43	18.7	6
2016	June	10	0.84	-5.5	-2.63	15.6	30
2016	June	15	0.40	-17.2	-3.19	8.3	58
2016	June	20	1.06	-21.3	-5.02	18.8	40
2016	June	27	1.98	-1.5	-2.64	19.7	1
2016	June	28	1.03	-1.7	-1.85	13.1	2
2016	July	1	1.63	-2.2	-2.74	19.7	15
2016	July	2	18.45	2.2	-1.96	17.9	2
2016	July	7	17.99	2.0	-2.16	19.3	4
2016	July	21	0.57				35
2016	July	22	1.64	-2.5	-1.99	13.4	5
2016	July	28	3.83	-37.2	-6.13	11.8	5
2016	July	29	1.07	-31.1	-4.76	7.0	33
2016	August	3	1.78	-44.9	-7.12	12.1	25
2016	August	14	9.70	-1.5	-2.25	16.5	9
2016	August	22	10.55	-0.8	-2.14	16.3	9
2016	September	1	1.59	6.5	-0.71	12.2	7
2016	September	5	2.23	4.3	-1.63	17.3	12
2016	September	13	5.21	-1.0	-2.41	18.3	10
2016	September	16	1.46	-17.0	-5.33	25.6	20
2016	September	17	1.24	-27.7	-4.99	12.2	2
2016	September	22	1.69	8.7	-0.79	15.0	1
2016	September	26	1.92	4.3	-1.04	12.6	2
2016	September	27	2.71	-1.2	-2.32	17.3	12
2016	September	28	10.08	7.7	-0.81	14.2	3.5
2016	October	11	5.25	6.9	-1.69	20.5	8.5
	MAXIMUM		*18.45*	*16.9*	*2.13*	*-0.1*	
	MINIMUM		*0.40*	*-44.9*	*-7.12*	*26.5*	
	WEIGHTED AVERAGE		*2.61*	*-9.4*	*-2.93*	*14.0*	

5.2.1. Chloride concentrations in rain water

Chloride concentrations in rainfall varied between 0.27 and 20.59 mg/L for all rainfall collectors (Figure 13). Excluding statistical outliers, which lie off the primary box and whisker plot, daily rainfall collector VL-R shows the greatest variation in chloride concentrations across the catchment (19.10 mg/L), with KK-R showing the smallest variation (7.16 mg/L). The weighted averages of all samples are 2.61, 2.73 and 3.98 mg/L for KA-R2, KK-R and VL-R respectively. Cumulative collector M-R has a measured chloride concentration of 7.10 mg/L, representing the highest average chloride concentration of all the rainfall collectors.

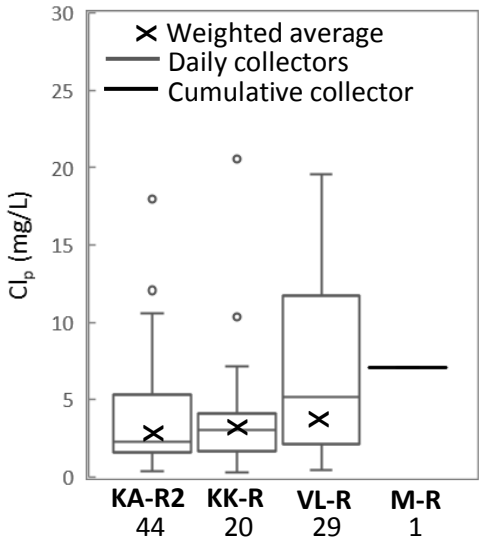

Figure 13: Chloride concentrations in rain water, including the number of samples per site

A reasonably good correlation exists between the amount of precipitation and chloride concentration (Figure 14). Chloride in precipitation and rainfall amount have an indirect correlation, where high chloride concentrations are associated with smaller rainfall events.

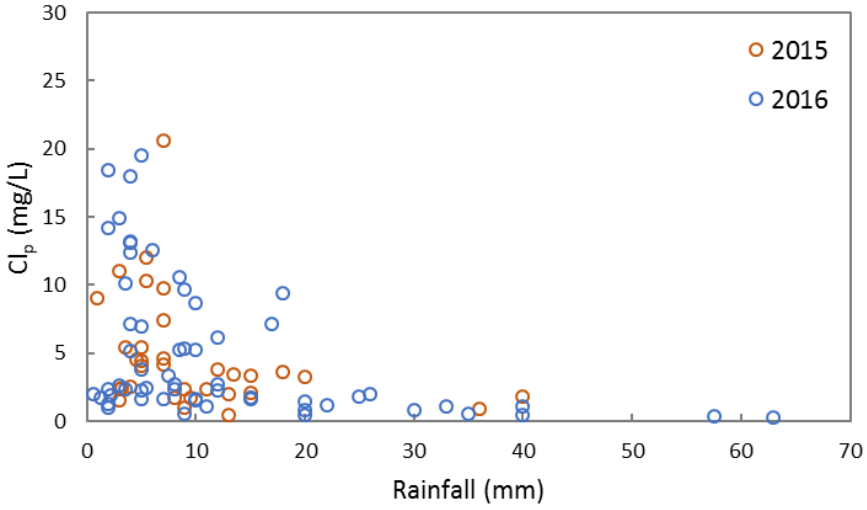

Figure 14: Chloride concentrations in precipitation in comparison to measured rainfall amounts at daily rainfall collectors

5.2.2. $\delta^{18}O$ and $\delta^{2}H$ in rain water

The $\delta^{18}O$ ratios of rain water range from -7.12‰ to 2.13‰ (Figure 15a), whilst the $\delta^{2}H$ values in rain water range from -44.9‰ to 16.9‰ (Figure 15b) for all rainfall collectors. Deuterium excess ratios range from -0.1‰ to 26.5‰, with a single negative value (-0.1‰) measured at KA-R2 (Figure 15c). The weighted averages at daily rainfall collectors KA-R2, KK-R and VL-R are -2.93‰, -2.71‰ and -2.56‰ for $\delta^{18}O$, and -9.4‰, -6.9‰ and -8.9‰ for $\delta^{2}H$ respectively. Cumulative collector M-R has an isotopic signature of -15.9‰ for $\delta^{2}H$, and -4.27‰ for $\delta^{18}O$, which is more negative in comparison to the weighted averages of the daily rainfall collectors. M-R shows a greater deuterium excess than the weighted average values of the daily rainfall collectors, where weighted d ratios at KA-R2, KK-R, VL-R and M-R are 14.0‰, 14.8‰, 11.5‰ and 18.3‰ respectively. The greatest isotopic variation occurs at KA-R2.

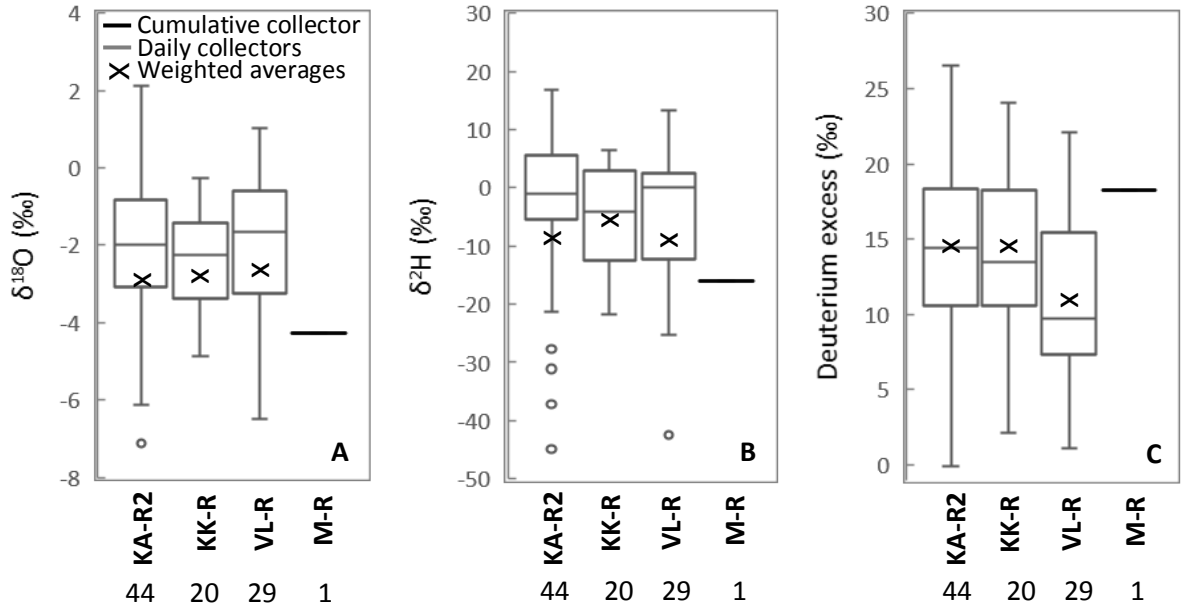

Figure 15: Stables isotope ratios in rain water for $\delta^{18}O$ (a), $\delta^{2}H$ (b) and deuterium excess (c) at rainfall collectors KA-R2, KK-R, VL-R and M-R

Stable isotope compositions show a general decrease in heavy isotopes with increasing rainfall amount for $\delta^{18}O$ (Figure 16a) and $\delta^{2}H$ (Figure 16b). This correlation is however weak, particularly for $\delta^{2}H$, with r-values of 0.07 and 0.18 for 2015 and 2016. While the deuterium excess shows no correlation with rainfall for 2016 (r = 0.01), a weak positive correlation between deuterium excess and increasing rainfall amount is noted for 2015 (r = 0.35) (Figure 16c).

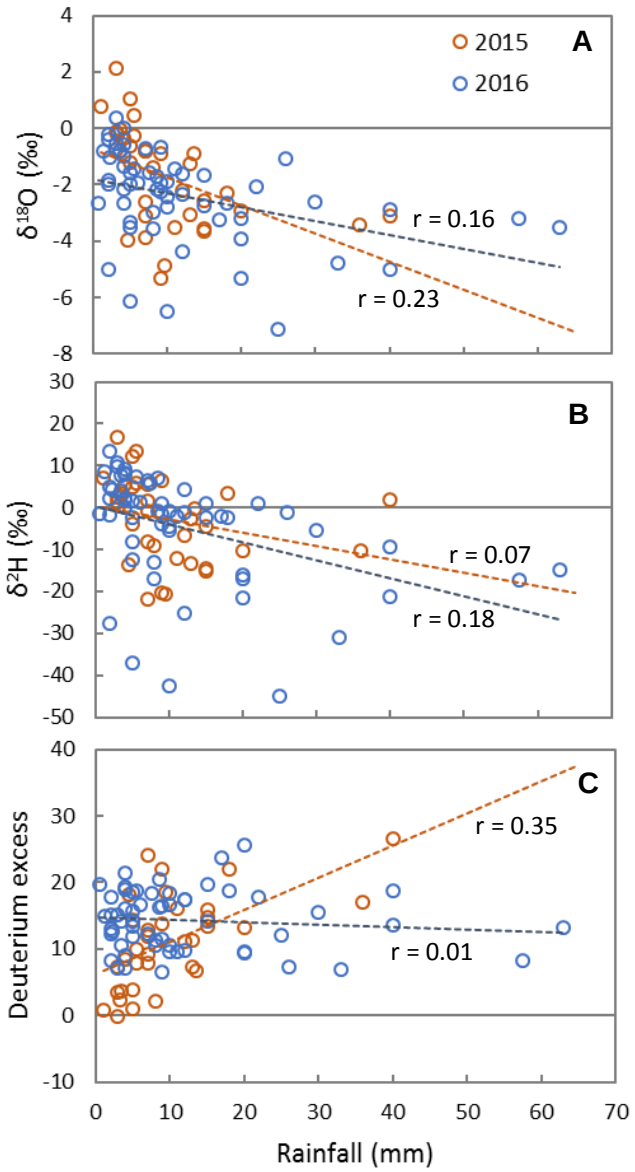

Figure 16: Isotopic compositions of δ^{18}O (a) and δ^{2}H (b) in comparison to rainfall, and the deuterium excess (c) in comparison to rainfall at daily collectors.

Seasonal variations correlate well with varying values of δ^{18}O (Figure 17a) and δ^{2}H (Figure 17b). A dramatic decrease in isotopic ratios is noted around July/August for 2016, with minimum δ^{2}H and δ^{18}O ratios of -44.9‰ and -7.12‰, in comparison to minimum ratios of -27.7‰ and -5.33‰ in the other months. A similar trend is observed in 2015, although this is less pronounced than 2016, with minimum δ^{2}H and δ^{18}O ratios of -21.8‰ and -5.31‰ in June and July. April, May, September and October show the most positive isotopic ratios for both 2015 and 2016. This is more pronounced for 2015 (maximum δ^{2}H and δ^{18}O ratios of 16.9‰ and 2.13‰ in September) in comparison to 2016 (maximum δ^{2}H and δ^{18}O ratios of 13.3‰ and 0.35‰ in May and April). It is therefore apparent that heavier isotopes dominated the rainfall for 2015 in comparison to 2016. This is mirrored in the deuterium excess-values (Figure 17c) where 2015 shows greater a variability in d (maximum difference of 26.6‰) in comparison to

2016 (maximum difference of 19.1‰), and thus greater fluctuations from the GMWL. It is also apparent that 2015 is characterised by a lower average d value (11.2‰) in comparison to 2016 (14.3‰).

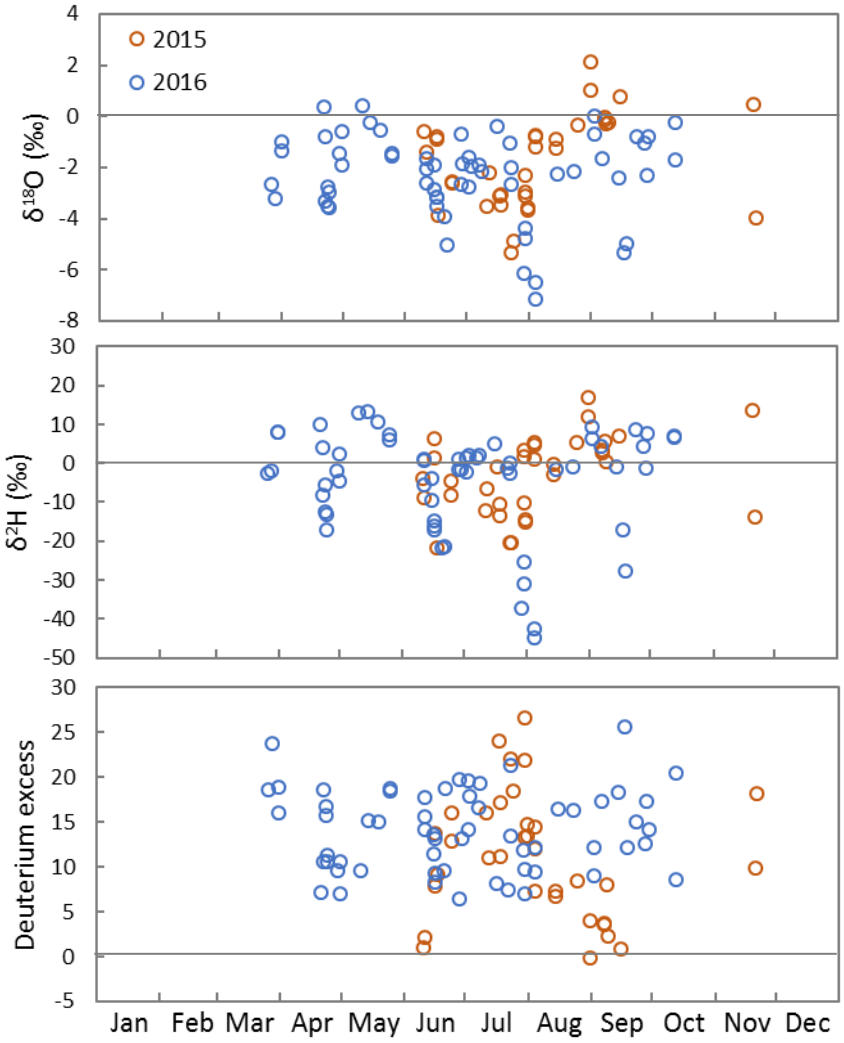

Figure 17: Seasonal variations in $\delta^{18}O$ (a), $\delta^{2}H$ (b) and d (c)

Stable isotope ratios are used as a comparative tool against the Global Meteoric Water Line (GMWL) of Craig (1961). The line of best fit between isotopic ratios for rain water samples from KA-R2, KK-R and VL-R is defined as the Local Meteoric Water line (LMWL). Due to the substantial isotopic variations between 2015 and 2016, it is necessary to determine the LMWL for these unique sampling seasons. Two LMWLs are therefore calculated from the 34 rain water samples collected in 2015, and the 59 rain water samples collected in 2016 (Figure 18).

The **2015 LMWL** is defined by the following equation (r = 0.80):

$$\delta^2H = 5.00\ \delta^{18}O + 5.91$$

The **2016 LMWL** is defined by the following equation (r = 0.89):

$$\delta^2H = 7.73\ \delta^{18}O + 13.63$$

When considering all the rainfall data for 2015 and 2016, a **general LMWL** with the following equation is produced (r = 0.82):

$$\delta^2H = 6.48\ \delta^{18}O + 9.85$$

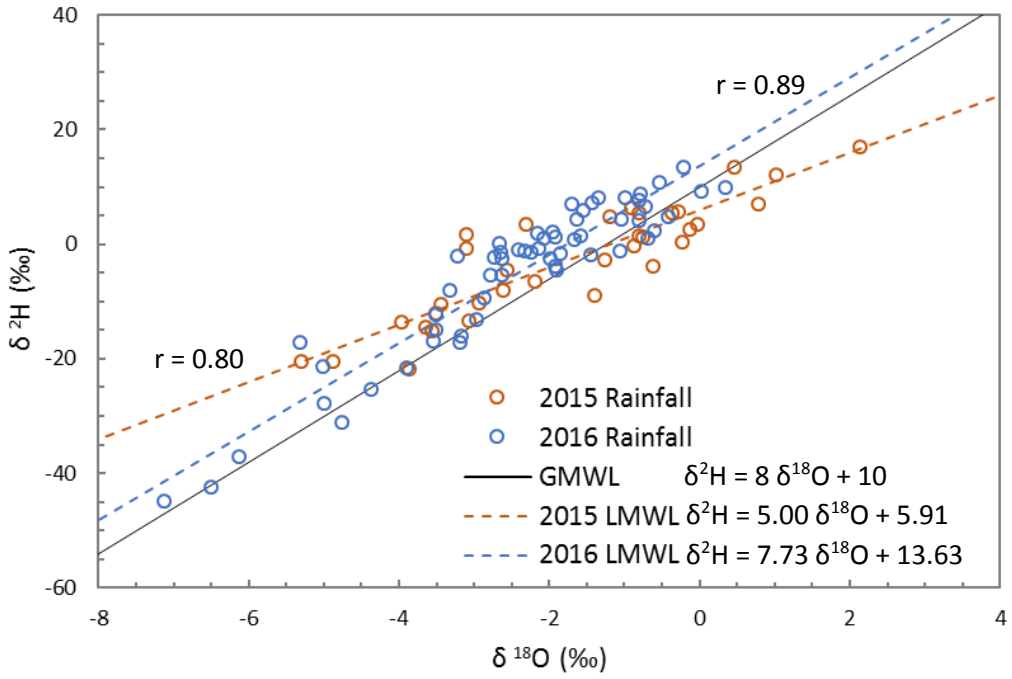

Figure 18: LMWL line for 2015 (34 samples from daily rainfall collectors) and 2016 (59 samples from daily rainfall collectors), in comparison to the GMWL defined by Craig (1961)

5.3. Groundwater

In total, 102 deep groundwater samples tapping into the secondary aquifer were collected from 41 boreholes across the study area (Figure 7). 58 samples were collected from 25 boreholes along the Krom Antonies River (Table 9 and Table 10), 25 samples from 8 boreholes along the Hol River (Table 11), and 11 samples from 5 boreholes along the Kruismans River, and 8 samples from 3 boreholes along Verloren River (Table 12).

Table 9: Deep groundwater samples collected along the Krom Antonies river, sites KA1 to KA10

Site	Latitude	Longitude	Borehole depth	Month	Year	ORP	pH	EC	TDS	Ca^{2+}	Mg^{2+}	Na^{+}	K^{+}	Cl^{-}	SO_4^{2-}	HCO_3^{-}	Charge Balance	δ^2H	$\delta^{18}O$	d-excess
			metres			*mV*		*mS/m*	*mg/L*	*mg/L*	*mg/L*	*mg/L*	*mg/L*	*mg/L*	*mg/L*	*mg/L*	*%*	*‰*	*‰*	*‰*
KA1	-32.71641	18.73737	96	Jun	2015	103	7.21	32.5	283.10	32.00	5.90	27.00	2.90	56.10	9.40	149.80	-11.93	-12.7	-3.41	14.6
				Nov	2015	120	6.80	22.0	188.10	25.09	4.63	24.07	1.72	41.10	7.28	84.20	0.62	-15.4	-3.20	10.2
				Mar	2016	148	7.17	32.4	261.91	38.20	6.11	28.16	1.87	49.60	11.17	126.80	-0.38	-12.7	-3.12	12.2
				Jun	2016		6.73	16.3	105.02	18.15	4.69	23.65	1.81	40.60	5.93	10.20	24.48	-10.6	-3.26	15.4
KA2	-32.71562	18.73474	122	Jun	2015	94	7.46	22.6	302.70	33.60	6.30	27.90	2.90	53.00	10.00	169.00	-12.45	-12.7	-3.43	14.7
				Sep	2015	57	7.33	37.0	307.58	33.78	5.97	27.73	1.99	45.00	10.32	182.80	-13.22	-12.4	-3.08	12.2
				Nov	2015	94	7.29	37.6	269.29	37.91	6.36	29.41	2.00	48.20	12.00	133.40	-0.66	-13.4	-3.45	14.2
				Mar	2016	168	7.35	36.4	312.35	45.53	7.38	31.43	2.84	50.00	12.76	162.40	-0.21	-13.0	-3.13	12.1
				Jun	2016		7.24	23.4	164.54	42.39	7.35	30.86	1.95	47.20	11.20	23.60	35.63	-12.0	-3.51	16.0
KA3	-32.71881	18.71124		Jun	2015	59	7.18	52.9	406.40	48.70	9.90	35.70	2.70	69.90	71.30	168.20	-12.15	-11.6	-2.83	11.0
				Sep	2015	-55	7.30	57.0	416.59	54.87	10.25	36.82	1.78	57.50	69.97	185.40	-7.83	-9.0	-2.72	12.7
				Mar	2016	179	7.41	49.5	421.26	61.54	10.41	37.85	2.27	60.30	40.48	208.40	-2.82	-11.0	-2.77	11.1
				Jun	2016		6.48	47.7	340.53	68.44	12.25	37.82	1.86	61.30	143.85	15.00	10.34	-11.0	-3.16	14.3
KA4	-32.71179	18.72179	45	Jun	2015	54	7.53	59.2	490.10	55.50	10.20	48.40	4.10	127.60	20.90	223.40	-13.89	-10.1	-3.22	15.7
KA5	-32.71639	18.71753	21	Jun	2015	103	7.49	66.8	517.50	59.10	12.30	48.70	2.90	128.20	21.90	244.40	-13.52	-13.0	-3.47	14.8
KA6	-32.69960	18.72625		Mar	2016	196	6.96	98.5	727.41	93.95	20.48	78.11	4.41	174.40	60.66	295.40	-5.45	-12.4	-3.01	11.6
				Jun	2016		6.73	76.5	805.96	124.56	29.16	80.89	3.59	176.60	356.56	34.60	-2.97	-11.7	-3.45	15.9
				Nov	2016	132.00	6.97	101.7	484.14	103.80	19.77	71.84	3.31	176.00	68.42	41.00	17.30	-11.5	-3.29	14.8
KA7	-32.70265	18.72857		Mar	2016	195	7.15	88.7	660.78	92.03	18.79	72.97	2.84	156.20	46.54	271.40	-2.28	-12.1	-3.19	13.4
				Jun	2016		7.15	69.5	576.61	120.93	25.16	96.47	3.72	229.20	64.32	36.80	19.17	-11.3	-3.26	14.8
KA8	-32.70832	18.71441	89	Mar	2016	168	6.91	103.5	668.34	101.17	26.66	73.13	3.21	224.10	86.07	154.00	-0.63	-13.2	-2.73	8.7
				Jun	2016		6.93	65.7	529.03	88.66	27.20	74.64	2.85	207.80	104.67	23.20	8.48	-11.0	-3.18	14.5
KA9	-32.69438	18.71268	96	Jun	2015	99	7.31	114.6	785.10	81.60	30.20	95.30	3.20	280.30	78.10	216.40	-9.62	-12.1	-3.46	15.6
				Sep	2015		7.10	121.4	772.59	98.63	32.93	109.69	3.15	251.50	74.09	202.60	2.15	-13.0	-2.84	9.7
				Nov	2015	62	7.10	126.6	735.26	91.33	29.88	102.37	2.72	259.90	73.86	175.20	-0.87	-13.6	-3.58	15.1
				Mar	2016	168	7.19	123.0	776.41	105.07	31.95	104.57	2.70	272.30	74.62	185.20	0.89	-15.9	-3.50	12.2
				Jun	2016		6.68	78.9	646.96	93.73	34.26	105.79	2.89	263.30	119.59	27.40	8.01	-12.4	-3.49	15.5
				Nov	2016	144.00	6.97	112.1	549.14	89.67	28.65	84.01	3.27	237.30	78.44	27.80	9.24	-11.7	-3.27	14.5
KA10	-32.68690	18.71872		Jun	2015	125	6.86	241.0	1258.60	99.00	86.60	161.80	5.50	519.40	231.10	155.20	-6.70	-11.1	-3.37	15.9

Table 10: Deep groundwater samples collected along the Krom Antonies river, sites KA11 to KA25

KROM ANTONIES

Site	Latitude	Longitude	Borehole depth	Month	Year	ORP	pH	EC	TDS	Ca^{2+}	Mg^{2+}	Na^{+}	K^{+}	Cl^{-}	SO_4^{2-}	HCO_3^{-}	Charge Balance	δ^2H	$\delta^{18}O$	d-excess
			metres			*mV*		*mS/m*	*mg/L*	*mg/L*	*mg/L*	*mg/L*	*mg/L*	*mg/L*	*mg/L*	*mg/L*	*%*	*‰*	*‰*	*‰*
KA11	-32.68173	18.71892	35	Jun	2015	73	6.46	158.3	880.40	53.80	40.60	179.80	4.30	392.50	108.60	100.80	-3.55	-13.7	-3.50	14.3
				Sep	2015	24	6.57	202.0	914.49	55.74	39.19	194.64	3.83	432.30	97.79	91.00	-3.80	-12.9	-3.07	11.6
				Nov	2015	170	6.28	198.6	1150.09	81.87	54.00	225.38	4.17	538.20	168.47	78.00	-3.98	-12.8	-3.53	15.4
				Mar	2016	149	6.30	178.4	1068.20	81.75	48.91	206.02	3.71	496.50	134.91	96.40	-3.47	-13.8	-3.09	10.9
				Jun	2016		6.48	99.2	862.76	61.09	42.23	201.41	3.50	438.70	101.24	14.60	2.16	-12.6	-3.52	15.5
				Nov	2016	88	6.32	220.0	1032.89	78.28	50.90	185.60	3.85	536.10	165.56	12.60	-7.16	-10.8	-2.99	13.1
KA12	-32.68670	18.69336		Jun	2015	121	7.38	206.0	1189.30	123.90	51.90	193.00	2.40	467.30	94.00	256.80	-1.14	-12.5	-3.08	12.1
KA13	-32.68817	18.68799	110	Jun	2015	148	4.43	64.2	316.50	5.40	17.80	77.00	1.60	213.10	0.00	1.60	-8.18	-14.4	-3.36	12.5
				Nov	2015	164	4.38	72.2	313.27	5.90	19.19	94.05	0.95	186.20	5.18	1.80	5.26	-15.5	-3.29	10.9
KA14	-32.67477	18.70884	70	Jun	2015	26	7.43	182.8	1171.70	101.40	51.10	165.00	3.60	367.40	184.40	298.80	-7.20	-13.9	-3.46	13.8
KA15	-32.66959	18.71507	120	Jun	2015	53	7.12	215.4	1427.10	131.70	61.40	200.50	4.10	406.50	244.10	378.80	-5.34	-13.6	-3.50	14.4
				Nov	2015	56	7.11	209.0	1326.27	145.38	57.33	201.81	3.12	430.80	223.83	264.00	-0.74	-14.8	-3.07	9.8
KA16	-32.67379	18.69106		Jun	2015	72	7.30	100.5	628.10	50.00	0.40	97.50	1.90	247.50	49.40	181.40	-23.40	-13.6	-3.31	12.9
KA17	-32.66681	18.70465	35	Jun	2015	53	6.95	298.0	1691.50	125.40	86.10	342.40	6.10	564.80	238.50	328.20	3.87	-14.3	-3.48	13.5
KA18	-32.66819	18.69016		Jun	2015	80	6.90	112.2	658.10	44.10	32.70	116.00	4.90	292.60	60.00	107.80	-5.66	-11.8	-2.98	12.0
KA19	-32.66009	18.68584	60	Jun	2015	37	7.73	125.6	803.60	64.90	26.30	120.20	1.90	325.20	66.50	198.60	-12.79	-14.9	-3.32	11.7
KA20	-32.65569	18.68276		Jun	2016		7.25	53.6	330.61	34.11	22.63	66.06	1.10	119.50	69.42	17.80	11.73	-14.6	-3.47	13.2
KA21	-32.65087	18.68316	117	Jun	2015	126	6.94	94.8	574.50	28.30	23.10	122.50	1.90	311.80	31.10	55.80	-8.75	-16.7	-3.66	12.6
				Sep	2015	67	7.09	106.6	553.88	32.87	21.77	128.54	1.29	268.10	31.51	69.80	-1.67	-14.6	-3.15	10.6
				Nov	2015	92	7.02	85.9	513.23	34.12	17.95	99.53	1.21	271.80	30.61	58.00	-10.21	-16.1	-3.62	12.9
				Mar	2016	185	7.45	93.8	494.44	46.88	18.93	97.51	1.25	211.90	32.78	85.20	0.70	-17.7	-3.70	11.9
KA22	-32.64929	18.70172	80	Jun	2015	84	7.08	185.8	1182.40	90.40	64.30	176.90	7.10	421.20	119.30	303.20	-4.47	-14.2	-3.55	14.2
				Nov	2015	114	7.17	201.0	1303.13	117.82	64.60	216.74	8.10	473.20	122.67	300.00	0.03	-18.4	-3.71	11.3
KA23	-32.64824	18.68735	120	Jun	2015	33	7.52	77.7	498.10	43.70	18.60	71.60	2.80	241.10	17.30	103.00	-12.40	-15.2	-3.30	11.2
KA24	-32.61935	18.69321	60	Jun	2015	97	5.87	69.7	398.80	23.40	19.50	67.30	4.00	219.50	35.30	29.80	-12.21	-15.0	-3.53	13.2
				Nov	2015	114	5.12	83.5	328.26	21.73	19.26	69.22	2.81	167.70	34.74	12.80	0.77	-19.0	-3.56	9.5
				Nov	2016	132	6.23	56.4	256.72	21.75	14.24	49.74	2.56	134.90	27.32	6.20	0.12	-15.5	-3.45	12.1
KA25	-32.61540	18.70818	100	Jun	2015	105	7.34	261.0	1563.30	147.10	71.70	238.00	8.60	503.50	196.60	397.80	-2.06	-16.5	-3.54	11.8
				Nov	2015	110	7.17	274.0	1660.44	196.64	75.10	292.08	8.42	649.60	217.40	221.20	4.40	-16.2	-3.58	12.4

Table 11: Deep groundwater samples collected along the Hol river

HOL																				
Site	**Latitude**	**Longitude**	**Borehole depth**	**Month**	**Year**	**ORP**	**pH**	**EC**	**TDS**	**Ca^{2+}**	**Mg^{2+}**	**Na^{+}**	**K^{+}**	**Cl^{-}**	**SO_4^{2-}**	**HCO_3^{-}**	**Charge Balance**	**$\delta^{2}H$**	**$\delta^{18}O$**	**d-excess**
			metres			*mV*		*mS/m*	*mg/L*	*mg/L*	*mg/L*	*mg/L*	*mg/L*	*mg/L*	*mg/L*	*mg/L*	*%*	*‰*	*‰*	*‰*
Hol1	-32.70018	18.60766	70	Jun	2015	90	6.77	65.8	502.60	34.80	24.10	64.00	1.80	186.90	44.20	146.80	-13.53	-16.4	-3.70	13.2
				Nov	2015	49	6.80	75.3	440.36	38.94	25.16	69.78	1.13	153.70	42.06	109.60	0.50	-15.2	-3.80	15.2
Hol2	-32.68716	18.63513	130	Jun	2015	111	7.38	613.0	2590.70	168.80	311.60	492.90	3.90	1085.20	156.50	371.80	16.37	-15.6	-3.55	12.8
				Sep	2015	93	7.25	358.0	3415.01	222.25	327.10	546.73	3.67	1871.00	135.25	309.00	1.00	-13.6	-3.23	12.2
				Nov	2015		7.39		3685.26	221.84	341.26	571.70	3.54	2114.00	148.32	284.60	-2.49	-16.3	-3.94	15.3
				Mar	2016	194	7.52	424.0	3525.99	227.11	344.85	547.81	3.43	1881.00	143.40	378.40	1.09	-14.4	-3.60	14.4
				Jun	2016		6.93	358.1	3144.34	217.58	340.67	547.38	3.07	1844.00	140.44	51.20	5.90	-14.3	-3.67	15.1
				Nov	2016	137	7.01	542.0	3095.95	198.50	297.80	450.51	2.97	1948.00	147.37	50.80	-4.22	-13.5	-3.28	12.7
Hol3	-32.65765	18.63124	20	Jun	2015	104	6.32	32.6	266.40	9.50	7.80	36.20	1.00	97.00	96.50	18.40	-30.03	-18.7	-3.73	11.1
				Nov	2015	109	6.15	29.8	159.56	8.95	6.32	42.33	0.42	82.70	5.86	13.00	2.73	-17.0	-3.62	12.0
Hol4	-32.60370	18.66606	100	Jun	2015	79	7.82	101.1	638.50	43.00	29.70	96.60	2.40	293.10	34.90	138.80	-12.01	-16.7	-3.25	9.3
				Nov	2015	109	7.63	99.7	568.32	49.42	28.52	108.77	1.78	254.10	31.74	94.00	1.16	-14.0	-2.90	9.2
				Nov	2016	129	7.41	102.0	454.73	44.44	27.22	94.75	1.76	238.00	28.95	19.60	6.06	-12.6	-2.81	9.9
Hol5	-32.60545	18.67117	120	Jun	2015	51	7.84	76.2	494.20	30.80	20.20	76.90	2.10	232.40	26.40	105.40	-14.48	-20.5	-3.87	10.5
				Nov	2015	29	7.25	83.6	461.30	37.63	23.47	91.62	1.65	201.30	29.63	76.00	1.92	-17.1	-3.57	11.5
Hol6	-32.59867	18.68295	130	Jun	2015	73	6.93	258.0	1245.70	101.90	73.80	213.70	7.50	499.80	70.00	279.00	1.27	-10.7	-2.40	8.5
				Sep	2015	62	6.79	458.0	2571.65	169.81	140.35	489.74	16.56	1189.00	89.79	476.40	-1.73	+0.6	+0.36	-2.2
				Nov	2015	97	6.93	358.0	2043.55	143.60	113.48	405.95	16.42	967.70	76.60	319.80	0.65	-2.1	-0.80	4.3
				Mar	2016	162	7.14	161.3	797.79	70.97	37.64	103.10	4.03	322.30	58.96	200.80	-9.60	-18.2	-3.40	9.0
				Jun	2016		7.23	117.3	940.74	59.95	38.35	114.80	4.45	645.40	56.18	21.60	-27.35	-15.0	-3.69	14.5
				Nov	2016	145	6.95	398.0	2034.08	169.00	130.60	369.60	8.99	1180.00	118.49	57.40	-1.67	-3.0	-0.89	4.1
Hol7	-32.59846	18.68295	125	Jun	2015	54	7.55	62.0	428.30	30.40	13.70	68.20	4.80	199.70	24.50	87.00	-13.80	-16.8	-3.79	13.5
				Mar	2016	162	7.03	77.5	413.77	38.61	15.77	74.45	3.91	166.80	21.63	92.60	-0.83	-17.5	-3.92	13.8
				Jun	2016		7.18	44.8	350.36	40.38	17.00	77.63	3.85	176.80	22.50	12.20	9.83	-16.8	-4.04	15.4
Hol8	-32.59814	18.68315	200	Jun	2015	59	7.34	83.3	581.60	47.40	24.70	84.00	5.70	267.20	41.40	111.20	-10.99	-15.6	-3.67	13.8

Table 12: Deep groundwater samples collected along the Kruismans and Verloren rivers

KRUISMANS

Site	Latitude	Longitude	Borehole depth	Month	Year	ORP	pH	EC	TDS	Ca^{2+}	Mg^{2+}	Na^{+}	K^{+}	Cl^{-}	SO_4^{2-}	HCO_3^{-}	Charge Balance	δ^2H	$\delta^{18}O$	d-excess
			metres			*mV*		*mS/m*	*mg/L*	*mg/L*	*mg/L*	*mg/L*	*mg/L*	*mg/L*	*mg/L*	*mg/L*	*%*	*‰*	*‰*	*‰*
Krs1	-32.66041	18.84732	150	Jun	2015	78	8.29	101.5	797.70	4.80	71.00	188.20	1.90	260.00	25.00	246.80	9.22	-15.6	-3.34	11.1
Krs2	-32.64875	18.84582	90	Jun	2015	112	8.38	23.1	180.30	8.40	6.70	29.00	1.40	46.70	26.90	61.20	-11.90	-15.1	-2.93	8.3
Krs3	-32.61298	18.80595	40	Jun	2015	114	6.05	57.0	301.00	7.40	12.40	71.00	1.00	183.30	12.10	13.80	-11.28	-16.4	-3.56	12.1
	-32.61298	18.80595		Sep	2015		5.68	56.5	276.10	6.57	13.00	79.93	0.57	151.90	13.33	10.80	1.55	-14.4	-3.22	11.4
	-32.61298	18.80595		Nov	2015	185	5.65	56.1	280.74	7.01	13.11	82.49	1.06	153.80	13.67	9.60	2.68	-15.0	-3.66	14.3
	-32.61298	18.80595		Mar	2016	173	5.6	55.7	283.04	7.41	12.96	78.02	0.59	158.30	13.96	11.80	-1.07	-15.5	-3.20	10.1
	-32.61298	18.80595		Jun	2016		5.7	40.9	281.28	6.53	13.51	82.54	0.67	161.40	14.02	2.60	1.59	-15.4	-3.65	13.8
Krs4	-32.60941	18.77602	285	Jun	2015	106	6.45	56.0	317.40	18.10	9.90	62.50	3.40	158.10	15.00	50.40	-10.62	-14.6	-3.67	14.8
	-32.60941	18.77602		Mar	2016	163	6.15	53.7	294.20	25.94	10.13	69.48	1.60	135.10	14.74	37.20	4.68	-15.1	-3.78	15.2
	-32.60941	18.77602		Nov	2016	124	6.61	49.8	222.75	17.55	7.69	57.28	1.42	120.80	12.00	6.00	3.60	-14.0	-3.45	13.6
Krs5	-32.60729	18.73510	120	Jun	2015		7.12	141.6	925.80	58.60	42.30	154.00	6.70	321.20	258.20	84.80	-8.77	-18.0	-4.21	15.7

VERLOREN

Site	Latitude	Longitude	Borehole depth	Month	Year	ORP	pH	EC	TDS	Ca^{2+}	Mg^{2+}	Na^{+}	K^{+}	Cl^{-}	SO_4^{2-}	HCO_3^{-}	Charge Balance	δ^2H	$\delta^{18}O$	d-excess
			metres			*mV*		*mS/m*	*mg/L*	*mg/L*	*mg/L*	*mg/L*	*mg/L*	*mg/L*	*mg/L*	*mg/L*	*%*	*‰*	*‰*	*‰*
Vrl1	-32.5878	18.68562	145	Jun	2015	58	8.22	60.0	405.10	27.30	14.10	57.50	4.80	168.80	16.60	116.00	-15.32	-17.9	-3.87	13.1
				Sep	2015	25	7.62	63.8	388.31	30.96	14.79	62.70	4.21	132.10	15.75	127.80	-4.69	-16.7	-3.53	11.6
				Nov	2015	56	7.56	59.0	351.92	31.55	15.05	63.22	4.23	126.30	13.98	97.60	1.95	-18.2	-4.02	14.0
				Mar	2016	152	7.20	82.2	446.81	41.54	20.52	79.12	4.21	190.70	23.93	86.80	0.07	-17.0	-3.88	14.1
				Jun	2016		6.91	162.4	925.04	57.64	47.77	223.42	5.21	522.00	50.80	18.20	1.76	-12.8	-3.29	13.5
				Nov	2016	109	7.64	62.0	295.15	33.31	15.23	59.88	4.32	148.60	18.21	15.60	7.69	-16.1	-3.56	12.4
Vrl2	-32.587	18.68417	70	Jun	2015	18	7.54	201.0	1021.40	58.60	51.10	219.90	5.70	453.70	45.80	186.60	0.09	-11.0	-2.76	11.1
Vrl3	-32.5264	18.66148	80	Jun	2015	73	5.96	45.2	288.10	10.50	11.90	45.10	4.50	129.00	48.30	38.80	-19.19	-16.3	-3.96	15.4

5.3.1. Groundwater depths

The depths of 41 of the boreholes sampled are presented for each tributary in Figure 19. The depth of nine boreholes (KA3, KA6, KA10, KA12, KA16, KA18, KA20, Krs6 and Hol3) are unknown.

The shallowest boreholes occur along the Krom Antonies River, with only 6 of the 17 recorded depths being greater than 100 metres. They range between 21 and 122 metres in depth. The deepest borehole sampled in this study occurs along the Kruismans River at Krs4, with a depth of 285 metres, and could possibly be tapping into a deeper aquifer. This is located 2.8km from the shallowest borehole on the Kruismans with a depth of only 40 metres. Sampling locations along the Hol River show deeper secondary boreholes than the Krom Antonies, where Hol1 is the only site with a depth < 100 metres. Borehole depths range between 70 and 200 metres along the Hol, with the deepest borehole (200m) occurring at the confluence (Hol8). The three boreholes situated along the Verloren River range in depth from 70 to 145 metres.

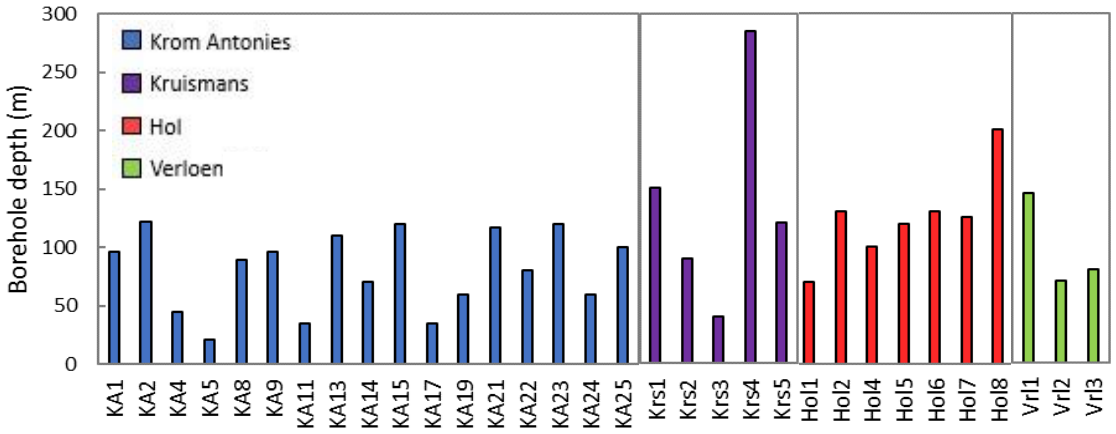

Figure 19: Borehole depths in the study area tapping into the secondary aquifer

5.3.2. EC, pH and ORP

For every sampling site, seasonal averages were calculated for EC, pH and oxidation-reduction potential (ORP), and are compared to one another in Figure 20. The Kruismans has the least saline groundwater in the study area (average EC = 74 mS/m), followed by the Verloren (average EC = 109 mS/m) and the Krom Antonies (average EC = 123 mS/m), with the most saline groundwater occurring along the Hol (average EC = 147 mS/m). However, for Hol groundwater, the statistical median indicates that this water has a similar salinity to the Krom Antonies, with two saline groundwater sites (Hol2 and Hol6) distorting the mean. pH values across the study area are very similar, with an average value of ~7 for each of the tributaries. The site with the highest pH occurs along the Kruismans (Krs2, pH = 8.4), with the

Krom Antonies exhibiting the lowest pH (KA13, pH = 4.4). ORP values range between 18 and 195 mV across the study area.

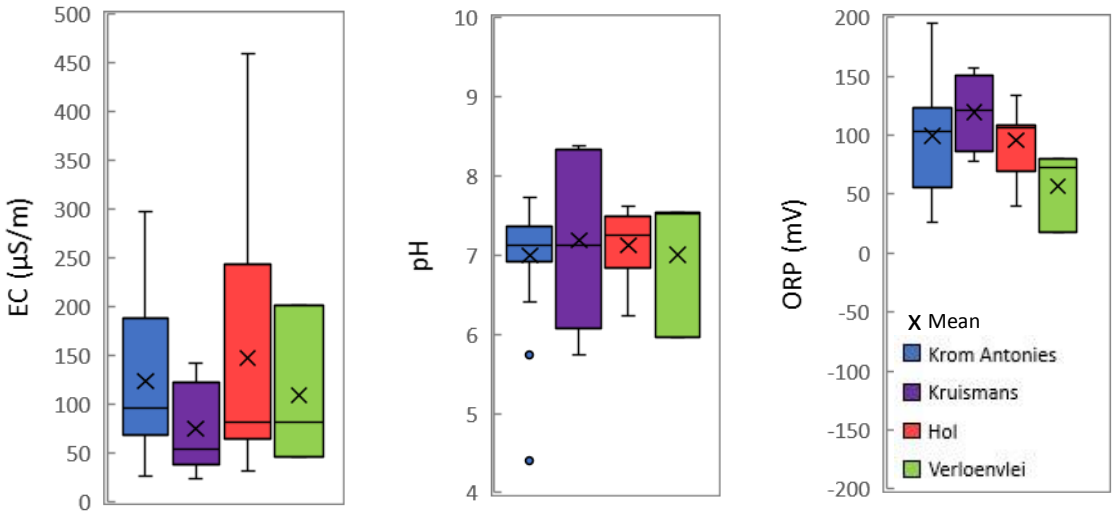

Figure 20: In-field measurements of EC (a), pH (b) and ORP (c)

Seasonal variations in electrical conductivity of deep groundwater is depicted in Figure 21. The Krom Antonies shows little seasonal variation in EC, with KA11 showing the largest variation of 121 mS/m. The Krom Antonies additionally shows a good spatial variation in EC values, with the uppermost Krom Antonies hosting some of the freshest groundwater in the study area (EC ~ 35 mS/m). This value increases downstream, with boreholes towards the east of the Krom Antonies showing greater EC values than those towards the west (Figure 22). The Kruismans shows little seasonal and spatial variation in salinity, with a maximum seasonal variation of 16.1 mS/m. The EC of groundwater along the Hol is <102 mS/m for boreholes Hol1, Hol3, Hol4, Hol5, Hol7 and Hol8. These values are comparable to boreholes KA1 to KA8 (EC <104 mS/m), and boreholes Krs1 to Krs4 (EC < 102 mS/m). Boreholes Hol2 and Hol6 are outliers and account for the most saline groundwater in the study area. Hol2 varies between 358 and 613 mS/m, with the most saline samples taken during June 2015 and November 2015, and the least saline in September 2015 and June 2016. Hol6 shows the most prominent seasonal variation, where EC values follow the pattern Sep 2015 > Nov 2016 > Nov 2015 > June 2015 > Mar 2018 > June 2016. Verloren groundwater has a maximum seasonal variation of 103.4 mS/m for Vrl1.

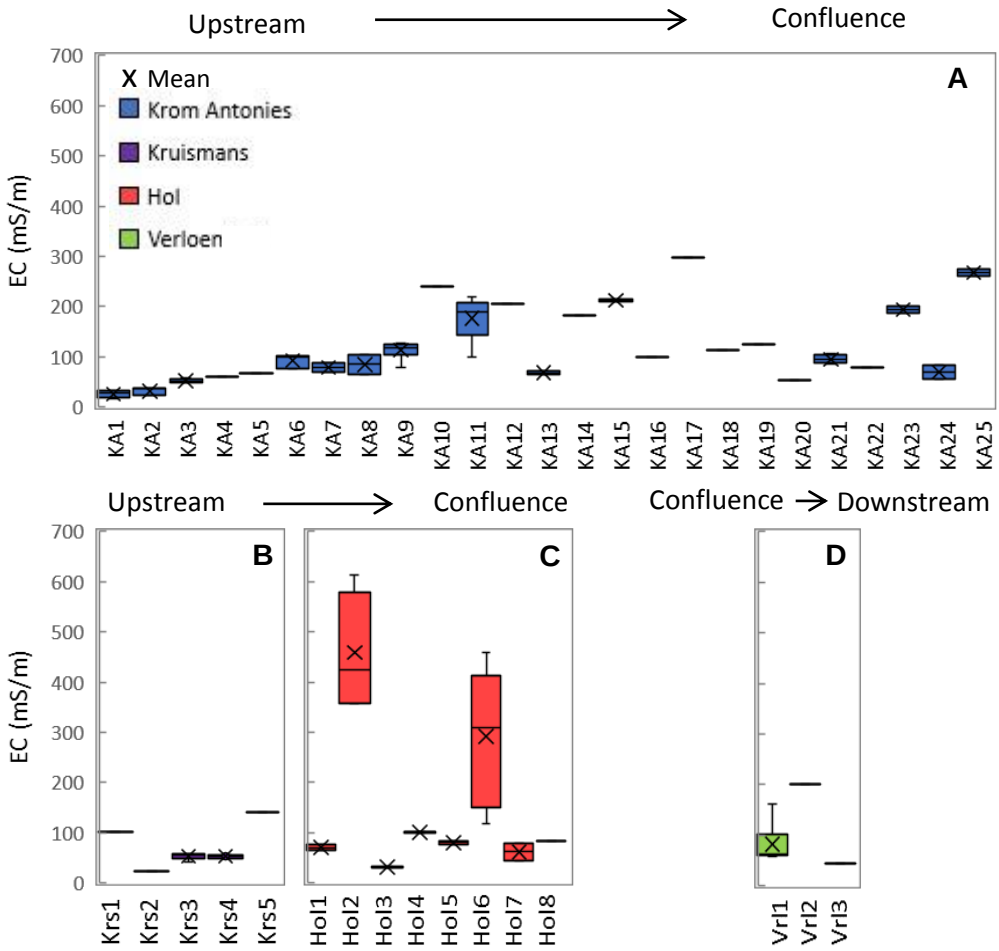

Figure 21: Seasonal variations in electrical conductivity for deep groundwater along the Krom Antonies (a), Kruismans (b), Hol (c) and Verloren (d) rivers

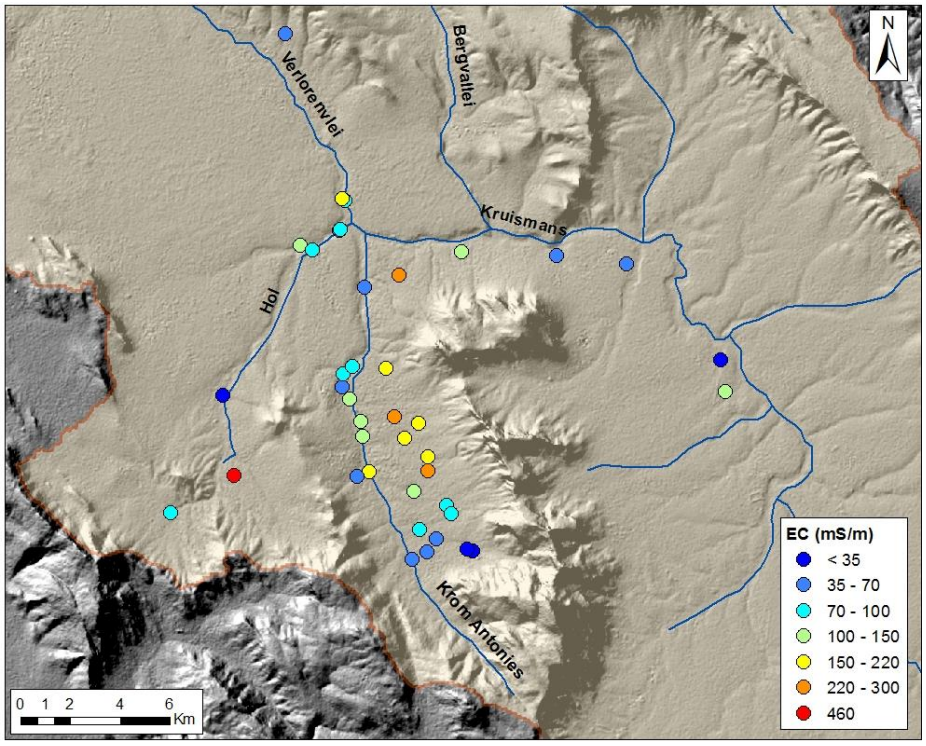

Figure 22: Spatial variations in EC (mS/m) across the study area

5.3.3. Major ion chemistry

5.3.3.1. Statistical variations of ion concentrations

The statistical variations of cation concentrations in groundwater are presented in Figure 23, where a seasonal average was calculated for each sampling site. Sodium is the most dominant cation in the study area, followed by calcium, magnesium and potassium. A single outlier exists for all major cations and corresponds to sample site Hol2. Magnesium and sodium concentrations of groundwater follow the trend of Hol > Krom Antonies > Verloren > Kruismans. This is not the case for calcium, where Krom Antonies > Hol > Verloren > Kruismans. Statistical percentiles indicate that cation concentrations of groundwater from most of the sampling sites along the Hol are significantly lower than the mean, and anomalous sites Hol2 and Hol6 are responsible for distorting the data.

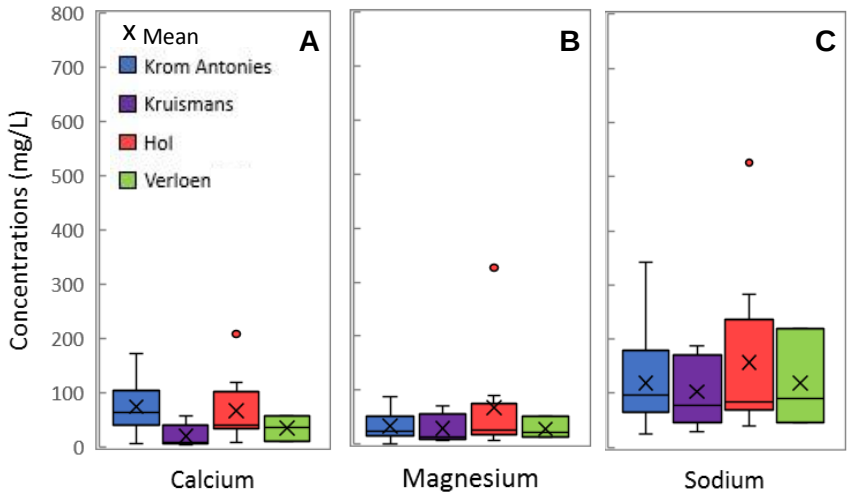

Figure 23: Major cations of calcium (a), magnesium (b) and sodium (c) in groundwater

The average anion concentrations of each tributary (where a seasonal average has been calculated for each sampling site) is presented in Figure 24. Chloride is the most dominant anion in the study area, followed by bicarbonate and sulphate. Statistical outlier Hol2 has an average chloride value of 1790 mg/L that far exceeds any other sampling site in the field area, and has been omitted from the plot. This resonates the patterns for the Hol cation concentrations, where Hol chloride concentrations are similar to the other tributaries, and the mean is distorted by Hol2 and Hol6. Chloride concentrations in groundwater follow the same trend as magnesium and sodium, where Hol > Krom Antonies > Verloren > Kruismans. Bicarbonate likewise follows the same trend as calcium, where Krom Antonies > Hol > Verloren > Kruismans. Average sulphate concentrations show a different trend where Krom Antonies > Kruismans > Hol > Verloren.

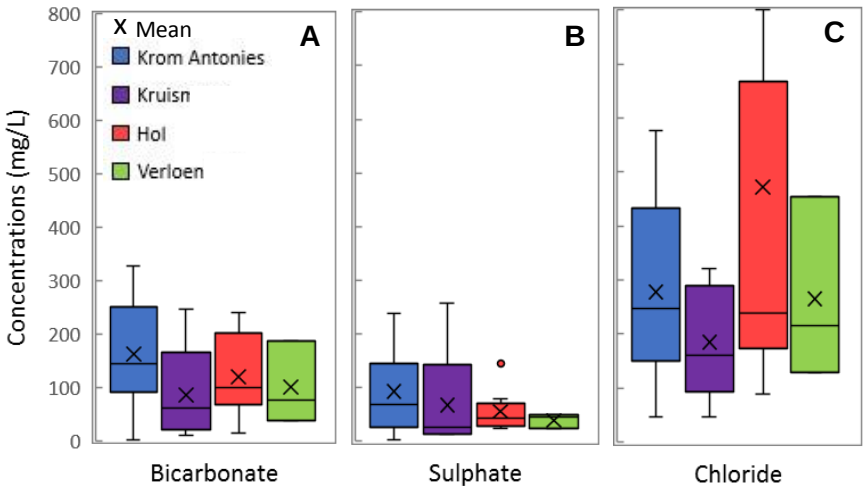

Figure 24: Major anions of bicarbonate (a), sulphate (b) and chloride (c) in groundwater. Outlier Hol6 (where Chloride = 1790.5 mg/L) has been emitted from the chloride plot only.

5.3.3.2. Groundwater characterisation

The geographical locations of the major tributaries of the Verlorenvlei catchment (namely the Krom Antonies, Kruismans, Hol and Verloren Rivers) are used as a proxy to characterise deep groundwater from the secondary Malmesbury aquifer. Groundwater types in the different tributaries have been characterised using a piper diagram (Figure 25). For sampling locations where multiple trips were conducted, the season with the lowest charge balance was selected for input into the diagram, and there is little variation in the type of groundwater between the seasons. Sites that were only sampled once in June 2015 and have a charge balance of >10% (i.e. KA16 and Vrl3) have been emitted from this plot.

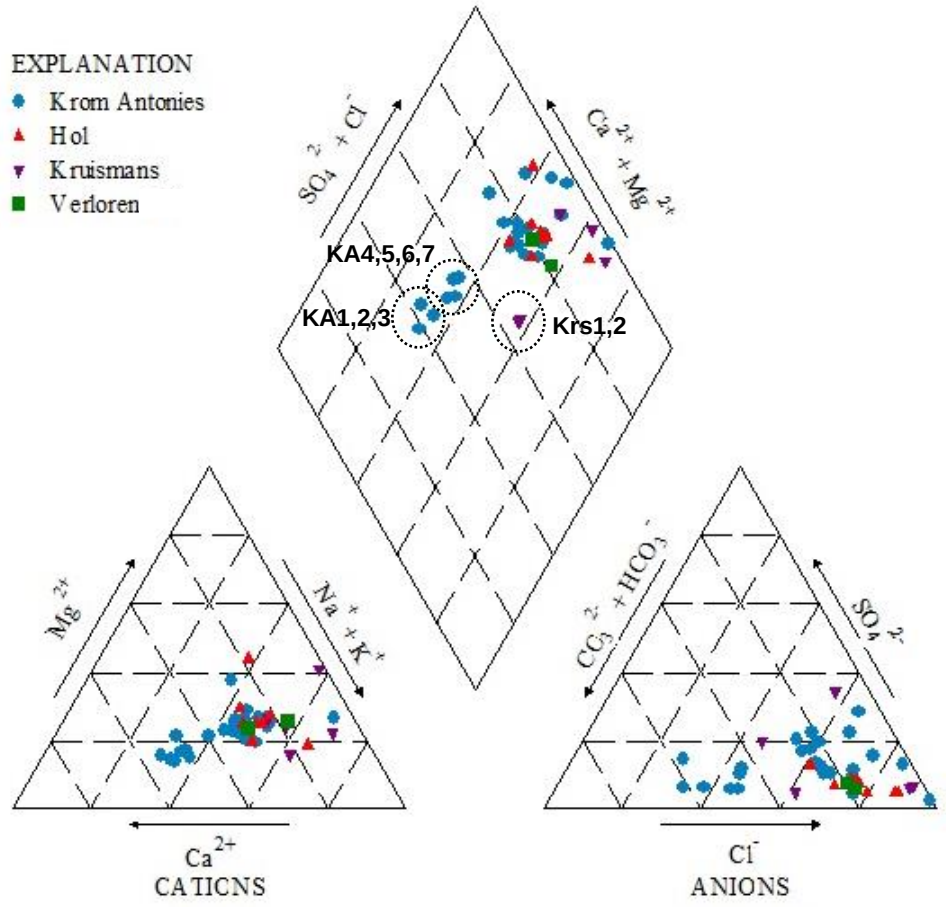

Figure 25: Piper diagram of groundwater in the study area

Most sampling sites have chloride as the dominant anion (except for KA1, KA2 and KA3) and fall between a mixture of Na^{+}-Cl^{-} and Ca^{2+}-Mg^{2+}-Cl^{-} type groundwater. Seven boreholes, occurring along the Krom Antonies, plot off the main sample group and represent the boundary between Ca^{2+}-HCO_3^{-} type groundwater (KA1, KA2 and KA3), and Ca^{2+}-Mg^{2+}-Cl^{-} type groundwater (KA4, KA5, KA6 and KA7). Two outliers also exist along the Kruismans river (Krs1 and Krs2), with groundwater of Na^{+}-Cl^{-} type, but an increase in bicarbonate in comparison to the other sampling sites.

5.3.4. $\delta^{18}O$ and $\delta^{2}H$ in groundwater

The standard $\delta^{2}H$ versus $\delta^{18}O$ plots are used to show all groundwater samples collected across the study area in 2015 and 2016, in reference to the GMWL (Craig, 1961) and the 2015 and 2016 LMWL (Figure 26). An evaporation line represents the line of best fit through the groundwater samples, and is validated by an r-value. Krom Antonies groundwater has $\delta^{2}H$ ratios of -19.0 to -9.0‰, and $\delta^{18}O$ ratios of -3.71 to -2.72‰. Most of the samples fall between the GMWL and 2015 LMWL, and show a weak evaporation trend (r = 0.36) parallel to the 2015 LMWL. Kruismans groundwater has $\delta^{2}H$ ratios of -14.0 to -18.0‰, and $\delta^{18}O$ rations of -4.21

to -2.93‰. Although similar in composition to the Krom Antonies, a weak trend (r = 0.31) indicates a stronger evaporative influence than Krom Antonies groundwater. The Hol shows the greatest variation in groundwater isotopic ratios across the catchment, with $\delta^{2}H$ ratios varying between -20.5 to +0.6‰, and $\delta^{18}O$ ratios between -3.94 to +0.36‰. A strong evaporation trend (r = 0.92) is largely influenced by a few individual outliers that are not necessarily true representatives of the groundwater, with the three most positive isotopic samples occurring at Hol6 and influencing this strong evaporation trend. Groundwater along the Hol also shows two isotopic classes: one that appears to follow a strong evaporation line parallel to the 2015 LMWL, and another that plots on the GMWL and includes isotopic ratios that are more negative in comparison to its counterpart. Verloren groundwater shows a similar evaporation trend (r = 0.86), and two outliers largely affecting this trend, with isotopic ratios of ranging between -18.2 to -11.0‰ for $\delta^{2}H$, and -4.02 to -2.76‰ for $\delta^{18}O$.

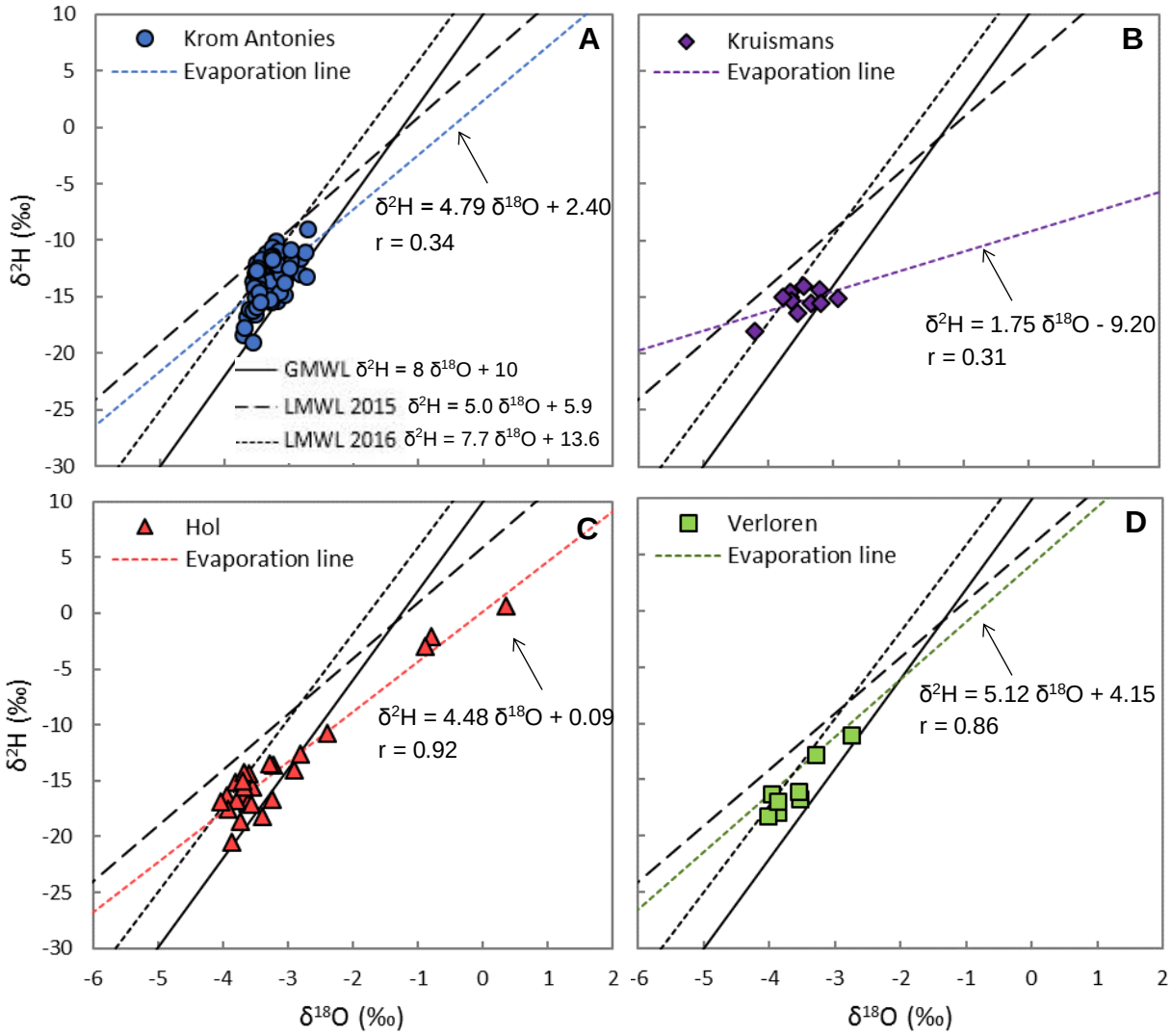

Figure 26: Stable isotope values of deep groundwater from the Krom Antonies (a), Kruismans (b), Hol (c) and Verloren (d) rivers, in comparison to the LMWL for 2015 and 2016, and the GMWL (Craig, 1961)

The seasonal variations in $\delta^{18}O$ ratios are depicted in Figure 27. The tributaries show no spatial variation in $\delta^{18}O$ values, and no seasonal correlations between individual boreholes. The Hol groundwater has the most significant seasonal fluctuations in the study area, with Hol6 showing a maximum seasonal variation of 4.05‰. $\delta^{18}O$ ratios follow the trend Sep '15 > Nov '16 > Nov '15 > Jun '15 > Mar '16 > Jun '16, and show an almost identical pattern to seasonal variations in EC.

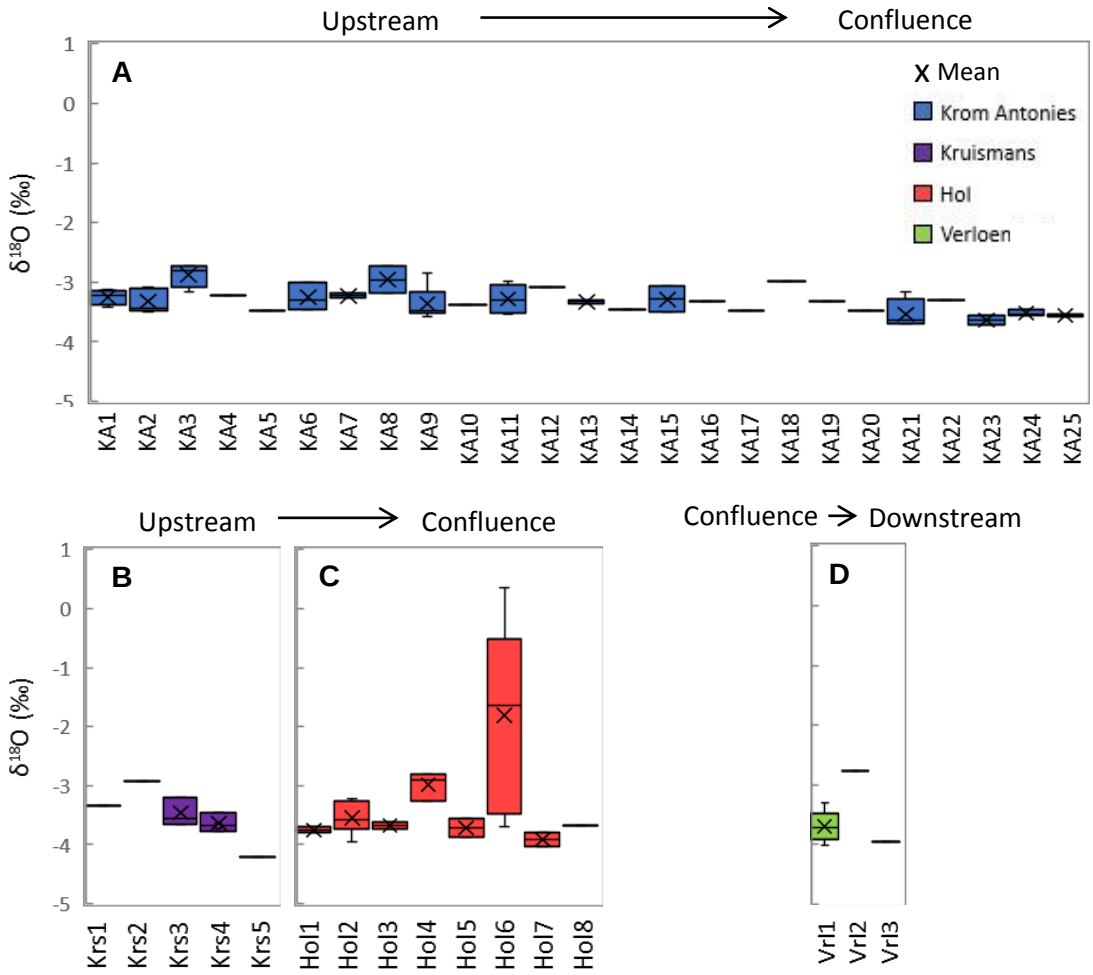

Figure 27: Statistical variations in δ18O ratios of deep groundwater over different sampling seasons along the Krom Antonies (a), Kruismans (b), Hol (c) and Verloren (d) rivers

The seasonal variations of δ^2H are depicted in Figure 28. In contrast to the lack of variation in $\delta^{18}O$ ratios, δ^2H ratios show a good spatial correlation along the Krom Antonies, with values increasing from the top to the bottom of the catchment. Groundwater originating in the upper Moutonshoek has more positive δ^2H ratios (approximately -15 to -9‰), which are comparative to the more negative δ^2H ratios of groundwater originating from the lower Krom Antonies (approximately -19 to -14‰). There is no seasonal correlation between individual boreholes. Kruismans and Hol groundwater shows no spatial or seasonal correlation in δ^2H ratios, with a maximum seasonal variation of 4.0‰ and 21.1‰ respectively. Hol groundwater shows the greatest variation in δ^2H ratios in the study area (21.1‰). A maximum variation of 18.9‰ occurs at Hol6 and accounts for the largest variation in the study area. δ^2H values at Hol6 show similar seasonal trend as for $\delta^{18}O$ ratios and EC values, where Sep ’15 > Nov ’15 > Nov ’16 > Jun ’15 > Jun ’16 > Mar ‘16

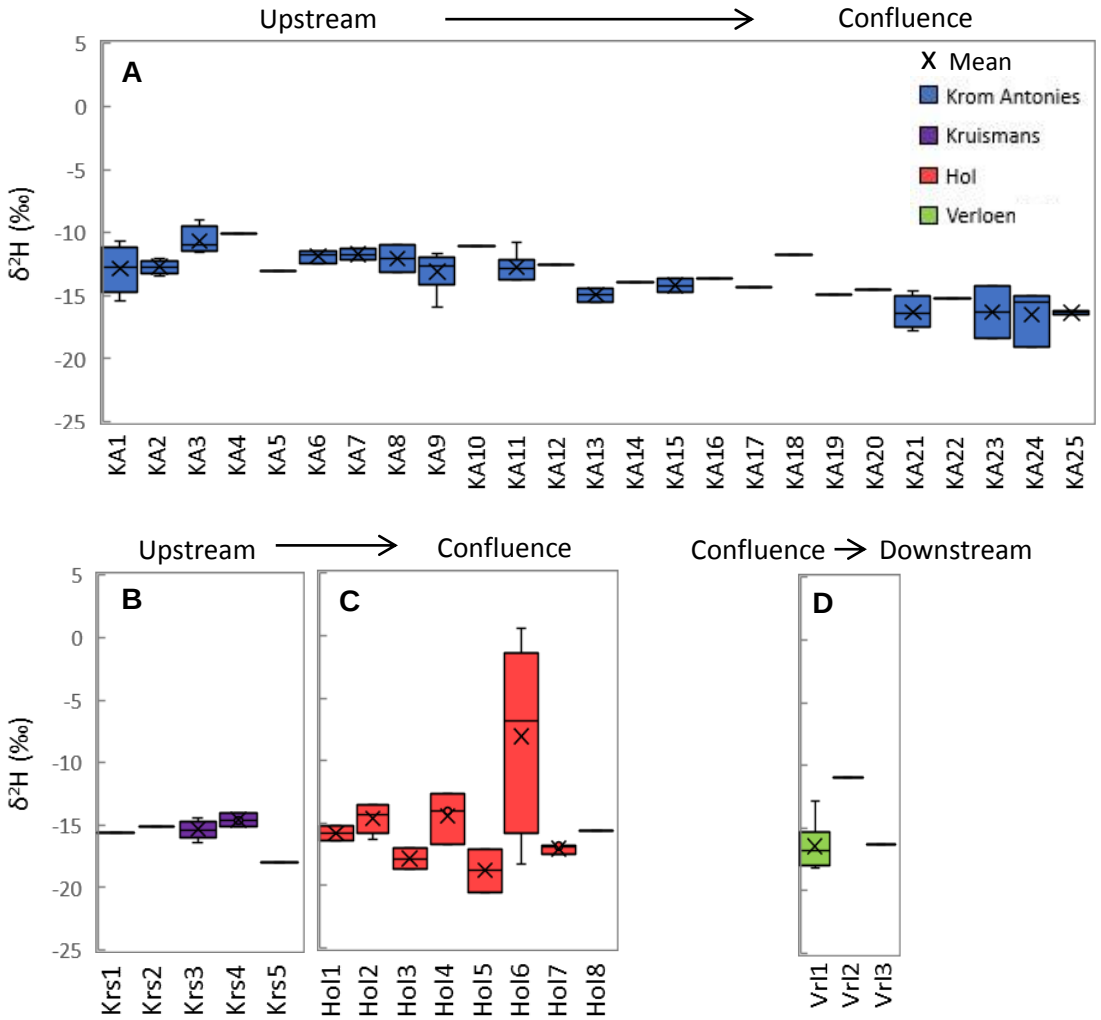

Figure 28: Statistical variations in δ^2H ratios of deep groundwater over different sampling seasons along the Krom Antonies (a), Kruismans (b), Hol (c) and Verloren (d) rivers

Seasonal variations in d values of groundwater are depicted in Figure 29. While δ^2H ratios vary considerably between the upper and lower catchment of the Krom Antonies, deuterium-excess values show much less spatial variation, with the upper catchment supporting d values of ~13.5‰, and the lower catchment ~12.0‰. However, boreholes KA1 to KA13 show a greater d range of 7.4‰, in comparison to boreholes KA14 to KA25, with a d range of 4.9‰. The Hol has three groundwater sites where d ~10‰ (Hol3, Hol4 and Hol5), which plot on the GMWL, as was noted in Figure 26. Hol6 shows the greatest variations in d across the study area, ranging from -2.23 to 14.51‰. The only negative d value in groundwater was sampled in September 2016 at Hol6, and correlates with the more positive δ^2H and $\delta^{18}O$ ratios.

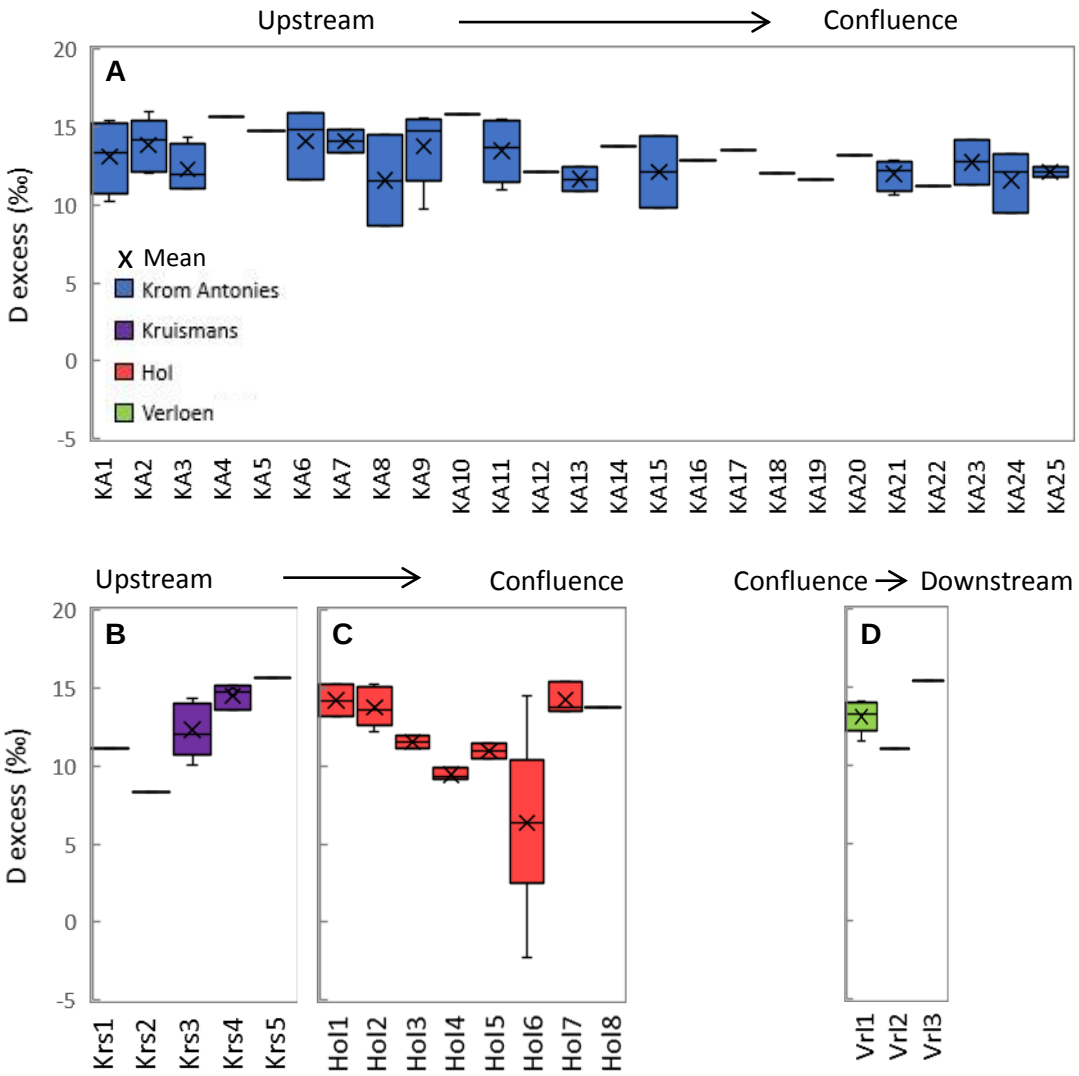

Figure 29: Statistical variations in the deuterium excess of deep groundwater over different sampling seasons along the Krom Antonies (a), Kruismans (b), Hol (c) and Verloren (d) rivers

6. DISCUSSION

6.1. Groundwater characterisation

6.1.1. Krom Antonies

Three types of deep groundwater occur along the Krom Antonies: a Ca^{2+}-HCO_3^- type in the upper-most catchment, and a Ca^{2+}-Mg^{2+}-Cl^- and Na^+-Cl^- type found in the middle and lower catchment (Table 13). This indicates a shift from calcium to sodium as the dominant cation, and bicarbonate to chloride as the dominant anion, as groundwater progresses down the catchment. Stable isotope data also indicates a distinct decrease in δ^2H ratios, and it is likely that groundwater recharged in the TMG of the Piketberg mountain range is mixing with other groundwater along its flow path. These spatial variations in stable isotope and major ion chemistry can be used to delineate groundwater zones along the Krom Antonies.

Table 13: Classification of groundwater types along the Krom Antonies

	Ca^{2+}-HCO_3^-	Ca^{2+}-Mg^{2+}-Cl^-	Na^+-Cl^-
KA1	x		
KA2	x		
KA3	x		
KA4		x	
KA5		x	
KA6		x	
KA7		x	
KA8		x	
KA9		x	
KA10		x	
KA11			x
KA12		x	
KA13			x
KA14		x	
KA15		x	
KA16			
KA17			x
KA18			x
KA19			x
KA20		x	
KA21			x
KA22		x	
KA23		x	
KA24			x
KA25		x	

Boreholes KA1 to KA3 have a Ca^{2+}-HCO_3^- type groundwater that is distinct from the rest of the catchment, and will be referred to as *Upper Krom Antonies*. Stable isotope ratios are further used to distinguish the *Upper Krom Antonies* from another distinct isotopic cluster.

Boreholes from the *Upper Krom Antonies* (KA1 to KA3), have more positive δ^2H ratios and greater variations in d (Figure 30). Alternatively, boreholes occurring in the lower reaches of the Krom Antonies (borehole KA19 to KA25) are characterised by a more negative δ^2H ratio and smaller variations in d (with an isotopic slope that runs parallel to the GMWL) (Figure 30). These boreholes have been termed the *Lower Krom Antonies,* and δ^2H ratios provide the tipping point between the *Upper Krom Antonies* (δ^2H ratios > -14.0‰) and *Lower Krom Antonies* (δ^2H ratios < -14.0‰). The only exception is sample KA1 from November 2015, originating in the *Upper Krom Antonies* with a δ^2H ratio of -15.4‰. Samples which show the same average isotopic signature as the *Upper Krom Antonies* but have chloride as the dominant anion have been termed the *Middle Krom Antonies* (Figure 30) and includes boreholes KA4 to KA18.

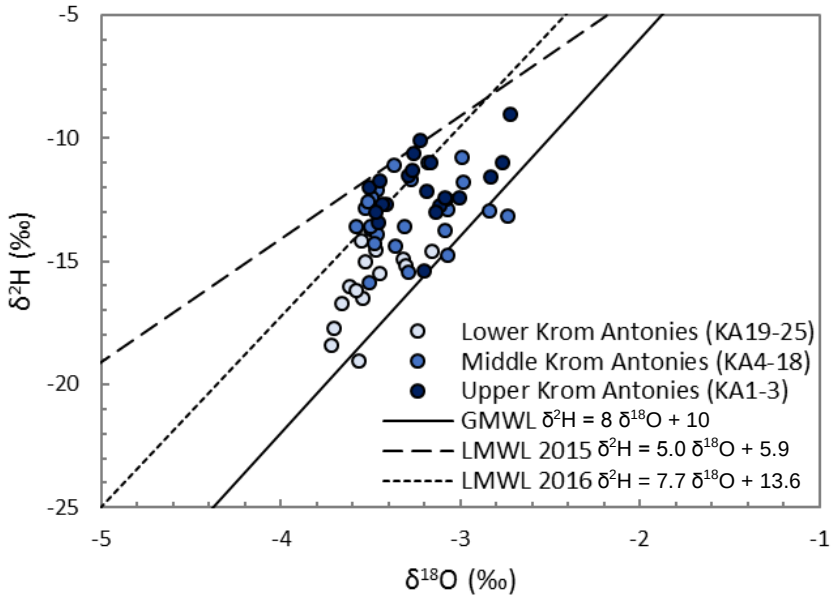

Figure 30: Stable isotope compositions of groundwater from the upper, middle and lower Krom Antonies, in comparison to the LMWL and GMWL

Figure 31 shows the delineated groundwater zones of the Krom Antonies based on major ion chemistry and δ^2H ratios.

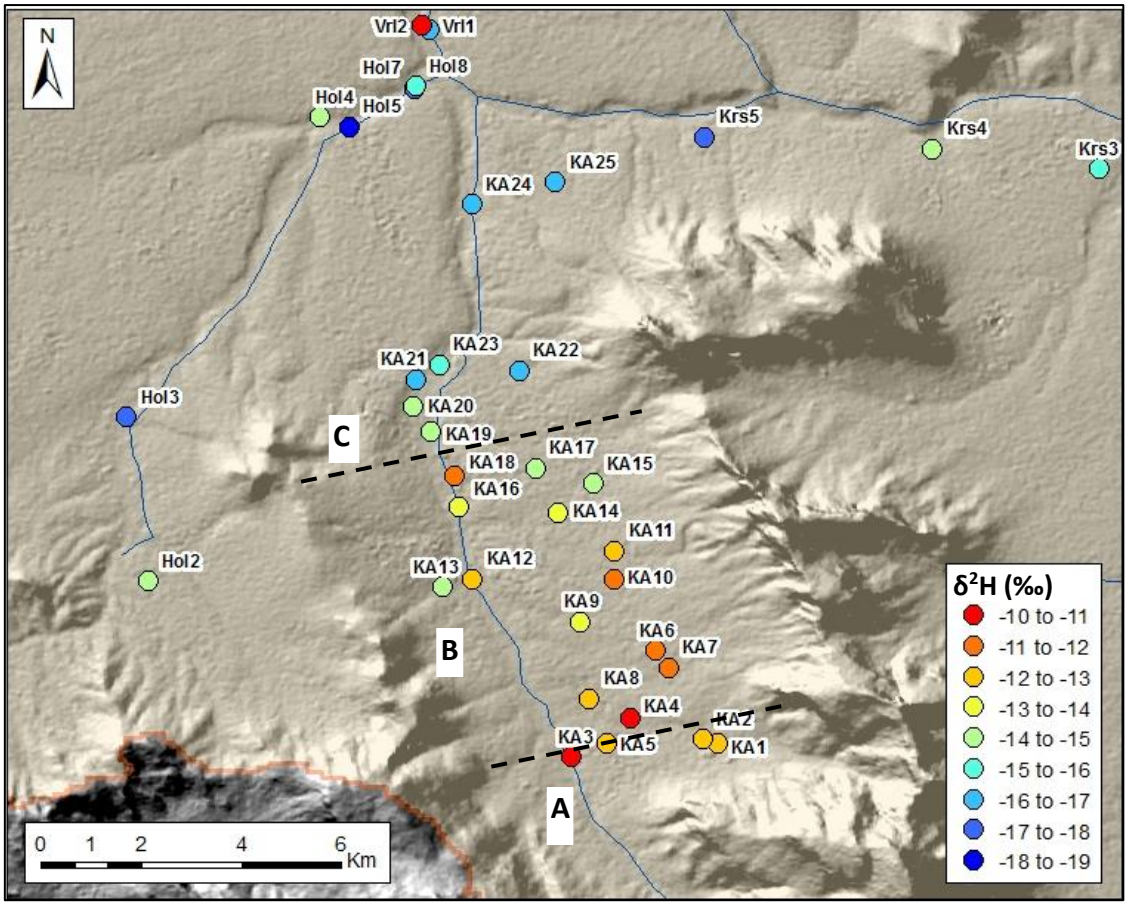

Figure 31: Delineation of groundwater zones along the Krom Antonies based on groundwater chemistry and δ^2H ratios, where A is the upper Krom Antonies, B the middle Krom Antonies, and C the lower Krom Antonies

6.1.1.2. Upper Krom Antonies

The only borehole in the *Upper Krom Antonies* that is known to be drilled into the TMG aquifer is located 180 metres south east of borehole KA1. It is therefore likely that boreholes KA1 to KA3 have been drilled through the TMG into the Malmesbury aquifer, and represent the nearest composition to TMG groundwater in the study area. TMG aquifers typically have a low salinity (10 - 100 mS/m) and low pH values (5.5 - 7), with groundwater being Na^+-Cl^- dominated (Smart and Tredoux, 2002). GEOSS (2012) and SRK (2009) both suggest that groundwater originating in the Piketberg mountain range is Na^+-Cl^- in nature. However, this study suggests that groundwater from the Malmesbury shale of the Upper Krom Antonies, which immediately underlies the TMG aquifer, is Ca^{2+}-HCO_3^- in nature. TMG groundwater in the study area is hosted in the Piekenierskloof formation (Watson *et al.*, 2017c), and an extensive groundwater study of the Olifants-Doorn catchment conducted by DWAF (2000) shows a compositional bimodality of groundwater from the Piekenierskloof formation which support a wide range of pH values (6.6 to 7.2) but similar EC values (<80 mS/m). Piper plots of DWAF (2000) show that while the majority of samples fom the Piekenierskloof formation are Na^+-Cl^- type, a fair

proportion plot on the Ca^{2+}-HCO_3^-/Ca^{2+}-Mg^{2+}-Cl^- zone. Vegter (1995) also showed that 40% of samples from the western limb of the TMG, where this study area is located, show a substantial increase in calcium and magnesium, in comparison to the rest of the TMG.

6.1.1.3. Middle Krom Antonies

The *Middle Krom Antonies* has an isotopic signature near identical to the *Upper Krom Antonies*, and is likely to have a similar source of recharge. However, the *Middle Krom Antonies* has higher EC values (Figure 32) and groundwater of Ca^{2+}-Mg^{2+}-Cl^- and Na^+-Cl^- composition, indicating the addition of salts, particularly sodium and chloride. Fractured shale aquifers are characterised by low permeability and groundwater flow velocities in comparison to sandstone aquifers, resulting in prolonged rock-water interaction (Domenico and Schwartz, 1990). In addition, most shale formations were deposited in saline environments, and limited flushing results in geological formations with a high concentration of adsorbed ions, and thus groundwater with greater dissolved ion concentrations (White *et al.*, 1963). Groundwater flow directions of the secondary aquifer in the Krom Antonies Valley follow the local topography (Watson *et al*., 2017a), with groundwater moving from the *Upper* to *Lower Krom Antonies.* Low flow velocities and increased rock-water interaction with the saline shales of the secondary aquifer is therefore likely to be a primary cause for the increase in salinity along the *Middle Krom Antonies*. Furthermore, satellite imagery of the catchment suggests that the TMG formation along the lower eastern limb of the Piketberg Mountain range dips away from the Krom Antonies catchment, resulting in increased recharge to the Kruismans basin (Figure 32). Little recharge may be directed to the Krom Antonies Valley, resulting in the accumulation of salts on the eastern part of the *Middle Krom Antonies* (Figure 32).

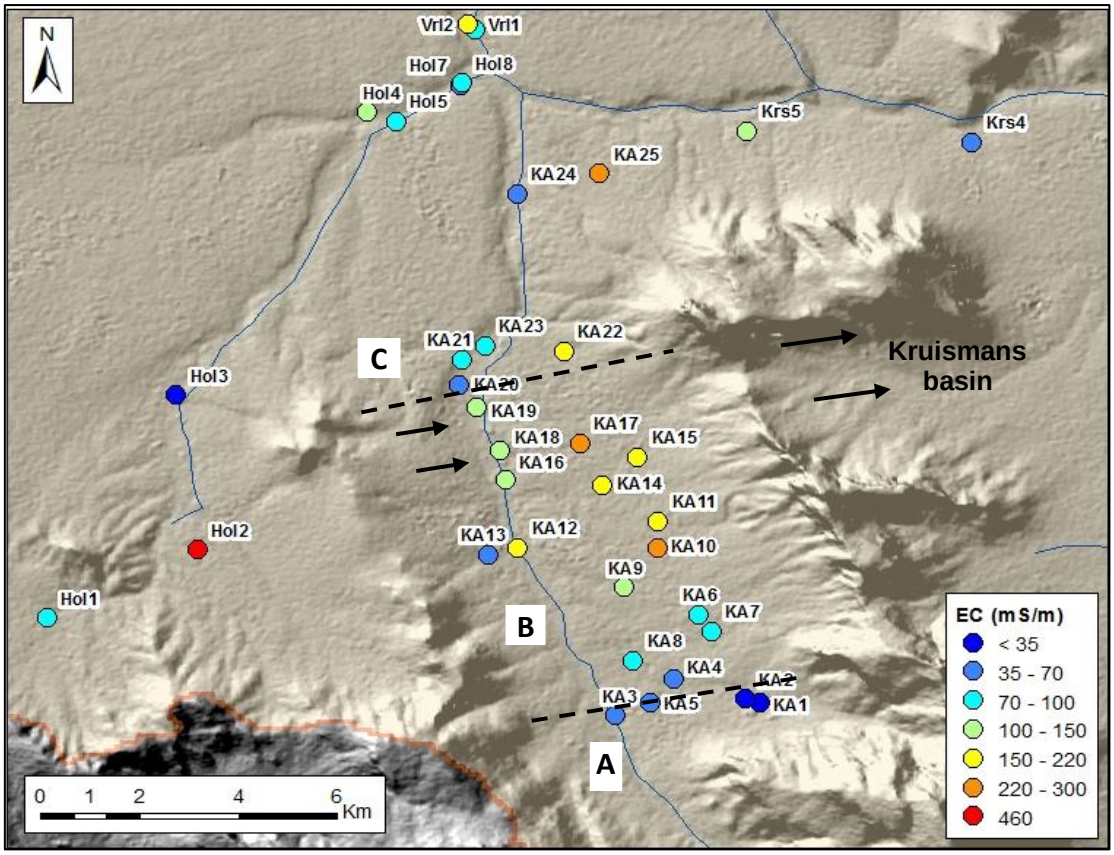

Figure 32: Spatial variation in EC values of groundwater where A is the upper Krom Antonies, B is the middle Krom Antonies, and C the lower Krom Antonies. Groundwater recharge direction in the Middle Krom Antonies in depicted

6.1.1.4. Lower Krom Antonies

Groundwater of the *Lower Krom Antonies* is characterised by δ^2H < -14.0‰, and the *Upper Krom Antonies* (δ^2H > -14.0‰) is therefore unlikely to be its primary source of recharge. Precipitation in the valley contributes little direct recharge to the secondary aquifer (Conrad *et al.*, 2004; Watson *et al*., 2017b), and is unlikely to contribute significantly to the decrease in δ^2H ratios of the *Lower Krom Antonies.* Shallow groundwater is also an unlikely source as samples from piezometers along the Krom Antonies river show δ^2H > -13.3‰ (Sigidi, 2017). Isotopic signatures of Hol groundwater (excluding isotopic outlier Hol6) are plotted against groundwater samples from the *Lower Krom Antonies* (Figure 33), and they show an almost identical isotopic signature. Furthermore, boreholes from the *Lower Krom Antonies* have an average EC value of 126 mS/m, indicating that the groundwater has picked up a significant amount of salts in comparison to the *Upper Krom Antonies*. Deep groundwater of the Hol has an average EC of 147 mS/m and hence groundwater mixing can geochemically account for the increase in EC and decrease in δ^2H and $\delta^{18}O$ ratios in the *Lower Krom Antonies*. Watson *et al.* (2017c) supports the influx of Hol groundwater near the confluence.

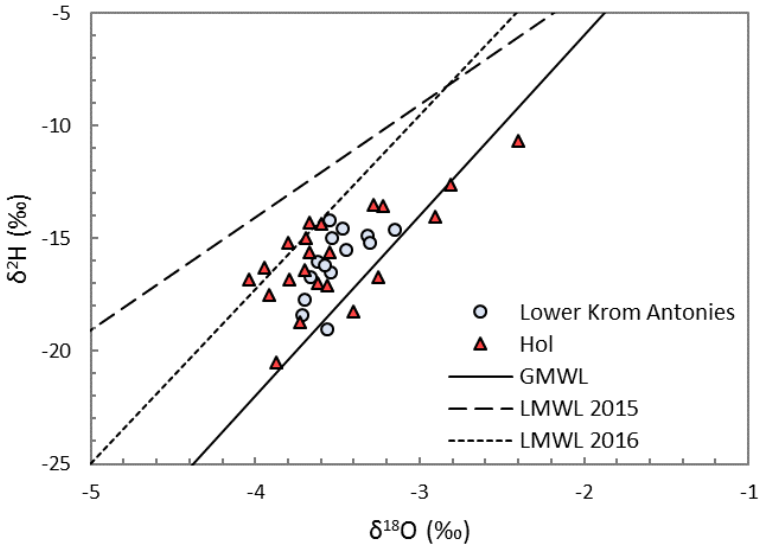

Figure 33: Groundwater from the lower Krom Antonies and Hol (excluding outlier Hol6), in comparison to the general LMWLs and GMWL

6.1.2. Hol

6.1.2.1. Hol2

The most saline groundwater in the study area occurs at Hol2 which lies just to the west of the Krom Antonies water shed, and derives groundwater from the same mountain range as the Krom Antonies (Watson *et al*., 2017a). However, the dip of the bedding planes along this mountain range direct most of the groundwater flow into the Krom Antonies catchment to the east (Figure 32), with little groundwater draining to the west (Watson *et al*., 2017a), resulting in the accumulation of salts at Hol2. The boreholes to the east of this watershed divide are comparatively less saline due to higher recharge (Figure 32). Similar saline conditions do not occur at Hol1 and Hol3, which have similar borehole depths to Hol2. They are situated outside of the boundaries of the Piketberg Mountain range (Figure 32), and are likely to not be effected by this local saline hotspot. GEOSS (2006) indicates the same zone of salinisation at Hol2.

6.1.2.2. Hol6

Borehole Hol6 shows the largest geochemical fluctuations in the catchment, with EC values more than doubling in summer (September and November) compared to winter (March and June), and stable isotope ratios following the same seasonal trends. Hol6 is utilised as a primary borehole for irrigation, with pumping commencing around November and continuing until March. It is therefore possible that water level draw-down induced by pumping during these months will result in the inflow of additional groundwater sources.

Meteoric waters typically have lower δ^2H and $\delta^{18}O$ ratios than evaporative systems, such as lakes and soil water, which are enriched in heavier isotopes (Gat, 1996), and evaporative sources could contribute to the positive stable isotope ratios noted at Hol6. Stable isotope ratios of shallow groundwater from the Hol primary aquifer (Sigidi, 2017) are compared to stable isotope ratios of borehole Hol6 (Figure 34). A near identical evaporation trend is observed for the shallow groundwater ($\delta^2H = 4.41\ \delta^{18}O + 0.28$) and Hol6 ($\delta^2H = 4.64\ \delta^{18}O + 0.31$). Shallow groundwater δ^2H ratios range between -20.6‰ and +2.0‰ (Sigidi, 2017), and are comparable to δ^2H ratios of Hol6. Furthermore, shallow groundwater samples from the Hol have an average EC of 740 mS/m (Sigidi, 2017). It is therefore likely that prolonged pumping of the secondary aquifer in the summer months results in significant drawdown and subsequent discharge from the primary to the secondary aquifer through the semi-pervious layer, characteristic of a leaky aquifer (Sayed and Hussainy, 2011). This would account for the anomalous EC and stable isotope ratios at Hol6 in September and November.

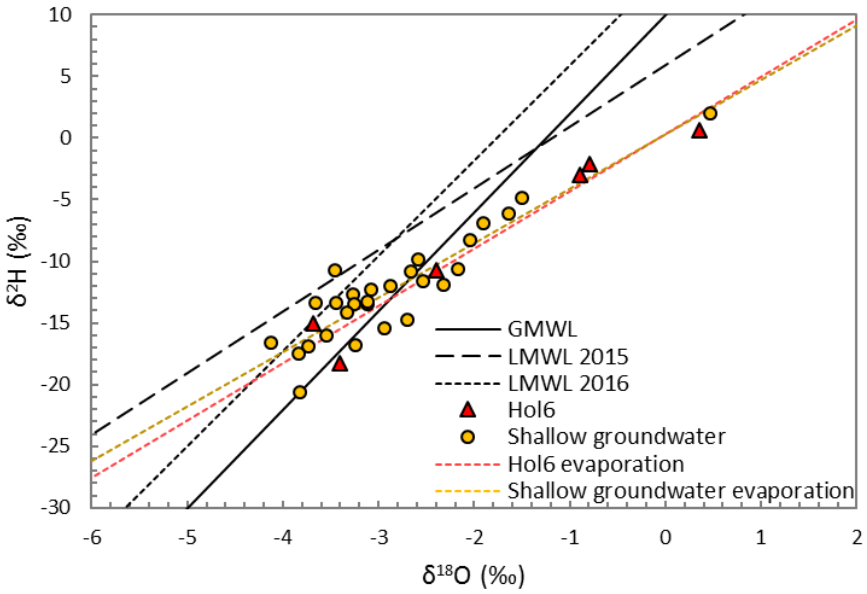

Figure 34: Deep groundwater samples from Hol6 in comparison to shallow groundwater samples from the Hol and confluence. Shallow groundwater data is from Sigidi (2017)

Similar seasonal variations are not apparent at Hol7 and Hol8, which are located within 60 metres from Hol6 and have a similar borehole depth. Hol7 is used for household purposes and Hol8 for small-scale irrigation from January to April, and are small water consumers in comparison to Hol6. This indicates that Hol6, although 130 metres in depth, may be in better hydraulic contact with the shallow aquifer than surrounding deeper aquifer system.

6.1.3. Kruismans

Borehole Krs4 is situated on the Redelinghuys fault and boundary between the flat plains of the Kruismans basin and sandstone formations of the TMG. Although Krs4 has a depth of 285

meters, similar chemistry to the surrounding boreholes indicates a similar source. Boreholes Krs1 to Krs3 have low EC values (< 102 mS/m), and are situated in the Kruismans basin. They present an interesting scenario, as the lack of local topography could support weak local flow systems, which has been shown elsewhere to result in stratified groundwater, and increased water-rock interaction and the accumulation of salts (Dahl *et al.*, 2007). This however is not the case, as EC values of Krs1 to Krs4 are comparable to the fresh *Upper Krom Antonies*. Furthermore, the high average ORP values (~120 mV) indicate that the groundwater has had recent contact with the atmosphere and has been recently recharged. Krs1 to Krs4 are the only boreholes in the study area situated in quaternary catchment G30B, which corresponds to a different GRU to G30D (GEOSS, 2006). This is particularly evident at Krs1 and Krs2, which show a clear increase in HCO_3^- in comparison to Krs3 to Krs5. This indicates a transition from HCO_3^- to Cl^- as groundwater moves towards the confluence. The source of recharge for the Kruismans secondary aquifer has not been quantified.

The effects of salinisation from the local shale are seen on the shallow groundwater samples of the Kruismans, which have an average EC of 746 mS/m (Sigidi, 2017). The significantly more fresh deep groundwater suggests that little interaction occurs between the primary and secondary aquifer of the Kruismans, and salinization of the secondary by the primary aquifer is not a cause for concern.

6.1.4. Verloren

The deep groundwater of the upper Verloren (sampled in this study) shows a similar isotopic and chemical signature to the deep groundwater of Hol and lower Krom Antonies. Groundwater studies along the lower Verloren River (beyond the boundaries of this study area) indicate that TDS concentrations vary between 500 and 3500 mg/L, with a chemical composition similar to diluted sea water (Maclear, 1994; Harck, 1995). It is therefore likely that additional salinisation occurs as groundwater progresses towards the coast, and is a cause of concern for the health of the wetlands.

6.2. Rain water characterisation

The El Niño-Southern Oscillation (ENSO) is a key role player for drought severity in the Western Cape, as most of the severe droughts have typically taken place during El Niño years (Araujo *et al.*, 2016). This is particularly evident during the rainy season, where the variation in sea-surface temperature (SST) and high pressure systems result in low rainfall and droughts in southern Africa (Camberlin *et al.*, 2001). El Niño years are also characterised by high temperatures in addition to low rainfall (Meque and Abiodun, 2015).

The El Niño event of 2015/2016 was one of the strongest recorded in history, taking place between spring (~September) 2015 and autumn (~March) 2016, with a weak El Niño occurring in 2014 (Lian *et al.*, 2017). This is apparent in the results presented in this study, where all collection points received on average 28% less rainfall in 2015 when compared to 2016, particularly for the winter months. The total annual rainfall for 2015 at KK-R was the lowest recorded since 2003, while 2016 was only slightly below average (Watson *et al*., 2017b).

6.2.1. Chloride composition

Precipitation amount and chloride concentration show a good correlation, with higher rainfall events having lower chloride values. This is attributed to the dilution of aerosol particles during higher rainfall events.

Weighted mean chloride values for the daily collectors show a maximum variation of 1.37 mg/L from one another, suggesting that they have a similar rainfall source. However, cumulative collector M-R has a significantly higher chloride content. Dry deposition and dust pollution on the Picketberg Mountain range is less than in the valley, and all rainfall collectors are made of the same material. This suggests that precipitation falling on the mountain does have a higher chloride content than precipitation in the valley.

6.2.2. Isotopic composition

The main factors that influence stable isotopic composition in precipitation are the amount of precipitation, continentality, temperature and altitude (Dansgaard, 1964; Mazor, 1991). There is also a possibility that water vapour originating from the Atlantic or Indian ocean may influence isotopic compositions, but this is unlikely to effect the west coast where most precipitation is derived from the Atlantic ocean (Diamond and Harris, 1997). The effects of altitude are apparent at M-R (elevation of 620 metres). Isotopic composition of precipitation at M-R is more depleted than the weighted averages for the daily rainfall collectors, and can be explained by the altitude effect, where the drop in temperature with increasing altitude results in condensation and isotopic depletion (Gat, 2001).

The amount effect implies that large quantities of rain have lower isotopic ratios, due to the rain-out effect of heavier isotopes, and less evaporation during the rainfall event (Dansgaard, 1964). Results show that this correlation does exist for both sampling years, albeit weak. On the other hand, seasonal variation shows a greater influence on stable isotope composition. Seasonal variability is a complex process influenced by numerous factors including temperature, humidity, source of the moisture, storm trajectories and convection patterns (Gat, 1983). The lowest $\delta^{18}O$ and $\delta^{2}H$ ratios are observed around the months of July and August,

which correspond to the coldest months in the study area (Schulze *et al.*, 2008), and thus produce precipitation with the lowest isotopic compositions. These strong seasonal variations are typical of temperate climates (Gat, 2001). Higher isotopic ratios are also recorded in 2015, and this is due to the effects of El Niño, where precipitation has been previously documented as having an isotopic signature that is heavier by 2‰ (Suwarman *et al.*, 2017).

Most arid regions show a LMWL slope < 8, as the secondary evaporation of falling droplets results in precipitation that does not represent the in-cloud composition (Gat, 2001). The general LMWL in this study is nearly identical to the Cape Town LMWL, collected from 12 years of data, where $\delta^2H = 6.41\ \delta^{18}O - 8.66$ (Harris *et al.*, 2010). However, the LMWL of 2015 and 2016 show significant differences, where 2016 shows a slight evaporation trend (slope = 7.73) and 2015 a far more pronounced evaporation trend (slope = 5.00). This is likely due to the El-Niño effects in 2015, which showed a particularly strong correlation with increasing temperature (Meque and Abiodun, 2015), and thus in-cloud evaporation. The lower d values for 2015 (~3.1‰ less than in 2016) are also attributed to the El-Niño effects, and Sánchez-Murillo *et al.* (2017) shows a similar increase in d (~3.6‰) from 2015 to 2016.

6.3. Recharge estimation using the CMB technique

Deep groundwater sites along the Krom Antonies are used for CMB recharge estimates, as the Krom Antonies is likely to represent the most recently recharged groundwater in the study area. Rainfall collector KA-R2 will be used to estimate recharge at boreholes in the *Upper Krom Antonies,* KK-R for boreholes in the *Middle Krom Antonies* and VL-R for boreholes in the *Lower Krom Antonies* (Figure 35). Chloride values from mountain collector M-R will also be used for recharge estimations in the *Upper Krom Antonies*, in order to assess the contibution of TMG groundwater to the secondary aquifer.

Long-term rainfall records are not available for all the rainfall collectors, and it is therefore necessary to use the rainfall values collected in 2016, as 2015 presents an anomalously dry year. The only limitation is that such a method will provide time specific recharge estimations. KA-R2 and VL-R rainfall values in 2016 show a good validation against AWS records, and therefore the annual total is reliable. Although rainfall was only collected at M-R from March to December in 2016, KA-R2 shows that 94% of the annual precipitation fell during this time frame. Using this percentage and the 330mm recorded at M-R, the assumption is made that the total annual rainfall for 2016 at M-R was 350mm. This agrees with Lynch (2004) who indicates that MAP at the location of KA-R2 is 125mm more than at the location of M-R.

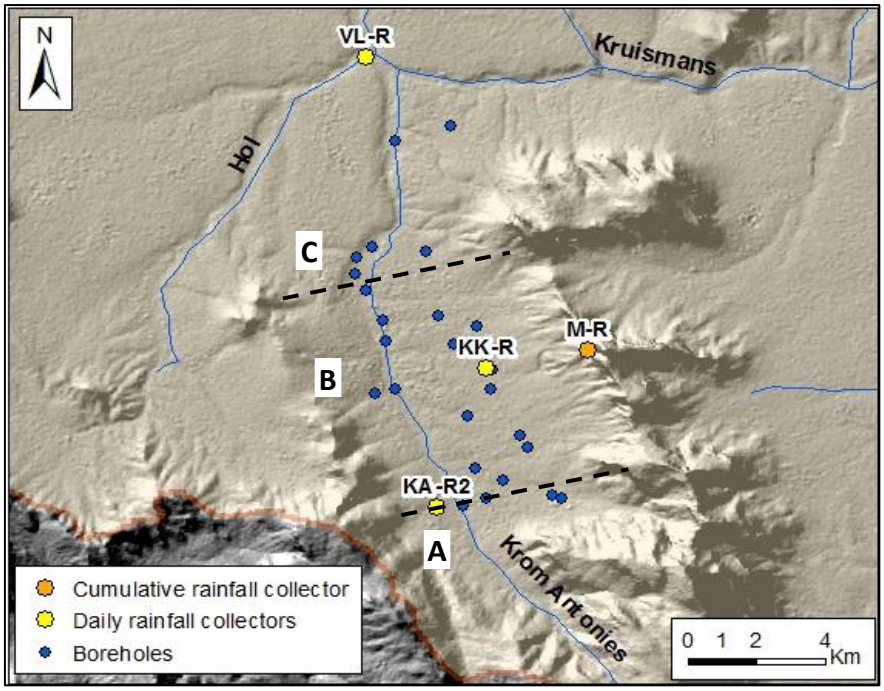

Figure 35: Rainfall collectors and boreholes used for recharge estimation, where A is the Upper Krom Antonies, B is the Middle Krom Antonies, and C is the Lower Krom Antonies

The CMB equation is used to calculate recharge, where P is annual precipitation, Cl_p the chloride concentration of rain water, and Cl_{gw} the chloride concentration of groundwater.

$$R = \frac{P \times Cl_p}{Cl_{gw}}$$

6.3.1. Recharge estimates

CMB calculations presented in Table 14 show the distribution of recharge estimates across the Krom Antonies catchment. Weighted average chloride concentrations of rain water for the whole sampling season, and average chloride concentrations of groundwater for the whole sampling season, are used as input values. These estimates are compared to recharge estimates by Watson *et al.* (2017b), underlined and presented above each rainfall collector.

The highest recharge estimates are calculated in the *Upper Krom Antonies*, and range between 20.0 and 26.6 mm/a (4.2 – 5.6%) and 40.0 to 53.0 mm/a (11.4 – 15.2%) for M-R and KA-R2 respectively. The highest recharge is calculated at KA1, followed by KA2 and KA3. These values correspond well with estimates by Watson *et al.* (2017b), particularly for borehole KA1. The recharge values decrease substantially in the *Middle Krom Antonies,* which range between 2.1 and 9.1 mm/a (0.5 – 2.1%), and the *Lower Krom Antonies,* which range between 1.8 and 8.6 mm/a (0.7 – 3.3%). These do not agree with estimates by Watson *et al.* (2017b), and support the additional input of salts in the *Middle* and *Lower Krom Antonies*,

which are likely to be distorting these estimates. Boreholes KA2 and KA3, which are situated slightly further down the catchment than KA1 (Figure 32), could also be effected by the additional input of salts. This would account for borehole KA1 producing the highest estimates that are most like Watson *et al.* (2017b). Recharge estimates from the *Upper Krom Antonies* suggest that the recharge that the TMG contributes ~48 mm/a to the secondary aquifer (represented by M-R), which is twice the amount of ~24 mm/a that direct infiltration in the valley contributes to recharge (represented by KA-R2).

Table 14: Spatial distribution of CMB calculations for the Krom Antonies, with recharge estimates of Watson et al. (2017b) presented above each collector

					8.0%		16.6%	
					KA-R2		M-R	
		#samples	Cl_{gw} (mg/L)		44		1	# samples
					2.61		7.1	Cl_p (mg/L)
					477		350	P (mm)
Upper Krom Antonies	KA1	4	46.9		26.6 mm/a	*5.6%*	53.0 mm/a	*15.2%*
	KA2	5	48.7		25.6 mm/a	*5.4%*	51.0 mm/a	*14.6%*
	KA3	4	62.3		20.0 mm/a	*4.2%*	40.0 mm/a	*11.4%*

					12.5%		5.4%	
					KK-R		VL-R	
		#samples	Average Cl_{gw} (mg/L)		20		29	# samples
					2.73		3.98	Cl_p (mg/L)
					426		259	P (mm)
Middle Krom Antonies	KA4	1	127.6		9.1 mm/a	*2.1%*		
	KA5	1	128.2		9.1 mm/a	*2.1%*		
	KA6	3	175.7		6.6 mm/a	*1.6%*		
	KA7	2	192.7		6.0 mm/a	*1.4%*		
	KA8	2	216.0		5.4 mm/a	*1.3%*		
	KA9	6	260.8		4.5 mm/a	*1.0%*		
	KA10	1	519.4		2.2 mm/a	*0.5%*		
	KA11	6	472.4		2.5 mm/a	*0.6%*		
	KA12	1	467.3		2.5 mm/a	*0.6%*		
	KA13	2	199.7		5.8 mm/a	*1.4%*		
	KA14	1	367.4		3.2 mm/a	*0.7%*		
	KA15	2	418.7		2.8 mm/a	*0.7%*		
	KA16	1	247.5		4.7 mm/a	*1.1%*		
	KA17	1	564.8		2.1 mm/a	*0.5%*		
	KA18	1	292.6		4.0 mm/a	*0.9%*		
Lower Krom Antonies	KA19	1	325.2				3.2 mm/a	*1.2%*
	KA20	1	119.5				8.6 mm/a	*3.3%*
	KA21	4	265.9				3.9 mm/a	*1.5%*
	KA22	2	447.2				2.3 mm/a	*0.9%*
	KA23	1	241.1				4.3 mm/a	*1.7%*
	KA24	3	174.0				5.9 mm/a	*2.3%*
	KA25	2	576.6				1.8 mm/a	*0.7%*

The impact of seasonal variations in groundwater chloride concentrations from the *Upper Krom Antonies* on recharge estimates at KA-R2 and M-R are presented in Table 15. Weighted average chloride values of all rainfall sampled at KA-R2 is used as an input parameter. Borehole KA1 shows the maximum seasonal variation in CMB estimates. This range is 16.9

mm/a at M-R, which translates to 31% of the average recharge value for KA1. Similarly, this range is 8.5 mm/a for KA-R2, which translates to 32% of the average recharge value for KA1. While seasonal groundwater variations do impact the CMB estimates, particularly for the low chloride concentrations at KA1, this impact is < 33% of the final value.

Table 15: The influence of seasonal groundwater variability on CMB estimates in the Upper Krom Antonies

		Cl_{gw} (mg/L)	KA-R2		M-R		
			44		1		# samples
			2.61		7.1		Cl_p (mg/L)
			477		350		P (mm)
KA1	AVERAGE	46.9	**26.6 mm/a**	***5.6%***	**53.0 mm/a**	***15.2%***	
	Nov '16						
	Jun '16	40.6	30.7 mm/a	*6.4%*	61.2 mm/a	*17.5%*	
	Mar '16	49.6	25.1 mm/a	*5.3%*	50.1 mm/a	*14.3%*	
	Nov '15	41.1	30.3 mm/a	*6.4%*	60.5 mm/a	*17.3%*	
	Sep '15						
	Jun '15	56.1	22.2 mm/a	*4.7%*	44.3 mm/a	*12.7%*	
KA2	AVERAGE	48.7	**25.6 mm/a**	***5.4%***	**51.0 mm/a**	***14.6%***	
	Nov '16						
	Jun '16	47.2	26.4 mm/a	*5.5%*	52.6 mm/a	*15.0%*	
	Mar '16	50.0	24.9 mm/a	*5.2%*	49.7 mm/a	*14.2%*	
	Nov '15	48.2	25.8 mm/a	*5.4%*	51.6 mm/a	*14.7%*	
	Sep '15	45.0	27.7 mm/a	*5.8%*	55.2 mm/a	*15.8%*	
	Jun '15	53.0	23.5 mm/a	*4.9%*	46.9 mm/a	*13.4%*	
KA3	AVERAGE	62.3	**20.0 mm/a**	***4.2%***	**40.0 mm/a**	***11.4%***	
	Nov '16						
	Jun '16	61.3	20.3 mm/a	*4.3%*	40.5 mm/a	*11.6%*	
	Mar '16	60.3	20.6 mm/a	*4.3%*	41.2 mm/a	*11.8%*	
	Nov '15						
	Sep '15	57.5	21.7 mm/a	*4.5%*	43.2 mm/a	*12.3%*	
	Jun '15	69.9	17.8 mm/a	*3.7%*	35.6 mm/a	*10.2%*	

The effects of varying chloride concentrations for different rainfall events on recharge estimates are presented for daily rainfall collector KA-R2 and *Upper Krom Antonies* groundwater in Table 16. Rainfall values from one year of data at KA-R2, 1 October 2015 to 30 September 2016, have been used for input into the table. The highest recharge estimates are calculated using the mean chloride concentrations in rain water, i.e. not weighted average. Alternatively, the lowest estimates are calculated using the mean chloride values from rainfall events >20 mm. This indicates the dilution effect of aerosol particles for high rainfall events. These are however both unrealistic scenarios, as rainfall events < 20mm are also likely to contribute to recharge, but larger rainfall events will still contribute the most. The weighted average concentration of chloride in rainfall is therefore likely to be the most representative of chloride contribution to groundwater. The weighted average recharge estimate for KA1 is 5.6%, and falls between the estimate of 7.4% for rainfall events > 5mm, and the estimate of 4.3% for rainfall events > 10mm. Watson *et al.* (2017b) estimated a recharge value of 8.0% at

KA-R2, indicating that rainfall events > 5mm might contribute the bulk of recharge to the secondary aquifer.

Table 16: The effects of varying chloride values of different rainfall events on the CMB estimates of boreholes in the Upper Krom Antonies

	Rainfall event	# samples	Cl_p (mg/L)	P (mm)	KA1		KA2		KA3	
					4		5		4	# samples
					46.9		48.7		62.3	Cl_{gw} (mg/L)
KA-R2	**Weighted average**	**34**	**2.6**	**414.6**	**23.2 mm/a**	**5.6%**	**22.4 mm/a**	**5.4%**	**17.5 mm/a**	**4.2%**
	All rainfall average	34	4.3	414.6	38.1 mm/a	9.2%	36.6 mm/a	8.8%	28.6 mm/a	6.9%
	> 5 mm average	20	3.5	372.0	27.7 mm/a	7.4%	26.6 mm/a	7.2%	20.8 mm/a	5.6%
	> 10 mm average	12	2.0	308.5	13.3 mm/a	4.3%	12.8 mm/a	4.2%	10.0 mm/a	3.3%
	> 15 mm average	8	2.1	258.5	11.5 mm/a	4.4%	11.0 mm/a	4.3%	8.6 mm/a	3.3%
	> 20 mm average	6	1.0	220.5	4.5 mm/a	2.0%	4.3 mm/a	2.0%	4.7 mm/a	2.1%

6.3.2. Comparison to other studies

Conrad *et al.* (2004) used a GIS-based approach to estimate recharge in the Sandveld, based on the parameters of lithology and rainfall. Conrad *et al.* (2004) estimates recharge at KA-R2 to be 1.4 mm/a, significantly less than the estimate for this study. Additionally, Conrad *et al.* (2004) estimates recharge at M-R to 80.1 mm/a, comparatively more than the estimation for this study. Although recharge estimates by Conrad *et al.* (2004) at KK-R (3.1 mm/a) and VL-R (0.8 mm/a) correspond well with the estimates of this study, it is known that these CMB estimates in this study are unlikely to represent true recharge due to the influx of salts in groundwater. DWAF (2004) calculated a recharge value of 28% in the mountains, and 5% at the base of the mountains, using the CMB method in the northern part of the catchment. These results are comparable to the estimates in this study.

Recharge estimates at M-R are slightly lower in comparison to TMG recharge estimates by Hay and Hartnady (2002), who estimated a spatial average of ~23% to the TMG aquifer in the Citrusdal area (located ~30 km from this study area). This could be due to the lower annual rainfall in catchment, where Parson (2002) suggests that TMG recharge of greater than 20% only occurs in areas where rainfall exceeds 600 mm/a.

6.4. Groundwater recharge mechanisms

CMB recharge estimates in the *Upper Krom Antonies* show that the TMG (represented by M-R) contributes twice the recharge to the secondary aquifer than localised recharge (represented by KA-R2) does. Watson et al. (2017b) shows a similar 2:1 ratio. When this ratio is applied to the average stable isotope compositions at M-R and KA-R2, the predicted groundwater isotopic signature of the *Upper Krom Antonies* is -13.6 for δ^2H and -3.79 for $\delta^{18}O$,

with a d value of 16.7‰ (Figure 36). This correlates well with actual groundwater isotopic ratios of the *Upper Krom Antonies*, supporting the fact the TMG contributes the most recharge to the secondary aquifer. The actual average d value is 13.1‰, and more negative in comparison to the predicted value. This indicates that evaporative losses have occurred before infiltration, through the processes of plant interception, streamflow, surface retention, evapotranspiration and runoff (Gat and Dansgaard, 1972), resulting in heavier isotope enrichment (Geyh, 2001). Modelled potential evaporation by Watson *et al.* (2017b) assigns an average value of 2 mm/day for the upper catchment during rainfall events, supporting the idea of evaporation before infiltration. The presence of these evaporative losses suggest that a combination of macropore diffusion and focussed recharge are at play in the catchment (Wood and Stanford, 1995).

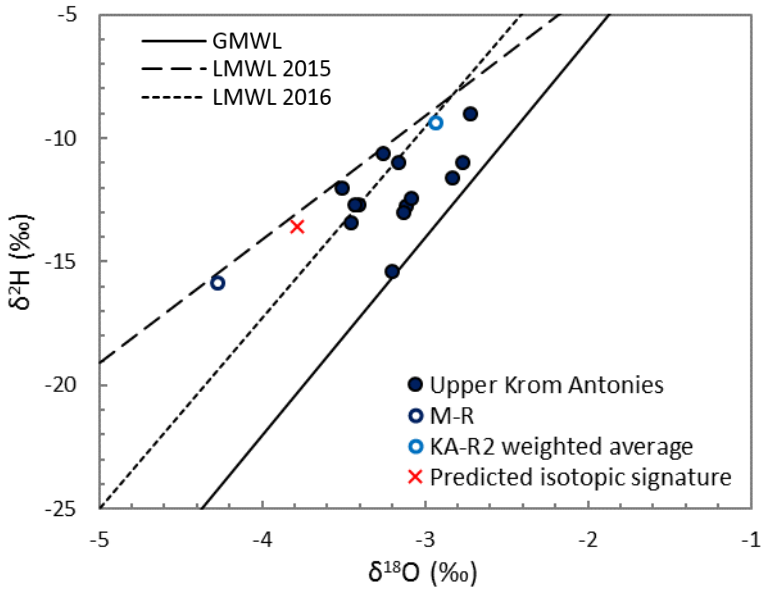

Figure 36: Weighted stable isotope ratios of rainfall collectors KA-R2 and M-R in comparison to boreholes KA1 to KA7. The predicted groundwater stable isotopic signature is caculated from the 2:1 ratio for recharge at M-R and KA-R2 respectively

6.4.1. Conceptual model of groundwater flow

A conceptual model of groundwater recharge for the Krom Antonies, in respect to the boreholes and rainfall collectors, is presented in Figure 37.

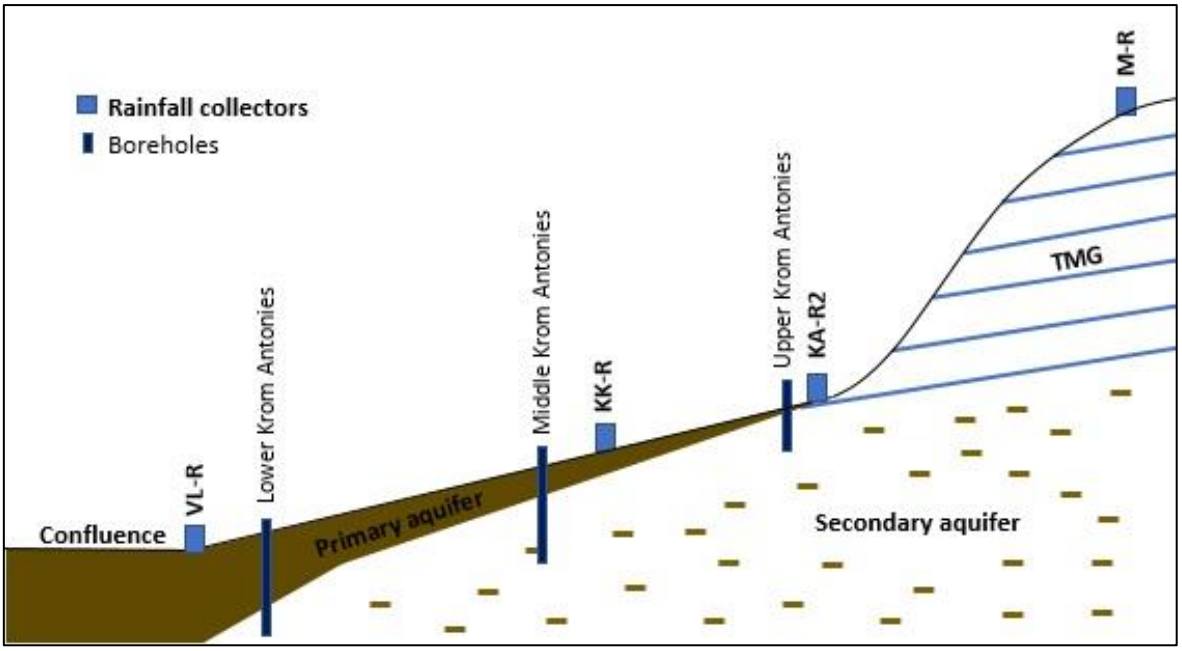

Figure 37: Conceptual model of recharge along the Krom Antonies

The primary aquifer is thin in the *Upper Krom Antonies* (Figure 37), and recharge from the TMG, and direct recharge to the secondary aquifer are likely to be the primary mechanisms, with CMB results indicating that the TMG contributes the most. While CMB recharge estimates in the *Middle Krom Antonies* are not reliable due to the influx of additional salt from the Malmesbury shale, stable isotope compositions indicate that the *Upper* and *Middle Krom Antonies* have similar recharge sources (Figure 30). Comparison between groundwater of the secondary and primary aquifer (Sigidi, 2017) originating in the *Upper* and *Middle Krom Antonies* indicate that the primary and secondary aquifers in the *Middle* and *Upper Krom Antonies* have a similar composition (Figure 38). This suggests that the high recharge to the secondary aquifer in the *Upper Krom Antonies* recharges the primary aquifer, contributing to baseflow in the form of a gaining stream. This would account for the lower EC values (~133 mS/m) of shallow groundwater along the Krom Antonies, comparatively less than the Hol (~740 mS/m) and Kruismans (~746 mS/m) (Sigidi, 2017).

The thick primary aquifer at the Lower Krom Antonies (Figure 37) implies minimal direct recharge to the Malmesbury aquifer, and stable isotope signatures indicate that the TMG aquifer also contributes little recharge (Figure 38). The Hol and Lower Krom Antonies groundwater has a more negative isotopic signature and recharge is likely to have occurred more inland or at higher altitudes (Breitenbach *et al.*, 2010). This groundwater would have longer flow paths, resulting in the smoothed isotopic signatures that are similar to the GMWL, as groundwater transitions through the aquifer (Gat, 1974). This is distinct from the *Upper Krom Antonies*, where the large isotopic variations represent the variations of local rainfall.

Deep groundwater from the *Lower Krom Antonies* is likely to contribute very little recharge to the shallow aquifer, as shallow groundwater has a more positive isotopic signature than its deep counterpart (Figure 38). Hol6 also shows the effects of pumping-induced recharge in the summer, where shallow groundwater contributes a fair portion of recharge to the deep aquifer. The *Lower Krom Antonies* and Hol can therefore be characterised as a losing stream.

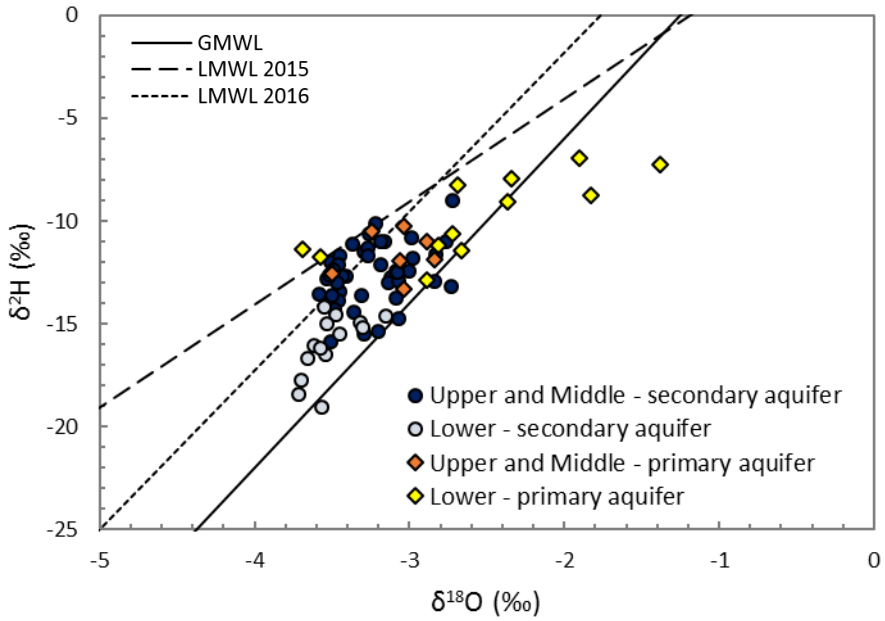

Figure 38: Deep groundwater from the Upper and Middle Krom Antonies, and Lower Krom Antonies, in comparison to shallow groundwater from the Upper and Middle Krom Antonies, and Lower Krom Antonies. Shallow groundwater data is from Sigidi (2017)

6.4.2. Implications for using the CMB technique in semi-arid areas

The CMB estimates correlate well with independent, physical methods from Watson *et al*. (2017b). The methodology for ground and rain water sampling presented in this study can be used to create a filtering technique for CMB input parameters. Major ion chemistry and stable isotopes are the main tools used, and provide easy recharge estimation in semi-arid catchments where groundwater salinisation is common and physical data is not always easily accessible.

The good spatial resolution and distribution of sampling points over the Krom Antonies catchment, and the good temporal variation over six sampling seasons, makes the methodology for delineating groundwater zones particularly robust. This study supports the fact that groundwater in the upper catchment is typically the least saline and most representative of recent recharge, and can sometimes be defined by a distinctly different groundwater type, as was the case for the *Upper Krom Antonies*. An increase in salinity only, while stable isotope ratios remain constant, indicate the same groundwater source, but where

salts have been added through water-rock interaction or low flushing of salts (e.g. the *Middle Krom Antonies*), and this groundwater is unsuitable for CMB calculations. Alternatively, a change in both the stable isotope composition and salinity indicates the influx of additional groundwater that is not representative of the catchment (e.g. the *Lower Krom Antonies*), and this groundwater should not be used for CMB estimates. Hol6 additionally reiterates the importance of sampling more than one season. Had only one sample been taken and assumed to be representative of average groundwater composition, the error of sampling shallow groundwater could have been made. Large seasonal fluctuations in groundwater geochemistry that correspond with pumping seasons can act as indicators for the effects of pumping-induced recharge, with strong evaporation trends further indicating that recharge is derived from shallow ground or surface water sources.

This study shows the importance of establishing a rainfall collector at a higher altitude in the catchment where recharge is suspected to be significant (e.g. rainfall collector M-R on the Piketberg Mountain range). The stable isotopes of this rain water could be more representative of groundwater in the valley, and the high altitude makes this collector less prone to dust pollution. Such a collector should be supplemented by rainfall collectors in the valley, which provide a robust spatial distribution. Comparing the stable isotopes of rain water from a range of collectors and groundwater from a range of boreholes can be used to validate the CMB recharge estimates. This study shows that the CMB method can be used to calculate recharge over smaller catchments, given that the flow systems are well constrained.

This study shows the importance of initially selecting more than one rainfall collector, to account for potential sampling errors (nine collectors were initially selected, but only four produced reliable results). Assessing the inclusivity of sampling for both the type of rainfall event, and the total annual rainfall, can indicate which rainfall collectors have the most representative sampling. It is also valuable to sample more than one rainy season, as extreme meteorological and weather events (such as El Niño) can produce data that is not representative of long-term averages. Stable isotopes of rain water are good indicators for such events, particularly when compared to other long-term rain water compositions.

6.5. Effects of regional pumping and climate change

Future climate change predictions across South Africa paint a bleak scenario, particularly for the west coast. In the Western Cape, winter rainfall is likely to decrease in the future, and will possibly be characterised by higher intensity rainfall events (Midgley *et al.*, 2005). These high intensity events are less likely to contribute significantly to recharge in the Verlorenvlei catchment (Watson *et al*., 2017a). Temperatures in the Sandveld are also predicted to

increase during the critical summer months from December to February, with a reduction in summer rainfall (Archer *et al.*, 2009), and an extension of the summer season (Cavé *et al.*, 2003). This is particularly worrisome for potato farmers who are heavily reliant on groundwater for irrigation during the summer months, and will result in increased groundwater abstraction in summer, placing more pressure on a groundwater system that already shows signs of high water stress (Archer *et al.*, 2009; Műnch *et al.*, 2013).

Saline shallow groundwater in the upper part of the Krom Antonies is not an issue yet, as the fresh secondary aquifer recharges the primary aquifer in the form of a gaining stream. However, increased pumping of TMG groundwater could decrease baseflow to the Krom Antonies River and result in the inflow of saline Hol groundwater reaching further up the catchment. Cavé *et al.* (2003) shows that an exponential relationship exists between rainfall and recharge, and a slight reduction in rainfall due to climate change could therefore result in a significant reduction in recharge, which may become negligible for rainfall < 400 mm/a.

Pumping-induced groundwater discharge from the primary to secondary aquifer at Hol6 has not been identified in previous literature, and could have severe consequences for the health of the secondary aquifer. As pumping increases and rainfall decreases across the catchment, such a scenario as at Hol6 could become more common across the lower catchment where the deep groundwater contributes little to baseflow. Sigidi (2017) shows that the inflow of shallow groundwater is particularly worrisome for the Hol and Kruismans, where average shallow groundwater EC values are 740 and 746 mS/m respectively. The salinity of the shallow groundwater is also likely to increase in the future, as surface run-off along the west coast is predicted to decrease to below 5 mm/a (Schulze, 2000), and dryland salinity could impact salinity down the catchment (Bugan, 2014). Although deep and shallow groundwater along the Kruismans show little signs of interaction, this could change in the future with increased pumping.

Pumping-induced recharge not only poses a threat of salinization to the secondary aquifer, but also threatens to decrease the quality and quantity of groundwater discharged into the Verlorenvlei wetlands. The wetlands rely heavily on groundwater baseflow during periods of low surface run-off and drought, and prolonged pumping is likely to result in a losing stream and reduced baseflow conditions. Furthermore, increases in pumping in the upper Krom Antonies catchment will reduce the contribution of TMG groundwater to the lower catchment.

7. CONCLUSIONS

The secondary aquifer of the Verlorenvlei catchment is generally characterised by good quality groundwater in comparison to the saline, primary aquifer. This is particularly true for the upper reaches of the Krom Antonies catchment in the Piketberg Mountain range, where groundwater has the lowest EC and chloride content in the study area. It also has a distinct Ca^{2+}-HCO_3^- type groundwater that has not been identified in previous literature, and is likely to represent the nearest composition to TMG groundwater. This is comparatively different to the Ca^{2+}-Mg^{2+}-Cl^- and Na^+-Cl^- type groundwater found in the rest of the catchment.

Chloride Mass Balance estimates from the upper Krom Antonies catchment indicate that direct recharge to the secondary aquifer varies between 20 and 27 mm/a (4.2 - 5.6% MAP), while the TMG aquifer contributes between 40 and 53 mm/a (11.4 - 15.2% MAP). These estimates correspond well with physical methods by Watson *et al.* (2017b), and prove robust for different groundwater sampling seasons and rainfall events. Ground and rain water $\delta^{18}O$ and $\delta^{2}H$ values from the upper Krom Antonies support the estimate that the TMG contributes double the recharge to the secondary aquifer, in comparison to direct recharge. Additionally, deuterium excess values of ground and rain water indicate the presence of evaporative processes before infiltration, suggesting a combination of macropore diffusion and focussed recharge. $\delta^{18}O$ and $\delta^{2}H$ values also show that deep groundwater contributes significant recharge to the primary aquifer in the upper and middle Krom Antonies, resulting in a gaining stream where deep groundwater contributes to baseflow.

Salinity increases significantly down the Krom Antonies catchment. This is reflected in the CMB results that underestimate recharge in the lower catchment and do not correlate well with physical-based methods. The middle and upper Krom Antonies have the same source of recharge, and increasing salinity in the middle Krom Antonies is attributed to decreased recharge and significant water-rock interaction with the Malmesbury shale. On the other hand, more negative stable isotope values of groundwater in the lower Krom Antonies show that little recharge is in fact derived from the TMG aquifer and upper catchment, contrary to previous literature. The lower Krom Antonies is mixing with deep groundwater from the Hol, and has a distinctly different source of recharge to the upper Krom Antonies, with $\delta^{18}O$ and $\delta^{2}H$ values indicating the likelihood of recharge at a higher altitude or more inland.

Although most deep boreholes along the Hol are comparable to the upper reaches of the Krom Antonies, two exceptions contribute significant salt to the lower Krom Antonies, and are a cause for concern. Salinisation at Hol2 is controlled by the dip of the Piketberg Mountain range, which directs most of the recharge into the Krom Antonies valley and results in the

accumulation of salts. Additionally, large groundwater abstraction at Hol6 during the summer months has resulted in the discharge of shallow groundwater to the deeper aquifer through the semi-confined layer. This is apparent by the elevated EC values and positive $\delta^{18}O$ and $\delta^{2}H$ values that are indicative of an evaporative environment, and closely match those of the shallow aquifer. This indicates a losing stream scenario, and deep groundwater does not contribute to baseflow.

Climate predictions indicate less rainfall and higher temperatures along the west coast, which will result in both decreased recharge and increased groundwater abstraction. Contributions from the TMG aquifer are likely to be significantly less in the lower Krom Antonies, resulting in more inflow of saline Hol groundwater. This will have severe impacts on the large expansion of agricultural activities in this area. The effects of pumping do not appear to be a problem for the Kruismans, where shallow and deep groundwater show little interaction. However, this study indicates that pumping-induced discharge from the primary to secondary aquifer is likely to become a problem for deep groundwater along the Hol, Verloren and lower Krom Antonies, which all have a similar source of recharge. This pumping-induced groundwater interaction has not been identified in previous literature, and should be carefully monitored in the future. Such a scenario does not only threaten the secondary aquifer with salinisation, but also the health of the wetlands through a reduction in deep groundwater baseflow.

Overall, the good spatial and seasonal variation in groundwater sampling shows the applicability of using major ion and stable isotope chemistry to constrain flow systems, recharge mechanisms, and identify the input of additional salts. This study also shows the importance of correct rain water sampling, as rain water indicated higher evaporation and the abundance of heavier isotopes in 2015, typical of an El Niño event. For recharge estimation, average $\delta^{2}H$, $\delta^{18}O$ and chloride values from both years were used, as these are most representative of long-term rainfall. This is supported by the general LMWL that is near identical to previous long-term isotopic studies in the Western Cape. Assessing the accuracy of rain water collection also proved valuable, to ensure that sampling is representative of both the type of rainfall event and the total annual rainfall. The study additionally showed the importance of establishing a rainfall collector in a high-altitude environment where rainfall is the most representative of recharge. Using this collector in combination with a collector in the valley proved particularly useful for validating the recharge mechanisms and estimates.

Although the CMB technique is typically used for regional recharge estimates in non-saline systems, in this study the at-point recharge estimates in the upper catchment are comparable to physical based methods. Since the estimates in the lower parts of the catchment via physical based recharge methods suggest negligible recharge, the approach used in this study

provides a meaningful estimate of recharge in the catchment as a whole. Therefore, the robust methodology for rain and groundwater evaluation presented in this study has far wider implications for CMB estimation, and provides a filtering technique that can be used for high resolution recharge estimates in semi-arid catchments threatened by groundwater salinisation.

8. REFERENCES

Airey, P., Calf, G. E., Campbell, B. L., Hartley, P. E. and Roman, D. (1979) Aspects of the isotope hydrology of the Great Artesian Basin, Australia, in *Isotope Hydrology 1978 (proceedings of a symposium): Vol. I*. Vienna: IAEA, pp. 205–219.

Allison, G. B. (1988) A review of some of the physical, chemical and isotopic techniques available for estimating groundwater recharge, in Simmers, I. (ed.) *Estimation of natural groundwater recharge: NATO ASI Series C 222*. Dordrecht: Reidel, pp. 49–72.

Allison, G. B., Barnes, C. J., Hughes, M. W. and Leaney, F. W. J. (1983) Effect of climate change and vegetation on oxygen-18 and deuterium profiles in soils, in *Isotope Hydrology 1983 (proceedings of a symposium)*. Vienna: IAEA, pp. 105–123.

Allison, G. B. and Hughes, M. W. (1977) The history of tritium fallout in Southern Australia as inferred from rainfall and wine samples, *Earth and Planetary Science Letters*, 36, pp. 334–340.

Allison, G. B. and Hughes, M. W. (1978) The use of environmental chloride and tritium to estimate total recharge to an unconfined aquifer, *Australian Journal of Soil Research*, 16, pp. 181–195.

Araujo, J. A., Abiodum, B. J. and Crespo, O. (2016) Impacts of drought on grape yields in Western Cape, South Africa, *Theoretical & Applied Climatology*, 123, pp. 117–130.

Archer, E., Conrad, J., Munch, Z., Opperman, D., Tadross, M. and Venter, J. (2009) Climate change, groundwater and intensive commercial farming in the semi-arid northern Sandveld, South Africa, *Journal of Integrative Environmental Sciences*, 6(2), pp. 139–155.

Balek, J. (1988) Groundwater recharge concepts, in Simmers, I. (ed.) *Estimation of natural groundwater recharge: NATO ASI Series C 222*. Dordrecht: Reidel, pp. 3–9.

Bazuhair, A. S. and Wood, W. W. (1996) Recharge in arid areas: examples from western Saudi Arabia, *Journal of Hydrology*, 186, pp. 153–159.

Beekman, H. E. and Xu, Y. (2003) Review of Groundwater Recharge Estimation in Arid and Semi-Arid Southern Africa, in Xu, Y. and Beekman, H. E. (eds) *Groundwater Recharge Estimation in Southern Africa*. Paris: UNESCO IHP, pp. 3–16.

Bredenkamp, D. B., Botha, L. J., van Tonder, G. J. and van Rensburg, H. J. (1995) *Manual on Quantitative Estimation of Groundwater Recharge and Aquifer Storativity: WRC Report No. TT 73/95*. Pretoria: Water Research Commission.

Breitenbach, S. F. M., Adkins, J. F., Meyer, H., Marwan, N., Kumar, K. K. and Haug, G. H. (2010) Strong influence of water vapor source dynamics on stable isotopes in precipitation observed in Southern Meghalaya, NE India, *Earth and Planetary Science Letters*. Elsevier B.V., 292(1–2), pp. 212–220.

Bugan, R. D. H. (2014) *Modeling and Regulating Hydrosalinity Dynamics in the Sandspruit River Catchment (Western Cape)*. Faculty of Agrisciences, Stellenbosch University: Unpublished PhD thesis.

Butler, J. J., Zlotnik, V. A. and Tsou, M. (2001) Produced by Pumping in the Vicinity of a Partially Penetrating Stream Stream, *Ground Water*, 39(5), pp. 651–659.

Camberlin, P., Janicot, S. and Poccard, I. (2001) Seasonality and atmospheric dynamics of the teleconnection between African rainfall and tropical sea-surface temperature: Atlantic vs. ENSO, *International Journal of Climatology*, 21, pp. 973–1005.

Cavé, L., Beekman, H. E. and Weaver, J. (2003) Impact of Climate Change on Groundwater Recharge Estimation, in Xu, Y. and Beekman, H. E. (eds) *Groundwater Recharge Estimation in Southern Africa*. Paris: UNESCO IHP, pp. 189–197.

Chen, X. (2001) Migration of Induced-Infiltrated Stream Water into Nearby Aquifers Due to Seasonal Ground Water Withdrawal, *Ground Water*, 39(5), pp. 721–728.

Conrad, J. E., Colvin, C., Sililo, O., Gorgens, A., Weaver, J. and Reinhardt, C. (1999) Fertiliser application to agricultural land: Verlorenvlei, in *Assessment of the impact of agricultural practices on the quality of groundwater resources in South Africa*. Pretoria: WRC Report No 641/1/99.

Conrad, J., Nel, J. and Wentzel, J. (2004) The challenges and implications of assessing groundwater recharge: A case study-northern Sandveld , Western Cape, South Africa, *Water SA*, 30(5), pp. 75–81.

Cook, P. G. and Solomon, D. K. (1997) Recent advances in dating young groundwater: Chlorofluorocarbons, 3H/3He and 85Kr, *Journal of Hydrology*, 191, pp. 245–265.

Craig, H. (1961) Isotopic Variations in Meteoric Waters, *Science*, 133, pp. 1702–1703.

CSIR (2009) *Development of the Verlorenvlei estuarine management plan: Situation assessment (Final Draft)*. Stellenbosch: Report prepared for the C.A.P.E. Estuaries Programme.

Dahl, M., Nilsson, B., Langhoff, J. H. and Refsgaard, J. C. (2007) Review of classification systems and new multi-scale typology of groundwater-surface water interaction, *Journal of Hydrology*, 344(1–2), pp. 1–16.

Dansgaard, W. (1964) Stable isotopes in precipitation, *Tellus*, 16(4), pp. 436–468.

De Beer, C. H. (2003) *The geology of the Sandveld area between Lambert's Bay and Piketberg: CGS Report No. 2003-0032*. Bellville: Council for Geosciences, Western Cape Unit.

De Vries, J. and Simmers, I. (2002) Groundwater recharge: An overview of processes and challenges, *Hydrogeology Journal*, 10, pp. 5–17.

De Vries, J. J., Selaolo, E. T. and Beekman, H. E. (2000) Groundwater recharge in the Kalahari, with reference to paleo-hydrologic conditions, *Journal of Hydrology*, 238, pp. 110–123.

Dennis, I. and Dennis, R. (2012) Climate change vulnerability index for South African aquifers, *Water SA: International Conference on Groundwater Special Edition*, 38(3), pp. 27–18.

Diamond, R. E. and Harris, C. (1997) Oxygen and hydrogen isotope composition of Western Cape meteoric water, *South African Journal of Geology*, 93, pp. 371–374.

Domenico, P. A. and Schwartz, F. W. (1990) *Physical and Chemical Hydrogeology*. New York: John Wiley & Sons, Inc.

DWAF (2000) *Reconnaissance investigation into the development and utilisation of Table Mountain Group artesian groundwater using the E10 catchment as a pilot study area: Final Report*. Report by Umvoto CC to the Department of Water Affairs and Forestry.

DWAF (2003) *Sandveld Preliminary (Rapid) Reserve Determinations. Langvlei, Jakkals and 646 Verlorenvlei Rivers. Olifants-Doorn WMA G30. Surface Volume 1: Final Report Reserve 647 Specifications*. DWAF Project Number: 2002-227.

DWAF (2004) *Assessment of the geohydrology of the Langvlei catchment: Report No. GH*

4000. Prepared by J.M. Nel: Department of Water Affairs and Forestry, Hydrological Services division.

Eriksson, E. and Khunakasem, V. (1969) Chloride concentration in groundwater, recharge rate and rate of deposition of chloride in the Israel Coastal Plain, *Journal of Hydrology*, 7(2), pp. 178–197.

Fontes, J. C. and Edmunds, W. M. (1989) *The use of environmental isotope techniques in arid zone hydrology - A critical review (IHP-III Project 5.2)*. Paris: UNESCO.

Freeze, R. A. and Cherry, J. A. (1979) *Groundwater*. New Jersey: Prentice-Hall, Inc.

Gardner, K. M. (1999) *Importance of Surface Water/ Groundwater Interactions*. Seattle: Environmental Protection Agency.

Gat, J. R. (1974) Local variability of the isotope composition of groundwater, in *Isotope Techniques in Groundwater Hydrology 1974 (proceedings of a symposium): Vol. II*. Vienna: IAEA, pp. 51–60.

Gat, J. R. (1983) Precipitation, groundwater and surface waters - Control of climate parameters on their isotopic composition and their utilization as palaeoclimatological tools, in *Palaeoclimates and palaeowaters: A collection of environmental isotope studies*. Vienna: IAEA, pp. 3–12.

Gat, J. R. (1996) Oxygen and hydrogen isotopes in the hydrologic cycle, *Annual Review Earth Planetary Science*, 24, pp. 225–262.

Gat, J. R. (2001) Volume II: Atmospheric water, in Mook, W. G. (ed.) *Environmental isotopes in the hydrological cycle: Principles and applications*. Vienna: IAEA-UNESCO, pp. 167–235.

Gat, J. R. and Dansgaard, W. (1972) Stable isotope survey of the fresh water occurrences in Israel and the northern Jordan rift valley, *Journal of Hydrology*, 16, pp. 177–212.

Gee, G. W. and Hillel, D. (1988) Groundwater recharge in arid regions: Review and critique of estimation methods, *Hydrological Processes*, 2(3), pp. 255–266.

GEOSS (2006) *Groundwater reserve determination required for the Sandveld, Olifants-Doorn water management area, Western Cape, South Africa: Report No. 2005/04-20*. Stellenbosch.

GEOSS (2012) *Geohydrological assessment of the Moutonshoek Area and environs - Sandveld, Western Cape: Report no. 2011_08-769*. Stellenbosch: GEOSS (Pty) Ltd.

Geyh, M. (2001) Volume IV: Groundwater saturated and unsaturated zone, in Mook, W. G. (ed.) *Environmental isotopes in the hydrological cycle: Principles and applications*. Vienna: IAEA-UNESCO, pp. 311–424.

Gresse, P. G., von Veh, M. W. and Frimmel, H. E. (2006) Namibian (Neoproterozoic) to early Cambrian successions, in Johnson, M. R., Anhaeusser, C. R., and Thomas, R. J. (eds) *The Geology of South Africa*. Johannesburg: Geological Society of South Africa, pp. 395–420.

Harck, T. R. (1995) *A geochemical investigation of the aquatic sediments, groundwater and surface water of the Verlorenvlei coastal lake, with special reference to nitrate transformations*. Faculty of Science, University of Cape Town: Unpublished MSc thesis.

Harris, C., Burgers, C., Miller, J. and Rawoot, F. (2010) O- and H-isotope record of Cape Town rainfall from 1996 to 2008, and its application to recharge studies of table mountain groundwater, South Africa, *South African Journal of Geology*, 113(1), pp. 33–56.

Hartnady, C. J. H., Newton, A. R. and Theron, J. N. (1974) The stratigraphy and structure of the Malmesbury Group in the southwestern Cape, *Bulletin of the Precambrian Research Unit, University of Cape Town*, 15, pp. 193–213.

Hay, E. R. and Hartnady, C. J. H. (2002) Towards 'Map-Centric' Simulation Modelling of Table Mountain Group Recharge, in Pieterson, K. and Parsons, R. (eds) *A Synthesis of the Hydrogeology of the Table Mountain Group - Formation of a Research Strategy: WRC Report N. TT 158/01*. Pretoria: Water Research Commission, pp. 103–107.

Herczeg, A. L. and Leaney, F. W. (2011) Review: Environmental tracers in arid-zone hydrology, *Hydrogeology Journal*, 19(1), pp. 17–29.

Hugman, R., Stigter, T. Y., Monteiro, J. P. and Nunes, L. (2012) In fluence of aquifer properties and the spatial and temporal distribution of recharge and abstraction on sustainable yields in semi-arid regions, *Hydrological Processes*, 26, pp. 2791–2801.

Kisters, A. F. M., Agenbach, C. and Frei, D. (2015) Age and tectonic significance of the volcanic Bloubergstrand member in the Pan-African Saldania Belt, South Africa, *South African Journal of Geology*, 118(3), pp. 213–224.

Kisters, A. F. M., Belcher, R. W., Armstrong, R. A., Scheepers, R., Rozendaal, A. and Jordaan, L. S. (2002) Timing and kinematics of the Colenso Fault: The Early Paleozoic shift from collisional to extensional tectonics in the Pan-African Saldania Belt, South Africa, *South African Journal of Geology*, 105, pp. 257–270.

Koeniger, P., Gaj, M., Beyer, M. and Himmelsbach, T. (2016) Review on soil water isotope-based groundwater recharge estimations, *Hydrological Processes*, 30(16), pp. 2817–2834.

Lerner, D., Issar, A. and Simmers, I. (1990) *Groundwater Recharge: A guide to understanding and estimating natural recharge*. Volume 8. Hannover, Germany: Verlag Heinz Heise.

Lerner, D. N. (2003) Surface water - ground water interactions in the context of groundwater resources, in Xu, Y. and Beekman, H. E. (eds) *Groundwater Recharge Estimation in Southern Africa*. Paris: UNESCO IHP, pp. 91–107.

Lian, T., Chen, D. and Tang, Y. (2017) Genesis of the 2014–2016 El Niño events, *Science China Earth Sciences*, 60(9), pp. 1589–1600.

Lihe, Y., Guangcai, H., Zhengping, T. and Ying, L. (2010) Origin and recharge estimates of groundwater in the Ordos Plateau, People's Republic of China, *Environmental Earth Sciences*, 60(8), pp. 1731–1738.

Lloyd, J. W. (1986) A review of aridity and groundwater, *Hydrological Processes*, 1(1), pp. 63–78.

Lynch, S. (2004) *Development of a raster database of annual, monthly and daily rainfall, for Southern Africa: Report No. 1156/1/04*. Pretoria: Water Research Commission.

MacDonald, A. M., Bonsor, H. C., Calow, R. C., Taylor, R. G., Lapworth, D. J., Maurice, L., Tucker, J. and Dochartaigh, B. E. (2011) *Groundwater resilience to climate change in Africa*. Nottingham: British Geological Survey.

Maclear, L. G. A. (1994) *A groundwater hydrocensus and water quality investigation of the Verlorenvlei primary aquifer - Elands Bay: Report No. GH 3835*. Cape Town: Department of Water Affairs, Geohydrology division.

Mazor, I. (1991) *Applied chemical and isotopic groundwater hydrology*. Buckinghamshire: Milton Keynes, Open University Press.

Meque, A. and Abiodun, B. J. (2015) Simulating the link between ENSO and summer drought in Southern Africa using regional climate models, *Climate Dynamics*, 44, pp. 1881–1900.

Midgley, G. F., Chapman, R. A., Hewitson, B., Johnston, P., De Wit, M., Ziervogel, G., Mukheibir, P., Van Niekerk, L., Tadross, M., Van Wilgen, B. W., Kgope, B., Morant, P. D., Theron, A., Scholes, R. J. and Forsyth, G. G. (2005) *A Status Quo, Vulnerability and Adaptation Assessment of the Physical and Socio-Economic Effects of Climate Change in the Western Cape: Report to the Western Cape Government, Cape Town, South Africa*. Stellenbosch: CSIR Report No. ENV-S-C 2005-073.

Miller, J. A., Dunford, A. J., Swana, K. A., Palcsu, L., Butler, M. and Clarke, C. E. (2017) Stable isotope and noble gas constraints on the source and residence time of spring water from the Table Mountain Group Aquifer, Paarl, South Africa and implications for large scale abstraction, *Journal of Hydrology*. Elsevier B.V., 551, pp. 100–115.

Mook, W. G. (2001) Volume I: Introduction, in Mook, W. G. (ed.) *Environmental isotopes in the hydrological cycle: Principles and applications*. Vienna: IAEA-UNESCO, pp. 1–164.

Műnch, Z., Conrad, J. E., Gibson, L. a., Palmer, A. R. and Hughes, D. (2013) Satellite earth observation as a tool to conceptualize hydrogeological fluxes in the Sandveld, South Africa, *Hydrogeology Journal*, 21(5), pp. 1053–1070.

Noble, R. G. and Hemens, J. (1978) *Inland water ecosystems in South Africa - review of research needs: Report No. 34*. South African National Scientific Programmes Report: CSIR.

Parsons, R. (2002) Recharge of Table Mountain Group Aquifer Systems, in Pietersen, K. and Parsons, R. (eds) *A Synthesis of the Hydrogeology of the Table Mountain Group - Formation of a Research Strategy: WRC Report N. TT 158/01*. Pretoria: Water Research Commission, pp. 97–102.

Parsons, R. (2004) *Surface Water - Groundwater interaction in a South African context: WRC Report No. TT 218/03*. Pretoria: Water Research Commission.

Roberts, D. L., Botha, G. A., Maud, R. R. and Pether, J. (2006) Coastal Cenozoic Deposits, in Johnson, M. R., Anhaeusser, C. R., and Thomas, R. J. (eds) *The Geology of South Africa*. Johannesburg: Geological Society of South Africa, pp. 605–628.

Robins, N. S. (1998) Recharge: the key to groundwater pollution and aquifer vulnerability, *Geological Society of London, Special Publications*, 130, pp. 1–5.

Rozendaal, A., Gresse, P. G., Scheepers, R. and de Beer, C. H. (1994) Structural setting of the Riviera W-Mo deposit, Western Cape, South Africa, *South African Journal of Geology*, 97(2), pp. 184–195.

Rozendaal, A. and Scheepers, R. (1995) Magmatic and related mineral deposits of the Pan-African Saldania belt in the Western Cape Province, South Africa, *Journal of African Earth Sciences*, 21(1), pp. 107–126.

Rushton, K. R. (1988) Numerical and conceptual models for recharge estimation in arid and semi-arid zones, in Simmers, I. (ed.) *Estimation of natural groundwater recharge: NATO ASI Series C 222*. Dordrecht: Reidel, pp. 223–238.

Rushton, K. R. and Ward, C. (1979) The estimation of groundwater recharge, *Journal of Hydrology*, 41(3–4), pp. 345–361.

Rust, I. C. (1967) *On the sedimentation of the Table Mountain Group in the Western Cape Province*. Department of Earth Sciences, Stellenbosch University: Unpublished DSc thesis.

Sami, K. and Hughes, D. A. (1996) A comparison of recharge estimates to a fractured sedimentary aquifer in South Africa from a chloride mass balance and an integrated surface-subsurface model, *Journal of Hydrology*, 179(1), pp. 111–136.

Sánchez-Murillo, R., Durán-Quesada, A. M., Birkel, C., Esquivel-Hernández, G. and Boll, J. (2017) Tropical precipitation anomalies and d-excess evolution during El Niño 2014-16, *Hydrological Processes*, 31, pp. 956–967.

Sanford, W. (2002) Recharge and groundwater models: An overview, *Hydrogeology Journal*, 10, pp. 110–120.

Sayed, S. A. S. and Hussainy, A. S. (2011) Analysis of pumping tests data from mutually leaky aquifers, *Water International*, 31(2), pp. 244–251.

Scanlon, B. R., Healy, R. W. and Cook, P. G. (2002) Choosing appropriate technique for quantifying groundwater recharge, *Hydrogeology Journal*, 10, pp. 18–39.

Scanlon, B. R., Keese, K. E., Flint, A. L., Flint, L. E., Gaye, C. B., Edmunds, W. M. and Simmers, I. (2006) Global synthesis of groundwater recharge in semiarid and arid regions, *Hydrological Processes*, 20, pp. 3335–3370.

Schulze, R. E. (2000) Modelling Hydrological Responses to Land Use and Climate Change: A Southern African Perspective, *Ambio*, 29(1), pp. 12–22.

Schulze, R. E., Maharaj, M., Warburton, M. L., Gers, C. J., Horan, M. J. C., Kunz, R. P. and Clark, D. J. (2008) *South African Atlas of Climatology and Agrohydrology: WRC Report No. 1489/1/08*. Pretoria: Water Research Commission.

Schuyt, K. D. (2005) Economic consequences of wetland degradation for local populations in Africa, *Ecological Economics*, 53, pp. 177–190.

Schwartz, F. W. and Zhang, H. (2003) *Fundamentals of Groundwater*. New York: John Wiley & Sons, Inc.

Sharma, M. L. and Hughes, M. W. (1985) Groundwater recharge estimation using chloride, deuterium and oxygen-18 profiles in the deep coastal sands of Western Australia, *Journal of Hydrology*, 81(1–2), pp. 93–109.

Sigidi, N. T. (2017) *Geochemical and isotopic tracing of salinity loads into the RAMSAR listed Verlorenvlei freshwater coastal estuarine lake, Western Cape, South Africa*. Department of Earth Sciences, Stellenbosch University: Unpublished MSc thesis.

Simmers, I. (ed.) (1988) *Estimation of natural groundwater recharge: NATO ASI Series C 222*. Dordrecht: Reidel.

Sinclair, S. A., Lane, S. B. and Grindley, J. R. (1984) Report No. 32: Verlorenvlei (CW 13), in Heydorn, A. E. F. and Morant, P. D. (eds) *Estuaries of the Cape. Part II, synopses of available information on individual systems*. Stellenbosch: CSIR Research Report 431.

Smart, M. and Tredoux, G. (2002) Groundwater quality and fitness for use, in Pieterson, K. and Parsons, R. (eds) *A Synthesis of the Hydrogeology of the Table Mountain Group - Formation of a Research Strategy: WRC Report N. TT 158/01*, pp. 118–123.

SRK (2009) *Preliminary Assessment of Impact of the Proposed Riviera Tungsten Mine on Groundwater Resources: Report No. 392947*. SRK Consulting Engineers and Scientists: Report prepared for Bongani Minerals (Pty) Ltd.

Suwarman, R., Ichiyanagi, K., Tanoue, M., Yoshimura, K., Mori, S., Yamanaka, M., Syamsudin, F. and Belgaman, H. A. (2017) El Niño Southern Oscillation Signature in Atmospheric Water Isotopes over Maritime Continent during Wet Season, *Journal of the*

Meteorological Society of Japan, 95(1), pp. 49–67.

Tankard, A., Welsink, H., Aukes, P., Newton, R. and Stettler, E. (2009) Tectonic evolution of the Cape and Karoo basins of South Africa, *Marine and Petroleum Geology*. Elsevier Ltd, 26(8), pp. 1379–1412.

Thamm, A. G. and Johnson, M. R. (2006) The Cape Supergroup, in Johnson, M. R., Anhaeusser, C. R., and Thomas, R. J. (eds) *The Geology of South Africaeology of South Africa*. Johannesburg: Geological Society of South Africa, pp. 443–460.

Toth, J. (1963) A theoretical analysis of groundwater flow in small drainage basins, *Journal of Geophysical Research*, 68, pp. 4795–4812.

Van Tonder, G. and Bean, J. (2003) Challenges in estimating groundwater recharge, in Xu, Y. and Beekman, H. E. (eds) *Groundwater Recharge Estimation in Southern Africa*. Paris: UNESCO IHP, pp. 19–29.

Van Weert, F., Van der Gun, J. and Reckman, J. (2009) *Global Overview of Saline Groundwater Occurrence and Genesis*. Utrecht: International Groundwater Resources Assessment Centre (IGRAC).

Van Wyk, E., Van Tonder, G. and Vermeulen, D. (2012) Characteristics of local groundwater recharge cycles in South African semi-arid hard rock terrains: Rainfall-groundwater interaction, *Water SA*, 38(5), pp. 747–754.

Vegter, J. R. (1995) *Ground water resources of South Africa, Map Sheet 2: Report TT74/95*. Pretoria: Water Research Commission.

Vegter, J. R. and Pitman, W. V (2003) Recharge and stream flow, in Xu, Y. and Beekman, H. E. (eds) *Groundwater Recharge Estimation in Southern Africa*. Paris: UNESCO IHP, pp. 109–123.

Verhagen, B. (2003) Recharge quantified with radiocarbon in three studies of Karoo aquifers in the Kalahari and independent corroboration, in Xu, Y. and Beekman, H. E. (eds) *Groundwater Recharge Estimation in Southern Africa*. Paris: UNESCO IHP, pp. 51–61.

Watson, A., Miller, J. and de Clercq, W. P. (2017a) Investigating Potential Additional Sources of Groundwater Flow into a Defined Watershed, *Procedia Earth and Planetary Science*. Elsevier B.V., 17, pp. 546–549.

Watson, A. P., Miller, J. A., Fleischer, M. and de Clercq, W. P. (2017b) Estimation of groundwater recharge via percolation outputs from a rainfall/runoff model for the Verlorenvlei estuarine system, west coast, South Africa., *Manuscript submitted for publication: Journal of Hydrology*.

Watson, A. P., Miller, J. A. and de Clercq, W. P. (2017c) Using MODFLOW to quantify the reduction in baseflow casued by abstractions within a RAMSAR listed wetland catchment in South Africa, *Manuscript in preparation for publication: Journal of Hydrogeology*.

Weaver, J. M. C., Talma, A. S. and Cave, L. C. (1999) *Geochemistry and isotopes for resource evaluation in the fractured rock aquifers of the Table Mountain Group: WRC Report No. 481/1/99*. Pretoria: Water Research Commission.

White, D. E., Hem, J. D. and Waring, G. A. (1963) Chemical composition of subsurface waters, in *Data of Geochemistry*. Washington: USGS Professional Paper 440-F.

Winter, T. C. (1999) Relation of streams, lakes, and wetlands to groundwater flow systems, *Hydrogeology Journal*, 7(1), pp. 28–45.

Winter, T. C. (2001) The concept of hydrologic landscapes, *Journal Of The American Water*

Resources Association, 37(2), pp. 335–349.

Winter, T. C., Harvey, J. W., Franke, O. L. and Alley, W. M. (1998) *Ground water and surface water: A single resource*. Denver, Colorado: U.S. Geological Survey Circular 1139.

Wood, W. W. (1999) Use and misuse of the chloride mass balance method in estimating ground water recharge, *Ground Water*, 37(1), pp. 2–3.

Wood, W. W. and Stanford, W. E. (1995) Chemical and isotopic methods for quantifying groundwater recharge in a regional, semi-arid environment, *Ground Water*, 33(3), pp. 458–468.

Xu, Y. and Van Tonder, G. J. (2001) Estimation of recharge using a revised CRD method, *Water SA*, 27(3), pp. 341–343.

Yuan, R., Song, X., Han, D., Zhang, L. and Wang, S. (2013) Upward recharge through groundwater depression cone in piedmont plain of North China Plain, *Journal of Hydrology*. Elsevier B.V., 500, pp. 1–11.